

Mapping of a Protein Interaction Network Required for Enterobactin Biosynthesis in
Escherichia coli

Paknoosh Pakarian

A thesis
In the Department of
Chemistry and Biochemistry

Presented in Partial Fulfillment of the Requirements for
the Degree of Doctor of Philosophy
at
Concordia University
Montreal, Quebec, Canada

August 2016

© Paknoosh Pakarian, 2016

CONCORDIA UNIVERSITY
SCHOOL OF GRADUATE STUDIES

This is to certify that the thesis prepared

By: **Paknoosh Pakarian**

Entitled: **Mapping of a Protein Interaction Network Required for Enterobactin Biosynthesis in *Escherichia coli***

and submitted in partial fulfillment of the requirements for the degree of

Ph.D. of Chemistry (Biochemistry)

complies with the regulations of the University and meets the accepted standards with respect to originality and quality.

Signed by the final examining committee:

| | |
|----------------------|---------------------|
| _____ | Chair |
| Dr. Jack Kornblatt | |
| _____ | External Examiner |
| Dr. Eric Masse | |
| _____ | External to Program |
| Dr. David Walsh | |
| _____ | Examiner |
| Dr. Paul Joyce | |
| _____ | Examiner |
| Dr. Alisa Piekny | |
| _____ | Thesis Supervisor |
| Dr. Peter D. Pawelek | |

Approved by

Dr. Peter D. Pawelek, Graduate Program Director

August 2016

André Roy, Dean of Faculty

Abstract

Mapping of a Protein Interaction Network Required for Enterobactin Biosynthesis in *Escherichia coli*

Paknoosh Pakarian, Ph.D.

Concordia University, 2016

Protein complexes are essential components of many biological processes. Therefore, protein-protein interactions are crucial for many essential cellular functions and are considered good targets for the development of novel therapeutics.

Siderophore biosynthesis is one of the biological processes that has an absolute requirement for protein-protein interactions. Siderophores are small iron-scavenging molecules that are synthesized and secreted by iron-starved bacteria to chelate ferric iron (Fe^{3+}) from the environment. Ferric iron, which is essential for survival and growth of most bacteria, is insoluble at neutral pH, or is bound to host iron storage proteins such as transferrin. By taking up Fe^{3+} -siderophore complexes, such bacteria can survive and proliferate in low-iron environments.

Enterobactin is a catecholate type siderophore of *E. coli* that is synthesized in its cytoplasm by seven enzymes, EntA-F and EntH. These sequentially-related enzymes function together to produce enterobactin, which is a cyclic trimer of 2,3-dihydroxy-N-benzoyl-L-serine. Enterobactin biosynthetic enzymes are organized in two functional modules: the DHB module (EntCBA) and the non-ribosomal peptide synthesis (NRPS) module (EntBDEF). Interactions between EntBDEF in the NRPS module have been previously reported. Our research group has since reported *in vitro* evidence of an interaction between EntA and EntE, the enzymes at the interface of the DHB and NRPS modules.

The research presented here is focused on the identification of novel protein-protein interactions in the DHB module as well as the study of subunit orientation in the Ent complexes.

The first research chapter is centered on the subunit orientation in the intracellular EntA-EntE complex. In this study Chrome Azurol S (CAS) assays and bacterial adenylate cyclase two-hybrid (BACTH) assays were employed to study the EntA-EntE complexation *in vivo*. CAS assays were used to validate the functionality of EntA and EntE BACTH constructs. BACTH experiments were then performed to identify the intracellular complexation of EntA and EntE and to determine the orientation of EntA relative to EntE in the complex. BACTH results were further validated by automated docking simulations.

The second research chapter focuses on the construction of two Fur-controlled bidirectional protein expression vectors. Ferric Uptake Regulator (Fur) is a protein involved in iron homeostasis in *E. coli*. When intracellular iron is abundant, Fur forms a complex with Fe^{2+} . This complex binds to the Fur box and inhibits the transcription of iron responsive genes such as *ent* genes. The Fur box is the consensus sequence that is located near or within the promoter region of iron responsive genes. The novel expression vectors are derivatives of low copy number plasmids pACYC184 and pBR322 and contain a bidirectional promoter, FLAG or HA tags, TEV cleavage site and a multiple cloning site (MCS) compatible with the MCS of BACTH vectors.

The third research chapter involves the identification of a novel protein-protein interaction between two enzymes in the DHB module, EntA and EntB. Furthermore, ternary complex formation between EntA, EntB and EntE was investigated in this chapter. BACTH was employed as the primary method for the detection of protein-protein interactions between EntA and EntB. Functionality of all the constructs used in the BACTH was confirmed using the CAS assay and growth studies. Automated docking simulations were also used to generate a model for an EntA-EntB-EntE ternary complex. The EntE-EntB interaction interface in the generated model was in accordance with the published crystal structure for the EntE-EntB complex and therefore supported our experimental results.

Acknowledgments

I owe the biggest debt of gratitude to my supervisor, Dr. Peter D. Pawelek. I am deeply grateful to you for your guidance, support and patience throughout my PhD studies. Without a doubt you are one of those people who had a great impact on my life. If one day I start my own research group, I have a clear idea of what type of supervisor I want to be.

I am also grateful to Drs. Paul Joyce, Alisa Piekny, Joanne Turnbull and Michael Sacher for all their help and time and useful discussions.

A big thank you goes to all my colleagues and staff in the Chemistry and Biochemistry Department.

&

My family. Expressing gratitude toward you in words is like pouring an ocean into a soda can. So I am going to keep it short and simple but I am sure you know exactly what I mean, Thank you and Love you.

Contributions of the Authors

Dr. Peter D. Pawelek has performed the blind docking for EntA-EntE and EntA-EntE-EntB complexes in Chapters 2 and 4, respectively.

Table of Contents

| | |
|--|------------|
| List of Tables | x |
| List of Figures | xi |
| List of Abbreviations | xii |
| Chapter 1: General Introduction | 1 |
| 1.1 Statement of the Problem and Its Significance | 1 |
| 1.2 Background | 2 |
| 1.2.1 Iron chemistry and bioavailability | 2 |
| 1.2.2 Iron homeostasis | 3 |
| 1.2.3 Mammalian iron binding proteins | 4 |
| 1.2.3.1 Bacterial iron acquisition from mammalian sources | 5 |
| 1.2.4 Siderophores | 6 |
| 1.2.4.1 Bacterial siderophores | 6 |
| 1.2.4.2 Fungal siderophores | 7 |
| 1.2.4.3 Plant siderophores | 8 |
| 1.2.4.4 Mammalian siderophores and iron sequestration | 10 |
| 1.2.5 Applications of siderophores | 10 |
| 1.2.5.1 Siderophores and bioremediation | 11 |
| 1.2.5.2 Siderophores as Trojan horse antibiotics | 11 |
| 1.2.6 Siderophores of <i>E. coli</i> | 11 |
| 1.2.6.1 Enterobactin: The catecholate siderophore of <i>E. coli</i> | 12 |
| 1.2.6.2 Enterobactin: Biosynthesis | 13 |
| 1.2.6.3 Enterobactin: Secretion | 18 |
| 1.2.6.4 Enterobactin: Uptake | 20 |
| 1.2.6.5 Enterobactin: Hydrolysis and iron release | 21 |
| 1.2.7 Specific aims | 21 |
| Chapter 2: Subunit Orientation in the <i>Escherichia coli</i> Enterobactin Biosynthetic EntA-EntE Complex Revealed by a Two-Hybrid Approach | 23 |
| 2.1 Preface | 23 |
| 2.2 Abstract | 23 |
| 2.3 Introduction | 24 |
| 2.4 Materials and Methods | 25 |

| | |
|--|-----------|
| 2.4.1 Reagents | 25 |
| 2.4.2 Preparation of BACTH constructs | 26 |
| 2.4.3 Modification of <i>entA</i> ⁻ and <i>entE</i> ⁻ knockout strains | 27 |
| 2.4.4 CAS assays and growth studies | 28 |
| 2.4.5 Bacterial adenylate cyclase two-hybrid (BACTH) assays | 29 |
| 2.4.6 Western blotting | 30 |
| 2.4.7 Automated Docking | 31 |
| 2.5 Results and Discussion | 31 |
| 2.5.1 Validation of BACTH constructs using CAS assays and growth studies | 32 |
| 2.5.2 Detection of the intracellular EntA-EntE interaction by BACTH | 38 |
| 2.5.3 Intracellular expression of BACTH fusion proteins | 41 |
| 2.5.4 Computational prediction of the EntA-EntE complex | 42 |
| | |
| Chapter 3: A Novel Set of Vectors for Fur-controlled Protein Expression Under Iron | |
| Deprivation in <i>Escherichia coli</i> | 46 |
| 3.1 Preface | 46 |
| 3.2 Abstract | 46 |
| 3.3 Background | 47 |
| 3.4 Methods | 49 |
| 3.4.1 Reagents, plasmids, software and primers | 49 |
| 3.4.2 Production of pFCF1 and pFCF2 | 49 |
| 3.4.3 Production of pFBH1 | 50 |
| 3.4.4 CAS assays | 51 |
| 3.4.5 Growth studies | 52 |
| 3.4.6 Western blotting | 53 |
| 3.5 Results | 54 |
| 3.5.1 Construction of pFCF1, pFCF2 and pFBH1 | 54 |
| 3.5.2 Assessment of iron-responsive promoter regions | 58 |
| 3.5.3 Iron-controlled protein expression | 60 |
| 3.5.4 Iron-controlled bidirectional expression from pFCF2 | 61 |
| 3.6 Discussion | 63 |
| 3.7 Conclusions | 65 |
| 3.8 Supplementary Material | 67 |

| | |
|---|------------|
| Chapter 4: Intracellular Co-Localization of the <i>Escherichia coli</i> Enterobactin Biosynthetic Enzymes EntA, EntB, and EntE | 69 |
| 4.1 Preface | 69 |
| 4.2 Abstract | 69 |
| 4.2 Introduction | 70 |
| 4.3 Material and Methods | 71 |
| 4.3.1 Reagents | 71 |
| 4.3.2 Preparation of constructs | 72 |
| 4.3.3 CAS assays and growth studies | 74 |
| 4.3.4 BACTH assays | 74 |
| 4.3.5 Computational docking | 75 |
| 4.4 Results and Discussion | 75 |
| 4.4.1 Intracellular interaction of <i>E. coli</i> EntA and EntB | 75 |
| 4.4.2 Computational docking of <i>E. coli</i> EntA, EntB, and EntE | 80 |
| 4.4.3 Interaction of EntA and EntE with the EntB IC domain | 83 |
| Chapter 5: General Discussion | 87 |
| 5.1 Subunit Orientation in the EntA-EntE Complex | 88 |
| 5.2 Design and Generation of Fur-controlled Protein Expression Vectors | 88 |
| 5.3 “ABE Complex”: Ternary Complex Formation between EntA, EntB and EntE | 89 |
| 5.4 Conclusion | 91 |
| Chapter 6: Work in Progress and Future Directions | 93 |
| 6.1 Identification of Residues at the Interaction Interface of EntA-EntE Complex | 93 |
| 6.2 Validation and Characterization of EntA and EntB Interaction | 93 |
| 6.3 Identification of Novel Protein Interactions in the DHB Module | 94 |
| 6.4 Membrane Localization of Enterobactin Biosynthetic Machinery | 96 |
| References | 98 |
| Appendix 1 | 108 |

List of Tables

Chapter 1

| | |
|---|----|
| Table 1: Summary of the proteins involved in the enterobactin biosynthesis pathway. | 18 |
|---|----|

Chapter 2

| | |
|--|----|
| Table 1: PCR primer sequences used for preparing BACTH constructs. | 27 |
|--|----|

| | |
|--|----|
| Table 2: BACTH Constructs: Summary of CAS assays and growth studies. | 37 |
|--|----|

Chapter 3

| | |
|---------------------------------------|----|
| Table 1: Plasmids used in this study. | 49 |
|---------------------------------------|----|

Chapter 4

| | |
|--|----|
| Table 1: PCR primers used in this study. | 73 |
|--|----|

List of Figures

Chapter 1

| | |
|--|----|
| Figure 1: Different types of bacterial siderophores. | 9 |
| Figure 2: Schematic of enterobactin, the catecholate siderophore of <i>E. coli</i> . | 12 |
| Figure 3: Enterobactin biosynthetic arms: DHB module and NRPS module. | 14 |
| Figure 4: <i>E. coli</i> biosynthetic pathway, DHB module. | 15 |
| Figure 5: <i>E. coli</i> biosynthetic pathway, NRPS module. | 17 |
| Figure 6: Enterobactin biosynthetic and inner membrane secretion machinery. | 20 |

Chapter 2

| | |
|--|----|
| Figure 1: Intracellular functionality of BACTH constructs determined by CAS assays and growth studies. | 35 |
| Figure 2: Three-dimensional X-ray crystallographic structures of EntA and EntE. | 37 |
| Figure 3: BACTH assays of the EntA-EntE interaction. | 40 |
| Figure 4: Verification of protein expression from BACTH constructs by Western blotting. | 42 |
| Figure 5: Automated docking of monomeric EntE to tetrameric EntA. | 44 |

Chapter 3

| | |
|--|----|
| Figure 1: The intercistronic bidirectional promoter region between <i>E. coli fepB</i> and <i>entC</i> . | 55 |
| Figure 2: Vector maps of pFCF1 and pFCF2. | 56 |
| Figure 3: Vector map of pFBH1. | 57 |
| Figure 4: Functional assays for pFCF1, pFCF2 and pFBH1. | 59 |
| Figure 5: Protein expression from pFCF1 and pFBH1. | 61 |
| Figure 6: Bidirectional expression from pFCF2. | 62 |

Chapter 4

| | |
|--|----|
| Figure 1: Bacterial two-hybrid assays of EntA with full-length EntB. | 79 |
| Figure 2: Computational modeling of the <i>E. coli</i> EntA-EntB-EntE complex. | 82 |
| Figure 3: Functional validation of EntB IC domain BACTH construct. | 84 |
| Figure 4: Intracellular co-localization of EntB IC domain with EntA and EntE. | 86 |

Chapter 6

| | |
|--|----|
| Figure 1: Functionality assays and protein purification for pGEX- <i>entA</i> construct. | 94 |
| Figure 2: CAS assays and growth studies for <i>entC</i> BACTH constructs. | 95 |

List of Abbreviations

ABC: ATP Binding Cassette

AC: adenylate cyclase

ACP: acyl carrier protein

APEC: avian pathogenic *E. coli*

ArCP: aryl carrier protein domain

AUC: analytical ultracentrifugation

BACTH: bacterial adenylate cyclase two-hybrid

CAP: catabolite activator protein

CAS: chrome azurol S

DHB: 2,3 dihydroxybenzoic acid

DHBS: 2,3 dihydroxybenzoyl-serine

DTT: dithiothreitol

DtxR: Diphtheria toxin repressor protein

DIP: 2,2'-dipyridyl

ExPEC: extraintestinal pathogenic *E. coli*

FP: fluorescent protein

Fur: ferric uptake regulator

HH: hereditary hemochromatosis

HRP: horseradish peroxidase

IC: isochorismatase domain

IPTG: isopropyl β -D-1-thiogalactopyranoside

ITC: isothermal titration calorimetry

Lpn 2: lipocalin 2

MCS: multiple cloning site

MFS: major facilitator superfamily

NRPS: non-ribosomal peptide synthesis

ORF: open reading frame

PALM: photoactivated localization microscopy

PCP: peptidyl carrier protein

PVDF: polyvinylidene difluoride

Scn: siderocalin

SDS-PAGE: SDS-polyacrylamide gel electrophoresis

TM: Transmembrane

UPEC: Uropathogenic *E. coli*

Chapter 1: General Introduction

1.1 Statement of the Problem and Its Significance

Antibiotic resistance in bacteria is a major health concern that is having serious effects on the population and the healthcare system. Furthermore, the development of novel antimicrobial agents has been limited or abandoned by some pharmaceutical companies over the years causing a gap in the treatment of patients. Therefore, the efficient design of novel antimicrobial agents to which bacteria have not acquired resistance is vital to maintain public health in the long run [1,2,3].

One recent lead discovery approach to develop novel therapeutics employs small molecules that disrupt protein-protein interactions [3,4]. Protein-protein interactions occur extensively in cells and are essential for a great number of cellular functions. For these reasons, they are considered as good targets for novel therapeutics. Our knowledge of protein-protein interactions has been greatly improved over the last two decades. Furthermore, advances have been achieved in designing small-molecule inhibitors that target protein-protein interactions [4,5].

One cellular process that is highly dependent on numerous protein-protein interactions in most microorganisms is siderophore-mediated iron uptake. Siderophores are small molecules that chelate ferric iron (Fe^{3+}) with high affinity [6-9]. There are numerous siderophore-mediated uptake systems that are found in different microorganisms, and each system involves numerous proteins for biosynthesis and secretion of siderophores, and import of ferric siderophores. Given its essential role for survival in iron-limited environments, siderophore-mediated iron uptake could be considered as a potential target for novel antibiotics [2,6].

Iron is an essential nutrient for almost all microorganisms. However, ferric iron (Fe^{3+}) is inaccessible to bacteria at physiological pH and under aerobic conditions. In mammalian cells, most Fe^{3+} is bound to proteins such as transferrin, or sequestered in ferritin [7]. To circumvent the problem of low bioavailability, many microorganisms produce and secrete siderophores in order to acquire Fe^{3+} from the extracellular environment, which can then be used as a cofactor in many metabolic processes required for cellular growth and survival [10]. Thus, siderophores can be considered as virulence factors when they support growth of pathogenic bacteria inside mammalian hosts [6]. Since protein-protein interactions are already recognized as good drug targets, and since siderophore-mediated iron uptake relies on numerous protein-protein interactions [2,6], disruption of protein interactions necessary to support bacterial growth in low-iron environments can thus be considered a good strategy in the development of novel therapeutics.

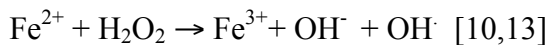
The research presented in this thesis focuses on the protein-protein interactions in the biosynthetic machinery required for the production of the *E. coli* siderophore, enterobactin.

1.2 Background

1.2.1 Iron chemistry and bioavailability

Most microorganisms require iron as a cofactor for different cellular processes such as amino acid biosynthesis, electron transport and DNA synthesis. Iron is one of the most abundant elements on earth and it readily converts between ferric (Fe^{3+}) and ferrous (Fe^{2+}) forms. As a transition state metal, iron is ideal for the catalysis of biochemical reactions and many enzymes require iron for their biological functions [10,11,12]. However, the bioavailability of iron is affected by pH and aeration. Under aerobic conditions at physiological pH, iron exists in its ferric form (Fe^{3+}), which has a low solubility outside of living organisms due to ready formation of

ferric hydroxide polymers. Bacteria can therefore not acquire enough freely soluble ferric iron to support their growth [12]. In mammalian hosts, serum iron concentration is around 10^{-24} M due to its sequestration in proteins such as transferrin and lactoferrin. Therefore, microbial growth is inhibited by low concentrations of free iron in serum [12]. In addition, excessive iron accumulation can be harmful to cells due to the production of reactive oxygen species *via* the Fenton reaction:



Therefore, the low concentration of free iron in the host organism protects against both bacterial infection and reactive oxygen species.

1.2.2 Iron homeostasis

Since the excessive iron can cause cellular damage, organisms have developed protective mechanisms to regulate iron homeostasis. In *E. coli*, iron homeostasis is achieved by the Ferric Uptake Regulator (Fur) protein and small RNA RyhB [14]. Fur is a dimeric protein that binds to the Fur box, a consensus sequence that is located near or within the promoter of the genes to be regulated. Under iron sufficient conditions, Fur makes a complex with Fe^{2+} that acts as a negative regulator of iron responsive genes by binding to the Fur box. In contrast, under conditions of iron deprivation Fe^{2+} is released from Fur. Fur then dissociates from the Fur box, resulting in the up-regulation of the expression of genes involved in iron uptake [15]. Fur homologues in other microorganisms such as cyanobacterium *Synechococcus*, *Salmonella enterica*, and *Pseudomonas aeruginosa* have been identified [16,17]. Fur homologues have also been reported in Gram-positive bacteria such as *Bacillus subtilis* and *Staphylococcus aureus* [18]. Diphtheria toxin repressor protein (DtxR) is another regulatory protein that is found in Gram-positive bacteria

such as *Corynebacterium diphtheria*. Despite the similarities between physiological roles of Fur and DtxR, no significant sequence homology between the two proteins has been observed [19].

RyhB is a small regulatory RNA that is under the control of Fur. Under iron deprivation where Fur dissociates from the Fur box, the expression of *ryhB* is up-regulated. RyhB down-regulates the expression of iron-containing proteins such as succinate dehydrogenase and superoxide dismutase, and channels the available iron toward biosynthesis of more essential iron-containing proteins [20,21]. Furthermore, RyhB promotes siderophore production and is important in pathogenicity of uropathogenic *E. coli* [20].

Iron homeostasis is also crucial in mammalian cells since excessive iron can cause variety of disorders such as neurodegenerative diseases and bacterial infections. It has been shown that mutation in genes involved in iron homeostasis in humans can cause hereditary hemochromatosis (HH), an iron overload disease that in some cases can lead to liver dysfunction [22]. Iron-binding proteins such as transferrin have been shown to play a critical role in iron homeostasis in the mammalian host [12].

1.2.3 Mammalian iron binding proteins

Iron is bound to proteins such as transferrin and lactoferrin in serum. Furthermore, iron is bound to proteins such as ferritin, hemoglobin and cytochromes inside the cell [23]. The majority of iron in mammalian cells is stored in hemoglobin and ferritin. In serum, iron is bound to transferrin, which is a glycoprotein and has two iron-binding sites and binds Fe^{3+} with high affinity ($K_d = 10^{-20}$ M). Mammalian cells internalize transferrin through specific receptors and iron is released from transferrin inside the cell [23,24].

Lactoferrin is also a glycoprotein and belongs to the transferrin protein family. Lactoferrin is found in mucosal fluids such as tears and saliva and it is abundant in milk [25,26]. Lactoferrin is known to have antibacterial activity due to its ability to sequester iron from pathogenic bacteria [25,27]. The dissociation constant of lactoferrin is similar to that of transferrin ($K_d = 10^{-22}$ M) [25,27,28]. Internalization of lactoferrin also occurs through a receptor-mediated process [26]. The majority of iron inside mammalian cells can be found in hemoglobin [23,29]. Hemoglobin is involved in oxygen transport in red blood cells; heme is the iron containing part of this protein that can be targeted by bacteria as an iron source [24]. Ferritin is another iron storage protein. Mammalian ferritin is composed of 24 subunits and it can store up to 4,500 iron atoms [30].

1.2.3.1 Bacterial iron acquisition from mammalian sources

To circumvent the low bioavailability of ferric iron in mammalian host, pathogenic microorganisms have developed various strategies to acquire Fe^{3+} from iron-binding proteins for their survival and growth [31]. In the mammalian host, bacteria can scavenge iron from iron-binding proteins such as transferrin, lactoferrin, hemoglobin and ferritin. Some bacteria such as *Haemophilus influenzae* and *Neisseria meningitidis* have specific outer membrane receptors by which they are able to directly acquire iron from transferrin, lactoferrin and heme [24,31,32]. Some bacteria also have hemoglobin binding-proteins such as HgBA in *Actinobacillus* [33].

Hemophore mediated iron-uptake is another mechanism of iron acquisition in some Gram-negative bacteria such as *Pseudomonas aeruginosa*, *Pseudomonas fluorescens*, *Yersinia pestis* and *Yersinia enterocolitica*. Hemophores secreted by these species either bind to free heme or scavenge heme from hemoglobin and transfer it to the cell through specific receptors [34]. Gram-positive pathogens such as *Bacillus anthracis* are also able to produce and secrete hemophores. Little is known about bacterial iron acquisition from ferritin. A recent study on *Bacillus cereus*

has shown that a surface protein, IIsA, recognizes and binds to ferritin and promotes iron release [32].

1.2.4 Siderophores

Siderophores are low-molecular-weight molecules that have very high affinity for iron. Siderophores are produced by many different microorganisms including bacteria and fungi. Siderophore production has also been observed in plants and mammals [35,36].

1.2.4.1 Bacterial siderophores

Siderophores can be found in both Gram-negative and Gram-positive bacteria. Most siderophores are composed of a peptide scaffold to which various iron-chelating moieties are covalently attached. Depending on the chemical structure of iron-binding groups, siderophores can be divided into the following major classes: catecholates and phenolates, hydroxamates, carboxylates and mixed types (Fig. 1) [13,37-39].

Catecholate-type siderophores have very high affinity for ferric iron. Enterobactin, bacillibactin, salmochelin and pyoverdine are examples of catecholate siderophores. Enterobactin is synthesized by enteric bacteria such as *E. coli* and *Salmonella* [31]. Since the enterobactin biosynthesis pathway is the main focus of this thesis, enterobactin structure and function will be discussed in more detail in section 1.2.6.

Bacillibactin is the most common catecholate siderophore that is synthesized by Gram-positive bacteria such as *B. subtilis*, *B. cereus*, *B. anthracis* [40]. A secondary siderophore, petrobactin, is also synthesized by *B. anthracis*. Salmochelin is the glycosylated version of enterobactin, which is synthesized by *Salmonella enterica* and uropathogenic *E. coli*. Glycosylation of the enterobactin makes it more hydrophilic that is useful for evading the host defense mechanisms [41,42].

Enterobactin glycosylation occurs through the *iroA* gene cluster that can be found in some pathogenic bacteria such as uropathogenic *E. coli* [42].

Pyoverdine is the catecholate siderophore of fluorescent *Pseudomonas* species such as *Pseudomonas aeruginosa*. It is composed of a dihydroxyquinoline chromophore which is attached to a peptide chain. Pyochelin is another siderophore of *Pseudomonas* which is categorized under phenolate family and has a lower affinity for ferric iron [43,44].

Hydroxamate siderophores are another group of common bacterial siderophores that exist in both Gram-positive and Gram-negative bacteria [13]. Desferrioxamine B, also known as Desferal is a hydroxamate siderophore that is used for treatment of iron overload diseases [31].

Carboxylate, phenolate and mixed type siderophores can also be found in different bacterial species [13].

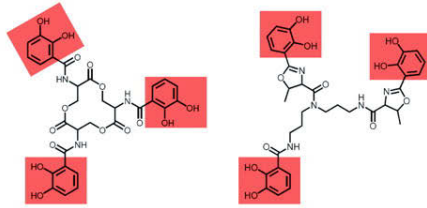
1.2.4.2 Fungal siderophores

Most fungal siderophores are hydroxamate type; however, some fungi produce carboxylate and catecholate type siderophores [45]. Similar to bacteria, fungi use siderophore-mediated iron uptake to survive and proliferate. *Aspergillus*, *Neurospora*, *Schizosaccharomyces*, *Rhodotorula* and *Ustilago* are species that are able to synthesize siderophores. There is no evident correlation between siderophore production and pathogenicity in fungi. It has been shown that non-pathogenic fungi such as *Schizosaccharomyces pombe* produce siderophores while pathogenic species (e.g., *Candida albicans*) do not. Both siderophore producing and non-producing fungal species are able to import xenosiderophores (i.e., siderophores generated by other bacteria or fungi) to survive and proliferate in low iron conditions [46].

1.2.4.3 Plant siderophores

Phytosiderophores such as avenic acid and deoxymugineic acid are produced by graminaceous plants (*e.g.* wheat, rice) and secreted into the rhizosphere to scavenge ferric iron. The Fe^{3+} -phytosiderophore complex is transported across the plasma membrane and ferric iron is then transferred to nicotianamine followed by a transfer to the phloem of the plants [35,36]. In addition to providing iron for plants under iron deprivation, it has been shown that phytosiderophores are useful for soil mineral weathering [47].

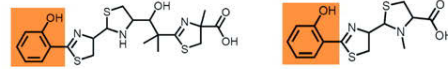
Catecholate Type



Enterobactin
(enteric bacteria,
Streptomyces spp.)

Vibriobactin
(*Vibrio cholerae*)

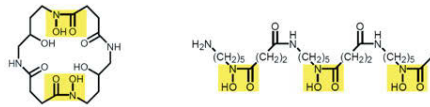
Phenolate Type



Yersiniabactin
(*Yersinia pestis*,
Yersinia enterocolitica)

Pyochelin
(*Pseudomonas aeruginosa*)

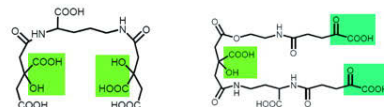
Hydroxamate Type



Alcaligin
(*Alcaligenes denitrificans*,
Bordetella pertussis,
Bordetella bronchiseptica)

Desferrioxamine B
(*Streptomyces pilosus*)

Carboxylate Type

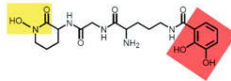


Staphyloferrin A
(*Staphylococcus* spp.)

Achromobactin
(*Erwinia chrysanthemi*)

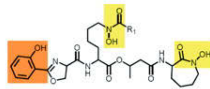
Mixed Types

Catecholate-Hydroxamate



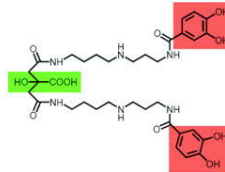
Heterobactin B
(*Rhodococcus erythropolis*)

Phenolate-Hydroxamate



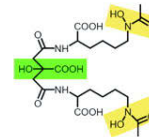
Mycobactin T
(*Mycobacterium tuberculosis*)

Citrate-Catecholate



Petrobactin
(*Bacillus anthracis*,
Bacillus cereus,
Marinobacter hydrocarbonoclasticus)

Citrate-Hydroxamate



Aerobactin
(*Enterobacter* spp.,
Escherichia coli,
Shigella flexneri)

Figure 1: Different types of bacterial siderophores. Iron-chelating moieties are highlighted in red: catecholate, orange: phenolate, yellow: hydroxamate and green: carboxylate/citrate.

This image is reused with permission from the American Society for Microbiology. Marcus Miethke, and Mohamed A. Marahiel *Microbiol. Mol. Biol. Rev.* 2007; 71: 413-451

Copyright © 2007, American Society for Microbiology

1.2.4.4 Mammalian siderophores and iron sequestration

Transferrin is recognized as the major iron transport protein in the extracellular environment of the mammalian cells [48,49]. In addition to transferrin, other iron-binding molecules have been identified in mammals. Given that at physiological pH and under aerobic conditions iron is insoluble, it is believed that a portion of iron is bound to endogenous mammalian siderophores [48,49]. Bao and colleagues have reported a novel catecholate iron-binding cofactor that binds to the ferric iron with high affinity [49]. In another study conducted by Devireddy and colleagues, the endogenous iron-chelating molecule was identified as 2,5-dihydroxybenzoic acid [49,50].

Another mechanism of iron sequestration in mammalian cells involves the protein siderocalin (Scn), also known as lipocalin 2 (Lpn 2) [49]. Siderocalin regulates iron homeostasis and iron transport in mammalian cells *via* binding to Fe³⁺-siderophore complexes such that the ferric siderophore complexes cannot be taken up by the producer bacteria [51,52]. Therefore siderocalin is considered a host defense mechanism against pathogenic bacteria [53]. Catecholate siderophores such as enterobactin are mainly recognized by siderocalins [52,53]. However, some bacteria synthesize and secrete siderophores that cannot be sequestered by siderocalin. Salmochelin is a glycosylated version of enterobactin that is synthesized by uropathogenic *E. coli* and *Salmonella* species. Glycosylation results in alterations to the bulkiness and hydrophobicity of the siderophore, allowing it to evade binding to siderocalin [52,54].

1.2.5 Applications of siderophores

Given their roles as metal chelators, siderophores are now being used in biotechnological processes. Two major applications involving siderophores are given below.

1.2.5.1 Siderophores and bioremediation

Siderophore-mediated bioremediation relies on the fact that some siderophores are able to form a complex with metals other than iron (*e.g.*, Al, Cu, Zn), although the binding affinity is typically lower than that found for iron-siderophore complexes [44]. Such metal-siderophore complexes are not imported into cells efficiently, however; sequestration of metals prevents them from diffusing to bacterial species present in the environment *via* the porin uptake system. Chelation of metals by siderophores is also beneficial for heavy metal detoxification of the environment [44,55].

1.2.5.2 Siderophores as Trojan horse antibiotics

The outer membrane in Gram-negative bacteria is considered a barrier for efficient entry of many antibiotics to bacterial cells. To circumvent this problem, thus addressing the emerging multi-drug resistance in bacteria, some antibiotics have been conjugated with siderophores so that they can enter the cell *via* siderophore transport system [56,57]. These types of antibiotics are known as Trojan horse antibiotics since they enter the cell through iron uptake pathway [58]. In one study, ciprofloxacin was conjugated to enterobactin and successfully transported to *E. coli* cells [56]. BAL30072 is an antibiotic in which a sulfactam is conjugated to dihydropyridone and it was shown to be active against 70% of carbapenem-resistant *Enterobacteriaceae* [57].

1.2.6 Siderophores of *E. coli*

E. coli species produce various types of siderophores. The two major siderophores of *E. coli* are aerobactin, a citrate-hydroxamate siderophore, and enterobactin which is a catecholate. Aerobactin has a lower affinity for iron compared to enterobactin and exists in extraintestinal pathogenic *E. coli* (ExPEC) such as Avian Pathogenic *E. coli* (APEC) or uropathogenic *E. coli*

(UPEC). Aerobactin is considered to be a virulence factor in APEC, UPEC and some other bacteria such as the human pathogen, *Klebsiella pneumoniae* [59-62].

1.2.6.1 Enterobactin: The catecholate siderophore of *E. coli*

Enterobactin (enterochelin) was first isolated from both *Salmonella typhimurium* and *E. coli* in 1970. Enterobactin is a catecholate siderophore that is synthesized and secreted in response to iron depletion by enteric bacteria [63,64]. The enterobactin structure is comprised of three 2,3-dihydroxybenzoate (DHB) molecules such that each group forms an amide bond with L-serine and three serine residues form a trilactone backbone [6,63]. Ferric iron is coordinated through three catecholate moieties that are linked to the triserine trilactone backbone (Fig. 2) [52,63]. Due to its chemical structure, enterobactin has the highest affinity for ferric iron of all known siderophores (K_D approximately 10^{-35} M at physiological pH) [6,42,65].

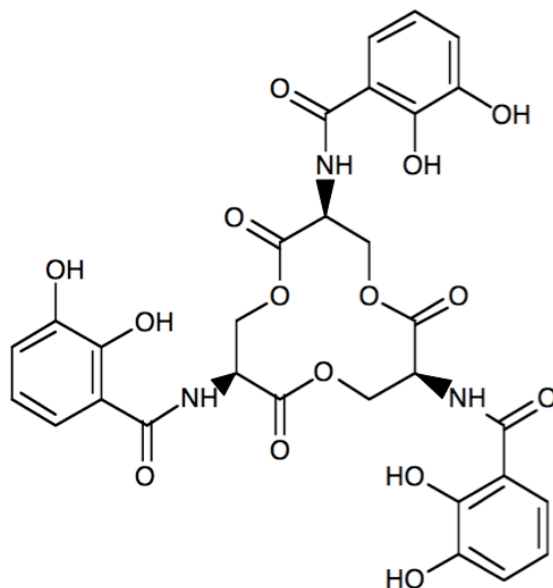


Figure 2: Schematic of enterobactin, the catecholate siderophore of *E. coli*.

1.2.6.2 Enterobactin: Biosynthesis

Enterobactin biosynthesis occurs in the *E. coli* cytoplasm and seven enzymes are involved in this process: EntC, EntB, EntA, EntE, EntF, EntD, and EntH. The enterobactin biosynthetic pathway is divided into two modules: the DHB module and the NRPS module (Fig. 3) [6,65]. In the DHB module, chorismate is converted into 2,3-dihydroxybenzoic acid (DHB) through the sequential action of three enzyme activities: EntC, EntB (N-terminal domain), and EntA. Chorismate is produced in the shikimate pathway and is a precursor for aromatic amino acid biosynthesis. Under iron deprivation and de-repression of Fur, chorismate is converted into isochorismate by isochorismate synthase, EntC. The second enzyme in the pathway is the N-terminal domain of EntB, isochorismatase (IC). EntB is a bifunctional enzyme that functions as an isochorismatase through its N-terminal domain (IC domain) and as an NRPS aryl carrier protein (ArCP) through its C-terminal domain (ArCP domain). Isochorismate is hydrolyzed into 2,3-dihydro-2,3-dihydroxybenzoate (diDHB) and pyruvate by the IC domain of EntB. EntA, also known as 2,3-dihydro-2,3-dihydroxybenzoate dehydrogenase, then converts diDHB to 2,3-dihydroxybenzoate (DHB) (Fig. 4) [6,65,66].

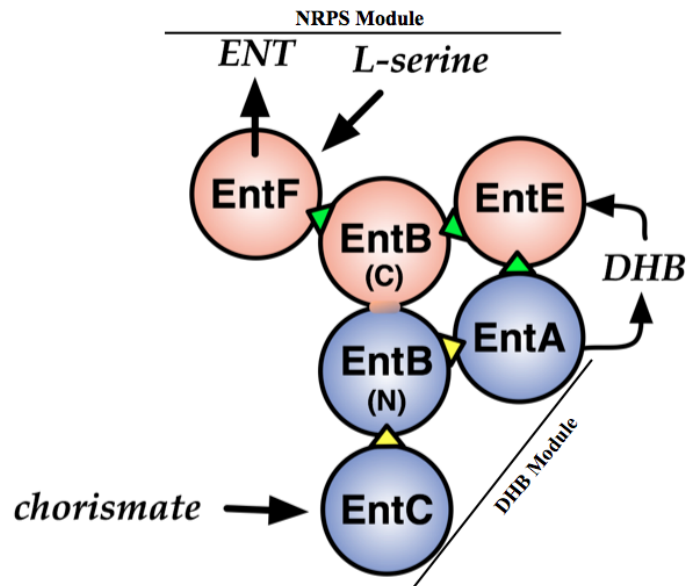


Figure 3: Enterobactin biosynthetic arms: DHB module and NRPS module. The DHB module is comprised of three enzymes, EntC, EntB (N-terminal domain) and EntA. In this part chorismate gets converted to DHB. NRPS module is composed of EntE, EntB (C-terminal domain) and EntF (EntD and EntH are not shown in this figure). In this module, enterobactin is synthesized from three molecules of DHB and three molecules of L-serine. (Green triangle represents known interactions while yellow triangle is indicative of hypothesized interactions).

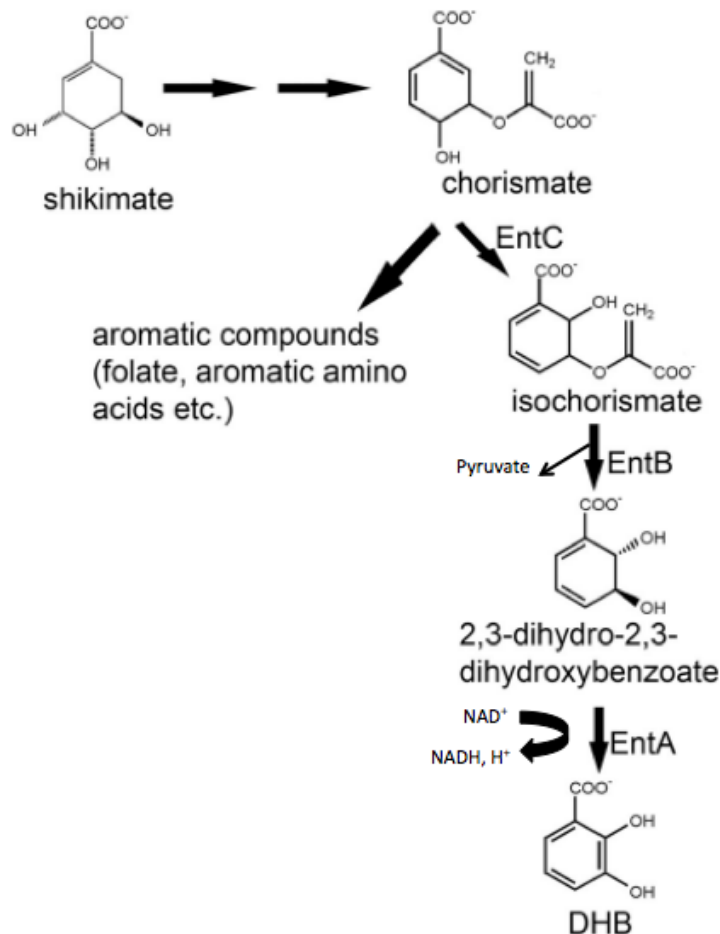


Figure 4: *E. coli* biosynthetic pathway, DHB module. Production of DHB from chorismate in the DHB module. EntC, IC domain of EntB and EntA are involved in this process. This image is adapted with permission from the American Society for Microbiology. Li Ma and Shelley M. Payne, *Journal of Bacteriology* 2012; 194: 6748-6757
Copyright © 2012, American Society for Microbiology

Following the production of DHB by EntA, three molecules of DHB condense with three molecules of L-serine to form enterobactin *via* the Non-Ribosomal Peptide Synthesis (NRPS) module [6]. NRPS is a ribosome-independent assembly line that is composed of large multidomain enzymes. Peptides synthesized through this process typically contain non-proteogenic amino acids, fatty acids and α -hydroxy acids [67,68]. The NRPS module in the enterobactin biosynthetic pathway is composed of EntD, EntE, the ArCP domain of EntB and

EntF. EntD is a phosphopantetheinyl transferase (PPTase) that catalyzes the phosphopantetheinylation of the ArCP domain of *apo-EntB* and the Thiolation domain (T) of *apo-EntF*, converting them to *holo-EntB* and *holo-EntF*. Phosphopantetheinylation activates EntB and EntF to work as aryl and acyl carriers, respectively [6,65,69,70]. EntE is a DHB-AMP ligase that activates DHB through adenylation. The DHB-AMP is then directly transferred to the phosphopantetheine group in the active site of *holo-EntB* to produce *acyl-holo-EntB* [9,69,71]. EntF, the last enzyme in the NRPS module, is composed of four domains: the adenylation domain (A), the condensation domain (C), the thiolation domain (T) that is also known as the peptidyl carrier protein domain (PCP), and the thioesterase domain (TE). The EntF A domain adenylates an L-serine molecule and transfers it to the phosphopantetheine group of the T domain. The DHB from the ArCP domain of *acyl-holo-EntB* then transfers to the C domain of *holo-EntF* and DHB-serine (DHBS) is produced through amide bond formation between the carboxyl group of DHB and the amino group of L-serine. DHBS is then transferred to the TE domain of EntF. A second round of DHBS synthesis occurs in the empty C domain and the TE domain catalyzes ester bond linkage between the two DHBS moieties. A third DHBS is synthesized in the empty C domain and ester bond formation yields a linear DHBS trimer, which is then cyclized and released from the TE domain (Fig. 5) [9,71-73].

EntH is a thioesterase that is under the control of Fur, and its gene is located downstream of *entA* in the *entCEBAH* operon. EntH removes misacylated molecules from the ArCP domain of EntB since accurate phosphopantetheinylation is critical for optimal production of enterobactin *in vivo* [74,75].

The protein-protein interactions between the NRPS module components are well characterized [6-9,76,77]. Our research group has identified an interaction between EntA, the last enzyme in the DHB module and EntE, the first enzyme in the NRPS module [65]. The present work mainly

focuses on the identification of protein-protein interactions between the enzymes in the DHB module; ternary complex formation between EntA-EntB-EntE and subunit orientation in EntA-EntE complex. A summary of the proteins involved in enterobactin biosynthesis is presented in Table1.

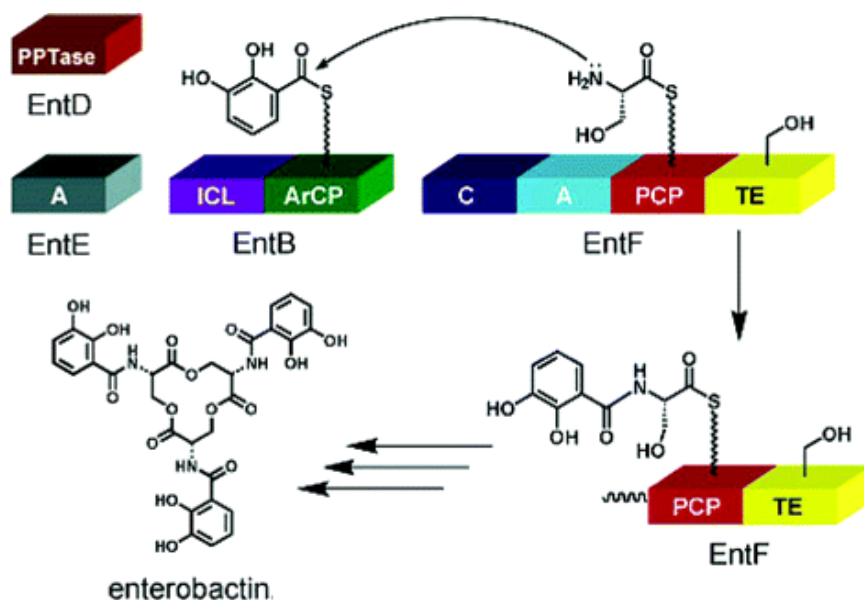


Figure 5: *E. coli* biosynthetic pathway, NRPS module. In this module enterobactin is synthesized from three molecules of DHB and three molecules of L-serine. EntD, EntE, ArCP domain of EntB and EntF are involved in this process.

This figure is adapted with permission from: Lai, J.R., Fischbach, M. A., Liu, D. R., Walsh, C.T., 2006, Localized Protein Interaction Surfaces on the EntB Carrier Protein Revealed by Combinatorial Mutagenesis and Selection, *J. Am. Chem. Soc.* 128 (34): 11002-11003.

Copyright © 2006, American Chemical Society

Table 1: Summary of the proteins involved in the enterobactin biosynthesis pathway

| Protein | Enterobactin biosynthetic module | Activity |
|---------|----------------------------------|---|
| EntC | DHB | Isochorismate synthase |
| EntB | DHB/NRPS | Isochorismatase /Aryl Carrier Protein |
| EntA | DHB | 2,3-dihydro-2,3-dihydroxybenzoate dehydrogenase |
| EntE | NRPS | AMP-ligase |
| EntF | NRPS | Peptidyl Carrier Protein |
| EntD | NRPS | phosphopantetheinyl transferase |
| EntH | NRPS | Thioesterase |

1.2.6.3 Enterobactin: Secretion

Following biosynthesis, enterobactin is secreted to the extracellular environment through an exporter or transport pump. Enterobactin cannot be transported across the *E. coli* inner membrane *via* passive diffusion due to its size (670 Da) and hydrophobic nature. It has been reported that EntS, a 43 KDa protein and a member of the major facilitator superfamily (MFS) of membrane proteins, is involved in the enterobactin efflux across the inner membrane [39]. EntS shows homology with proteins in the 12-TM helix MFS class of membrane proteins that employ the proton motive force to transport various small-molecule substrates such as antibiotics across the inner membrane [39,78]. It has also been shown that enterobactin transport across the outer membrane of *E. coli* is mediated by TolC [79]. TolC is an outer membrane protein that functions in conjunction with periplasmic proteins and about thirty different inner-membrane accessory proteins [80] to form a tri-partite channel spanning the entire *E. coli* cell envelope. Multiple inner

membrane proteins belonging to the resistance-nodulation-cell division (RND) family (AcrB, AcrD and MdtABC) have been shown to be involved in TolC-dependent enterobactin secretion [81]. The TolC system is known to have a role in exporting many different compounds, from harmful substances to intracellular metabolites. It has been reported that enterobactin accumulates in the periplasmic space of *E. coli tolC* strains that can lead to bacterial growth impairment [80]. However, another study showed that enterobactin secretion was reduced but not disrupted in *E. coli tolC* strains [81]. Enterobactin secretion is therefore thought to be a two-step process in which the EntS and TolC systems are involved [80,82,83].

Given our current understanding, our laboratory hypothesizes that the enterobactin biosynthetic machinery is anchored to the cytoplasmic membrane *via* an interaction between EntF, the final enzyme in the NRPS module, and EntS, the enterobactin inner membrane transporter (Fig. 6). Membrane fractionation studies have revealed that a small fraction of EntB, EntE and EntF proteins existed in membrane fractions in addition to the cytoplasmic fraction [84]. More recent studies have confirmed membrane association between pyoverdine biosynthetic enzymes in *Pseudomonas aeruginosa* [85] subcellular fractionation, pull-down assays and fluorescence microscopy were employed to study the membrane association of the pyoverdine biosynthetic NRPS module proteins to the membrane. The presence of such “siderosomes” in bacteria are thought to increase the efficiency of siderophore biosynthesis and secretion [85]. The membrane localization of enterobactin biosynthetic and secretion system has been of interest and briefly studied during the course of this work.

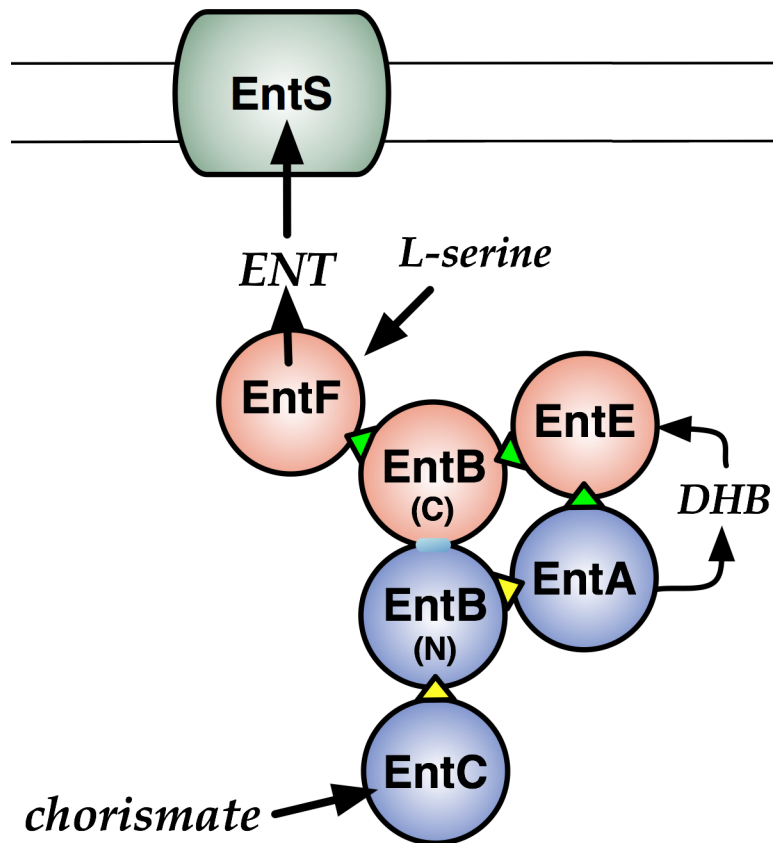


Figure 6: Enterobactin biosynthetic and inner membrane secretion machinery.

1.2.6.4 Enterobactin: Uptake

To initiate uptake, FepA, an outer membrane receptor, binds the iron-enterobactin complex from the extracellular environment *via* extracellular loops. The ferric siderophore is then transported through the barrel of FepA into the periplasm. This process is energized by a TonB-dependent mechanism. TonB, ExbB and ExbD are three inner membrane proteins. TonB spans the periplasmic space and is able to transduce the proton motive force to the outer membrane receptor to import the Fe³⁺-enterobactin across the outer membrane [86,87]. This is followed by

the transfer of the complex to the cytoplasm *via* FepBDGC, that is comprised of a periplasmic transport protein, two integral membrane subunits and a cytoplasmic ATP Binding Cassette (ABC) subunit [13].

1.2.6.5 Enterobactin: Hydrolysis and iron release

In the *E. coli* cytoplasm, iron is released from ferric enterobactin after import. Two classes of proteins known to be involved in iron release are ferric siderophore reductases and ferric enterobactin esterase (Fes). It has been shown that FhuF, a ferric siderophore reductase, could remove iron from the ferrioxamine B, a siderophore that has a lower affinity for ferric iron compared to enterobactin [88]. Ferric enterobactin esterase (Fes) is the enzyme involved in iron release from enterobactin. Fes hydrolyzes enterobactin to DHBS monomers, dimers or trimers followed by the release of iron into the *E. coli* cytoplasm. It has been shown that *E. coli* strains deficient in *fes* grow poorly under iron deprivation [89].

1.2.7 Specific aims

The enterobactin uptake pathway and protein-protein interactions between enzymes in the NRPS module of enterobactin biosynthesis have been well studied. However, the enterobactin secretion system and the protein-protein interactions between the enzymes involved in the DHB module of enterobactin biosynthesis have not yet been fully characterized. During the course of this work we aimed to study the enterobactin biosynthetic pathway, DHB module, in more detail. The overall goals of this thesis are outlined below:

- 1) Our research group has previously reported *in vitro* evidence of an interaction between EntA and EntE. The work presented in Chapter 2 is a follow-up study in which bacterial two-hybrid and docking simulations were used to identify the subunit orientation in EntA-EntE complex.

This knowledge is useful for future studies to identify the residues at the interaction interface of EntA-EntE complex and eventually these findings may lead to design of small-molecule inhibitors to disrupt EntA-EntE interaction and perturb siderophore mediated iron acquisition by *E. coli* in mammalian host.

2) As mentioned in section 1.2.2, iron homeostasis is crucial for bacteria as well as the mammalian host. In *E. coli*, iron homeostasis is mainly achieved by the action of a global regulator known as Fur. Chapter 3 of this thesis focuses on the design and generation of two sets of compatible vectors that are under the control of Fur. These vectors are useful for inducing gene expression and performing experiments under iron-deprivation and are good alternatives to conventional expression vectors (*e.g.* IPTG-inducible vectors). Here we used these vectors to demonstrate that epitope-tagged enterobactin biosynthetic enzymes could be expressed in an iron-controlled manner.

3) Chapter 4 is centered on the identification of novel protein-protein interactions in the DHB module. More specifically, an interaction between EntA and EntB was identified using the bacterial two-hybrid approach. Also, we hypothesized that EntA, EntB and EntE form a ternary complex and to further validate this hypothesis a docking simulation was performed.

4) The study of membrane localization of the enterobactin biosynthetic apparatus is a work in progress and is beyond the scope of this thesis. However, the experimental design and preliminary preparations will be briefly discussed in Chapters 5 and 6. The preliminary work to study the EntB-EntC complexation will also be discussed.

Chapter 2: Subunit Orientation in the *Escherichia coli* Enterobactin Biosynthetic EntA-EntE Complex Revealed by a Two-Hybrid Approach

2.1 Preface

The work presented in Chapter 2 has been published in the journal *Biochimie*:

Pakarian, P. & Pawelek, P.D. (2016) Subunit Orientation in the *Escherichia coli* Enterobactin Biosynthetic EntA-EntE Complex Revealed by a Two-Hybrid Approach. *Biochimie* 127, 1-9.

2.2 Abstract

The siderophore enterobactin is synthesized by the enzymes EntA-F and EntH in the *Escherichia coli* cytoplasm. We previously reported *in vitro* evidence of an interaction between tetrameric EntA and monomeric EntE. Here we used bacterial adenylate cyclase two-hybrid (BACTH) assays to demonstrate that the *E. coli* EntA-EntE interaction occurs intracellularly. Furthermore, to obtain information on subunit orientation in the EntA-EntE complex, we fused BACTH reporter fragments T18 and T25 to EntA and EntE in both N-terminal and C-terminal orientations. To validate functionality of our fusion proteins, we performed Chrome Azurol S (CAS) assays using *E. coli entE⁻* and *entA⁻* knockout strains transformed with our BACTH constructs. We found that transformants expressing N-terminal and C-terminal T18/T25 fusions to EntE exhibited CAS signals, indicating that these constructs could rescue the *entE⁻* phenotype. While expression of EntA with N-terminal T18/T25 fusions exhibited CAS signals, C-terminal fusions did not, presumably due to disruption of the EntA tetramer *in vivo*. Bacterial growth assays supported our CAS findings. Co-transformation of functional T18/T25 fusions into *cyd⁻ E. coli* BTH101 cells resulted in positive BACTH signals only when T18/T25 fragments were fused to

the N-termini of both EntA and EntE. Co-expression of N-terminally fused EntA with C-terminally fused EntE resulted in no detectable BACTH signal. Analysis of protein expression by Western blotting confirmed that the loss of BACTH signal was not due to impaired expression of fusion proteins. Based on our results, we propose that the N-termini of EntA and EntE are proximal in the intracellular complex, while the EntA N-terminus and EntE C-terminus are distal. A protein-protein docking simulation using SwarmDock was in agreement with our experimental observations.

2.3 Introduction

The Gram-negative bacterium *Escherichia coli* employs siderophore-mediated iron acquisition as a dominant means of importing extracellular iron under conditions of iron starvation [13]. The two major siderophores of *E. coli* are the hydroxamate siderophore aerobactin and the catecholate siderophore enterobactin [63,90]. Enterobactin consists of three dihydroxybenzoate groups linked by a triserine lactone core. It is synthesized in the *E. coli* cytoplasm and then secreted in the *apo* form to chelate extracellular Fe^{3+} . Uptake of ferric enterobactin is then mediated by a TonB-dependent uptake system [91]. Biosynthesis of enterobactin occurs in a pathway containing two major functional arms: (1) synthesis of 2,3-dihydroxybenzoic acid (DHB) from chorismate as catalyzed by the sequentially-related enzymes EntC, EntB (N-terminal isochorismatase domain), and EntA; (2) condensation of three molecules of DHB with three molecules of L-serine *via* a non-ribosomal peptide synthesis (NRPS) 'assembly line' comprised of the enzymes EntE, EntB (C-terminal aryl carrier protein domain), EntD, and EntF [92]. The thioesterase EntH has been shown to play a proofreading role in enterobactin biosynthesis [74]. Expression of the genes encoding the enterobactin biosynthetic enzymes (*entA-F, H*) is up-regulated during conditions of low intracellular iron, due to de-repression by the Ferric Uptake Regulator (Fur) protein.

Obligate protein-protein interactions in the NRPS arm have been known for many years [6,8,9,71,93]. In addition, we have previously reported *in vitro* evidence of an interaction between EntA, the terminal enzyme in the DHB synthetic arm of the pathway, and EntE, the initial enzyme in the NRPS arm of the pathway [65]. The existence of an EntA-EntE interaction, in addition to those within the NRPS module, is consistent with recent reports of membrane-associated "siderosomes" in *Pseudomonas aeruginosa* that are involved in pyoverdine and pyochelin biosynthesis [85,94]. We found that the EntA-EntE interaction stimulated EntE activity approximately 4-fold, presumably by inducing conformational alterations at the EntE active site. Furthermore, biophysical approaches revealed that the affinity of the EntA-EntE interaction increased when EntA was in the tetrameric form relative to the dimeric form [65]. Here we demonstrate intracellular EntA-EntE complex formation in *E. coli* using a bacterial adenylate cyclase two-hybrid (BACTH) approach. BACTH constructs were functionally validated by Chrome Azurol S (CAS) assays and growth studies. Our BACTH assays revealed relative orientations of EntA and EntE subunits within the intracellular complex. Automated docking simulations supported our BACTH observations.

2.4 Materials and Methods

2.4.1 Reagents

All chemicals were purchased from Bioshop Canada, Inc. (Burlington, Ontario) unless noted otherwise.

2.4.2 Preparation of BACTH constructs

Genes encoding *E. coli* EntA and EntE were PCR-amplified from pCA24N-*entA* and pCA24N-*entE* vectors, respectively, obtained from the ASKA collection [95]. PCR primers (Table 1) were designed such that *KpnI* and *EcoRI* sites were incorporated flanking the open reading frames. Amplification was performed using Phusion High-Fidelity DNA polymerase (New England Biolabs) according to the manufacturer's standard protocol. For recombinant BACTH fusion protein expression, PCR-amplified *entA* and *entE* genes were subcloned in-frame between *KpnI* and *EcoRI* sites of pUT18C and pKT25 (Euromedex) such that fragments of the catalytic domain of *B. pertussis* adenylate cyclase (T18 and T25) were fused N-terminally to EntA and EntE with vector-encoded polypeptide linker sequences N-HCRSTLEDPRVP-C (T18) and N-AAGSTLEDPRVP-C (T25) between EntA/EntE and T18/T25 fragments. For C-terminal T18/T25 fusions, PCR-amplified *entA* and *entE* genes were similarly subcloned into pUT18 and pKNT25 (Euromedex). Although the BACTH vectors with N-terminal T18/T25 fusions encoded 12-residue linkers, the linker between the *EcoRI* site and the DNA encoding C-terminal T18 and T25 fusions in the pUT18 and pKNT25 vectors had a length of only nine nucleotides encoding three residues. For subcloning our genes into these vectors, we used primers encoding an additional 9-residue HA tag linker (N-YPYDVPDYA-C) (Table 1). PCR products encoding EntA/EntE-HA fusions were subcloned between *KpnI* and *EcoRI* sites of pUT18 and pKNT25 vectors such that T18 and T25 fragments were fused C-terminally to EntA/EntE-HA upon induction of protein expression. All constructs were verified by DNA sequencing (Genome Quebec Innovation Centre, McGill University).

Table 1: PCR primer sequences used for preparing BACTH constructs

| Vector | Gene | Primer Sequence (5'-3') |
|------------------|-------------|--|
| pUT18C, pKT25 | <i>entA</i> | F: TAGGGGTACCTATGGATTTCAGCGGTAAAAATGTCTGGG |
| | | R: CTACGGAATTCTTATGCCCCAGCGTTGAGCC |
| | <i>entE</i> | F: TAGGGGTACCTATGAGCATTCCATTCACCCGCTGGC |
| | | R: CTACGGAATTCTCAGGCTGATGCGCGTGACG |
| pUT18, pKNT25 | <i>entA</i> | F: TAGGGGTACCTGATTTCAGCGGTAAAAATGTCTG |
| | | R: CTACGGAATTCGACGCATAATCCGGCACATCATACGGATATGCC CCCAGCGTTGAG |
| | <i>entE</i> | F: TAGGGGTACCTAGCATTCCATTCACCCGCTG |
| | | R: CTACGGAATTCGACGCATAATCCGGCACATCATACGGATAGGCT GATGCGCGTGAC |

F = forward, R = reverse. Underlined sequences indicate *KpnI* (forward) and *EcoRI* (reverse) restriction sites. Double underline indicates HA tag.

2.4.3 Modification of *entA*⁻ and *entE*⁻ knockout strains

BACTH constructs containing *entA* or *entE* genes were individually transformed into respective *entA*⁻ or *entE*⁻ single knockout strains to determine if the plasmid-borne *entA/entE* gene products fused to T25 or T18 could rescue the knockout phenotypes. We used modified *E. coli* BW25113 (*F*⁻, $\Delta(\textit{araD-araB})567$, $\Delta(\textit{lacZ4787}>::\textit{rrnB-3})$, λ ⁻, *rph-1*, $\Delta(\textit{rhaD-rhaB})568$, *hsdR514*) [96] strains obtained from the KEIO collection [97] that had *entA* or *entE* genes disrupted by insertion of a kanamycin resistance cassette. Since the T25-encoding BACTH constructs contained a kanamycin resistance gene (*kanR*) as a selective marker, we removed the chromosomally-inserted

kanR genes from the KEIO strains by using the Wanner Lambda Red Gene disruption kit (The Coli Genetic Stock Center (Yale CGSC)) [96]. Briefly, pCP20 plasmid was used for temperature-sensitive removal of *kanR* genes flanked by FRT (FLP Recognition Target) sequences. Competent knockout strains were transformed with pCP20 and were incubated overnight at 30 °C on LB plates containing 100 µg ml⁻¹ ampicillin. Colony picks were streaked on LB plates (no antibiotic) and incubated at 43 °C overnight. The loss of chromosomal *kanR* antibiotic resistance gene and pCP20 plasmid was verified by re-streaking colonies onto LB agar containing 50 µg ml⁻¹ kanamycin and 100 µg ml⁻¹ ampicillin, respectively.

2.4.4 CAS assays and growth studies

Competent modified knockout background strains (*kanR⁻ entA⁻* or *kanR⁻ entE⁻*) were transformed with respective BACTH constructs. Strains transformed with pKT25 or pKNT25 constructs were plated on LB agar containing 50 µg ml⁻¹ kanamycin, whereas strains transformed with pUT18C or pUT18 constructs were selected on LB plates supplemented with 100 µg ml⁻¹ ampicillin. Strains transformed with pCA24N-derived constructs were plated on LB agar containing 34 µg ml⁻¹ chloramphenicol. Empty vectors were also transformed into *entA⁻* and *entE⁻* modified knockout background strains as controls. All plates were incubated overnight at 30 °C. Colonies from transformation plates were used to inoculate LB broth supplemented with 50 µg ml⁻¹ kanamycin or 100 µg ml⁻¹ ampicillin or 34 µg ml⁻¹ chloramphenicol as appropriate. The cultures were incubated with shaking at 30 °C. Overnight cultures were diluted 1:100 in LB broth supplemented with 50 µg ml⁻¹ kanamycin or 100 µg ml⁻¹ ampicillin or 34 µg ml⁻¹ chloramphenicol and grown at 30 °C until an OD₆₀₀ between 0.5 – 0.7 was observed. Cultures were then diluted 1:1,000 in M9 medium composed of 1X M9 salts [98] supplemented with 0.3% (w/v) casamino acids, 0.2% (w/v) D-glucose, 1 mM MgCl₂, 100 µM CaCl₂, 0.0002% (w/v)

thiamine HCl and 50 $\mu\text{g ml}^{-1}$ kanamycin or 100 $\mu\text{g ml}^{-1}$ ampicillin or 34 $\mu\text{g ml}^{-1}$ chloramphenicol. Cultures diluted in minimal medium were grown at 30 °C overnight. CAS-agar plates were prepared according to Payne *et al.* [38] and then spotted with 1 μL overnight cultures in M9 medium and incubated at 30 °C for 16 to 20 hours. The CAS signal was interpreted as the presence of an orange halo, indicative of enterobactin biosynthesis [99]. Each CAS assay was performed at least in triplicate to ensure reproducibility.

For bacterial growth studies, single colony picks of *E. coli* cells (wild-type and knockout strains +/- transformed plasmids) were used to inoculate cultures as described above. Cultures were grown at 30 °C until they reached an OD₆₀₀ of 1.00, and then centrifuged for 1 min at 21,000 x g and cell pellets were resuspended in 1X M9 medium with appropriate antibiotics (see above). All cell suspensions were adjusted to a final OD₆₀₀ of 1.00. Bacterial suspensions were then diluted 1:1,000 in 1X M9 medium plus 50 μM 2,2'-dipyridyl and incubated at 30 °C for 18 hours with shaking. After incubation, the OD₆₀₀ of all cultures were measured. Growth experiments were performed in triplicate for each transformant/strain investigated.

2.4.5 Bacterial adenylate cyclase two-hybrid (BACTH) assays

BACTH constructs that could rescue *entA*⁻ or *entE*⁻ knockout phenotypes were co-transformed into competent *E. coli* BTH101 cells (*F*⁻, *cya*⁻⁹⁹, *araD139*, *galE15*, *galK16*, *rpsL1* (*Str*^R), *hsdR2*, *mcrA1*, *mcrB1*) (Euromedex). Co-transformants were incubated on LB plates containing 100 $\mu\text{g ml}^{-1}$ ampicillin and 50 $\mu\text{g ml}^{-1}$ kanamycin at 30 °C for two days. Colony picks were used to inoculate 3 ml of LB medium containing 100 $\mu\text{g ml}^{-1}$ ampicillin, 50 $\mu\text{g ml}^{-1}$ kanamycin and 0.5 mM IPTG. Inoculated cultures were grown at 30 °C overnight [100]. β -galactosidase assays of overnight cultures were performed in triplicate as described by Miller [101] except that reactions were incubated at room temperature. For plate assays, 1 μl of each overnight culture was spotted

onto MacConkey agar base (Difco) plates containing 100 $\mu\text{g ml}^{-1}$ ampicillin, 50 $\mu\text{g ml}^{-1}$ kanamycin, 0.5 mM IPTG and 1% maltose. Spotted plates were incubated at 30 °C for 18-24 hours [100]. Plate assays were also performed at least in triplicate with reproducible results. BACTH signals (i.e., interaction of fusion gene products in co-transformants) were interpreted as the formation of red colonies on MacConkey agar plates [102], and by elevated Miller units (at least 5-fold) relative to appropriate controls in β -galactosidase assays.

2.4.6 Western blotting

BACTH expression constructs encoding EntA/EntE-T18/T25 fusions were transformed into competent *E. coli* BW25113. One colony of each transformant was used to inoculate 2 ml of LB broth containing 100 $\mu\text{g ml}^{-1}$ ampicillin or 50 $\mu\text{g ml}^{-1}$ kanamycin. Cultures were incubated at 30 °C overnight with agitation. Overnight cultures were diluted 1:100 in 5 ml LB broth containing 100 $\mu\text{g ml}^{-1}$ ampicillin or 50 $\mu\text{g ml}^{-1}$ kanamycin and were incubated at 30° C with shaking until an OD₆₀₀ between 0.5-0.7 was reached. IPTG was then added to a final concentration of 0.5 mM, and induced cultures were grown at 30 °C for an additional 16 h. Cells (100 mg wet weight) from overnight cultures were pelleted by centrifugation at 3,000 x g at 4° C for 30 minutes and then resuspended in lysis buffer (50mM Tris pH8, 1% n-octyl-B-D-thioglucopyranoside, 3 $\mu\text{g/ml}$ DNase, 3 $\mu\text{g/ml}$ RNaseI, 30 $\mu\text{g/ml}$ lysozyme, 1mM DTT, 1X Proteinase Inhibitor Cocktail) and incubated on a nutating mixer for 30 minutes at room temperature. Aliquots of total cell lysates were separated on 8% SDS-polyacrylamide gels. Lysates from untransformed *E. coli* BW25113 cells were used as negative controls. Following gel electrophoresis, separated proteins were transferred onto a PVDF membrane using a Mini-Trans Blot Electrophoretic Transfer Cell (Bio-Rad Laboratories). The membrane was blocked using 5% skim milk powder in PBST (137 mM NaCl, 2.7 mM KCl, 10 mM Na₂HPO₄, 1.8 mM

KH₂PO₄, 0.2% Tween 20) for 1h at room temperature. Blocked membranes were incubated with one of the following primary antibodies for 1h at room temperature: (i) mouse monoclonal anti-Cya A (3D1) antibody (1:10,000 dilution, Santa Cruz Biotechnology) that recognizes the T18 fragment, (ii) goat polyclonal anti-Cya A (bN-13) (1:1,000 dilution, Santa Cruz Biotechnology) that recognizes the T25 fragment, or (iii) mouse monoclonal anti-HA antibody (1:5,000, Thermo Fisher Scientific) that recognizes the HA tag linker incorporated into our C-terminally tagged BACTH constructs. Goat anti-mouse conjugated with horseradish peroxidase (HRP) (1:15,000 - 1:10,000 dilution, Santa Cruz Biotechnology) and donkey anti-goat conjugated with HRP (1:5,000 dilution, Santa Cruz Biotechnology) were used as secondary antibodies. HRP activity was visualized using a SuperSignal™ West Pico Chemiluminescent Substrate (Thermo Fisher Scientific).

2.4.7 Automated Docking

Atomic coordinates of EntE monomer and EntA tetramer X-ray crystallographic structures were submitted to the SwarmDock server [103] for a blind docking experiment. The submitted EntE ligand consisted of residues 2-536 from the structure of the tethered EntB-EntE chimera (PDB code: 3RG2) reported previously [77]. The submitted receptor was the EntA tetramer (PDB code: 2FWM, biological assembly (chains A-D)) [104]. All SwarmDock parameters were left as default (number of normal modes: 5, docking type: full blind).

2.5 Results and Discussion

Our laboratory previously demonstrated that *E. coli* EntA and EntE form a complex *in vitro* [65]. Furthermore, we found that this interaction has a higher affinity when EntA is in the tetrameric state. Here we employed the bacterial adenylate cyclase two-hybrid (BACTH) system to study the intracellular interaction between EntA and EntE, and to gain further insights into the role of

EntA oligomerization in EntA-EntE complex assembly. BACTH has previously been used to identify intracellular interactions between the thioesterase EntH and the ArCP domain of EntB [74]. In this study, we employed BACTH to investigate an interaction between enterobactin biosynthetic enzymes at the functional hinge between DHB biosynthesis and downstream NRPS processes. We prepared combinatorial BACTH constructs that encoded EntA and EntE with N- and C-terminal fusions to fragments (T18 and T25) of the catalytic domain of *B. pertussis* adenylate cyclase [102].

2.5.1 Validation of BACTH constructs using CAS assays and growth studies

Prior to using our T18/T25 fusion constructs in BACTH assays, we performed validation experiments to investigate whether constructs encoding our T18/T25-EntA/EntE fusion proteins were functional in respective *entA*⁻ or *entE*⁻ backgrounds. Given that addition of polypeptide tags may potentially alter protein activity [105], we wanted to ensure that intracellular enzymatic functions of BACTH fusion proteins were not impaired by the N- or C-terminal addition of adenylate cyclase fragments T18 and T25. BACTH constructs were transformed into competent *E. coli entA*⁻ or *entE*⁻ knockout cells, and CAS agar assays were performed to determine if transformants produced orange halos indicative of enterobactin biosynthesis [99]. The presence of halos indicated that the T18/T25-fusion protein could rescue the knockout phenotype, thus confirming retention of Ent protein functionality. Fig. 1A shows CAS assay outcomes of the untransformed *E. coli* control strains: wild-type BW25113 (Fig. 1A: wt), BW25113 *entA*⁻ (Fig. 1A: *entA*⁻), and BW25113 *entE*⁻ (Fig. 1A: *entE*⁻). As expected, wild-type BW25113 cells produced an orange halo indicative of enterobactin biosynthesis, whereas the *entA*⁻ and *entE*⁻ knockout strains exhibited no halo due to impaired enterobactin production. Growth studies on untransformed strains indicated that wild-type BW25113 cells (Fig. 1A, bar graph 1) exhibited

the highest cell density in comparison to BW25113 *entA*⁻ and *entE*⁻ strains, which grew poorly in iron-deprived medium (Fig. 1A, bar graph 2 & 3). To ensure that observed CAS signals were independent of the nature of the polypeptide sequences fused to EntA or EntE, we performed control assays in which *E. coli* BW25113 cells were transformed with pCA24N-based expression constructs encoding EntA and EntE with N-terminal hexahistidine tags. We previously used these constructs to express and purify functional H6-EntA and H6-EntE [65]. Transformation of pCA24N-H6-*entA* into an *entA*⁻ background was found to successfully rescue the knockout phenotype resulting in a CAS halo (Fig. 1B, upper panel) and resulted in elevated growth relative to *entA*⁻ cells transformed with empty pCA24N vector (Fig. 1B, bar graph 1 & 2). Similar results were found for BW25113 cells transformed with pCA24N-H6-*entE* into an *entE*⁻ background (Fig. 1B, lower panel; Fig. 1B, bar graph 3 & 4).

We then assessed the functionality of our BACTH constructs. BW25113 *entA*⁻ cells transformed with pKT25-*entA* (Fig. 1C upper panel: T25-EntA) produced an orange halo, indicating that recombinant EntA with T25 fused to the N-terminus did not disrupt intracellular EntA function. However, cells transformed with pKNT25-*entA* (Fig. 1C upper panel: EntA-T25), which expressed recombinant EntA with T25 fused to the C-terminus, did not produce a halo. Consistent with our CAS assays, growth studies showed that only N-terminally tagged T25-EntA could complement the knockout phenotype, whereas C-terminally tagged EntA-T25 grew as poorly as the empty vector control (Fig. 1C, upper bar graph: 1-4). This demonstrates that EntA with C-terminally fused T25 fragment could not rescue the *entA*⁻ phenotype. Similar results were found for fusion of T18 to EntA, where fusion of T18 to the N-terminus of EntA rescued the knockout phenotype (Fig. 1C, lower panel: T18-EntA), but not fusion of T18 to the EntA C-terminus (Fig. 1C, lower panel: EntA-T18). Growth studies on transformants expressing T18-EntA and EntA-T18 also indicated that only T18-EntA could complement the *entA*⁻ knockout

phenotype, whereas transformants expressing EntA-T18 did not exhibit higher growth than the vector control (Fig. 1C, lower bar graph: 1-4). The functional assessment of *entE*-harboring BACTH constructs is shown in Figure 1D. Here, transformants expressing T25-fused EntE produced orange halos whether T25 was fused N- or C-terminally (Fig. 1D, upper panel: T25-EntE, EntE-T25). Transformants expressing T25-EntE or EntE-T25 exhibited higher growth in comparison with vector control transformants, indicating the ability of these fusion proteins to rescue the *entE*⁻ knockout phenotype (Fig. 1D, upper bar graph: 1-4). Fusion of the T18 fragment to EntE also resulted in functional constructs independent of the position of T18 relative to EntE (Fig. 1D, lower panel: T18-EntE, EntE-T18), although T18-EntE exhibited a more intense halo than EntE-T18. Growth studies demonstrated that transformants expressing either T18-EntE or EntE-T18 could rescue the *entE*⁻ knockout phenotype relative to vector controls (Fig. 1D, lower bar graph: 1-4). For both *entA*⁻ and *entE*⁻ knockout strains, no CAS halos were observed when cells were transformed with empty BACTH vectors (Figs. 1C and 1D, upper and lower panels: T25-vec, vec-T25, T18-vec, vec-T18). Since the *entA* and *entE* genes occur in an operon (*entCEBAH*) in the *E. coli* chromosome [74], possible loss of functionality in single-gene knockouts may be due to polar effects on downstream genes in the operon. However, Datsenko and Wanner (2000) [96] demonstrated that their single-gene disruptions in *E. coli* BW25113 had no polar effects on downstream gene expression. Consistent with this, we found that complementation of our *entE*⁻ knockout strain with *in trans* expression of T18- or T25-fused EntE resulted in positive CAS signals, demonstrating functionality of downstream *entB*, *entA*, and *entH* genes in the operon in an *entE*⁻ background.

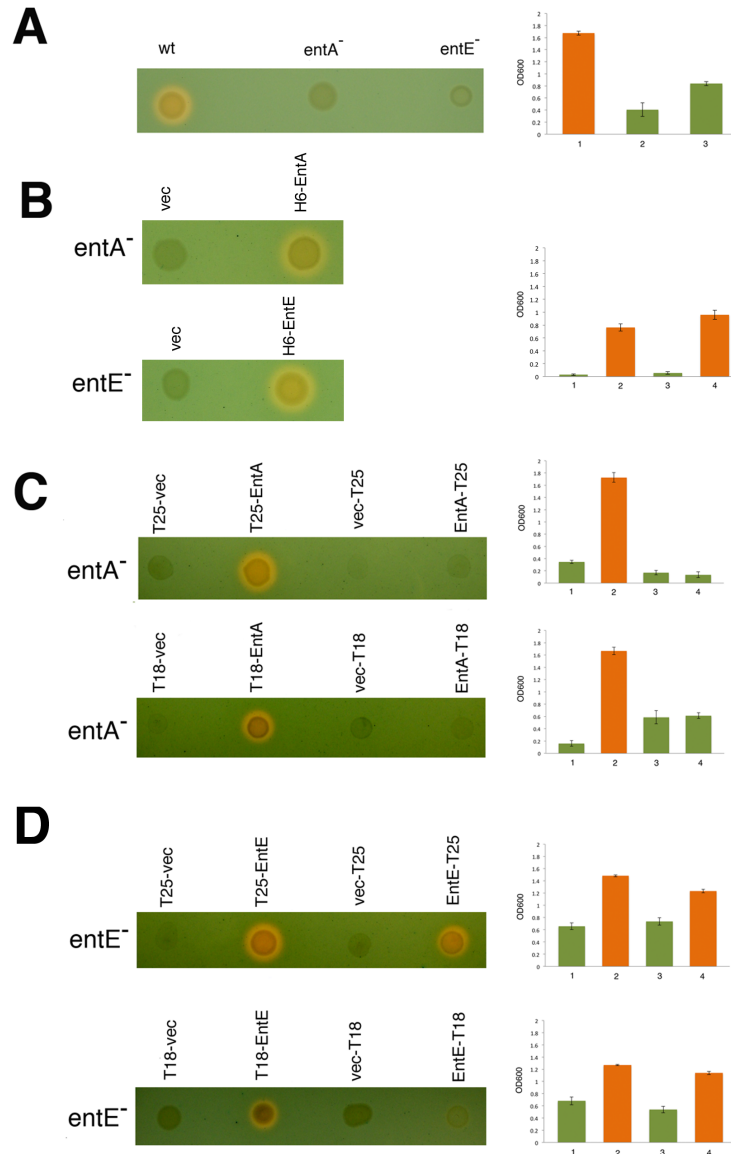


Figure 1: Intracellular functionality of BACTH constructs determined by CAS assays and growth studies. Images to the left are photographs of CAS agar plates spotted with various *E. coli* strains and transformants. Enterobactin secretion is indicated by orange halos. Graphs to the right show growth studies of corresponding strains and transformants. All growth studies were performed in iron-depleted minimal medium. Orange bars indicate strains/transformants that exhibited a positive CAS signal; error bars represent standard deviations from mean values (n=3). See Results & Discussion section 2.5.1 for details on all strains and transformants. (A) Untransformed *E. coli* strains. (B) *E. coli* knockout strains transformed with expression constructs harboring hexahistidine-tagged EntA (upper panel) and EntE (lower panel). (C) *E. coli entA⁻* cells transformed with BACTH constructs expressing EntA with N-terminal fusions (T25-EntA and T18-EntA) and C-terminal fusions (EntA-T25 and EntA-T18). (D) *E. coli entE⁻* cells transformed with BACTH constructs expressing EntE with N-terminal fusions (T25-EntE and T18-EntE) and C-terminal fusions (EntE-T25 and EntE-T18). For parts A, C and D, growth assays from left to right correspond to the order of strains/transformants shown in the corresponding CAS assays. For part B, growth assays 1 and 2 correspond to the CAS assays shown in the upper panel. Growth assays 3 and 4 correspond to the CAS assays shown in the lower panel.

Our CAS assay and growth study outcomes are summarized in Table 2. We found that T18-EntA and T25-EntA were able to complement the *entA*⁻ phenotype as seen in our CAS assays (Table 2, column 4, rows 1 and 3). However, EntA-T18 and EntA-T25 could not rescue the *entA*⁻ phenotype, suggesting a disruption of EntA intracellular function (Table 2, column 4, rows 2 and 4). The X-ray crystallographic structure of tetrameric EntA (PDB code: 2FWM) [104] revealed that the C-terminus of each monomeric subunit projects towards the interior of the tetramer, whereas the N-termini extend away from the protein (Fig. 2A). The introduction of T18 and T25 fusions to EntA C-termini may therefore prevent formation of EntA tetramers *in vivo*, thus negatively affecting enterobactin biosynthesis. In contrast, all EntE fusions examined (T18-EntE, T25-EntE, EntE-T18, EntE-T25) could rescue the *entE*⁻ phenotype, demonstrating that these fusions did not disrupt the intracellular function of EntE (Table 2, column 5, rows 1-4). Inspection of the published X-ray crystallographic structure of monomeric EntE (PDB code: 3RG2) [77], which was expressed as a tethered EntE-EntB fusion, indicates that the N- and C-termini both project away from the center of protein mass (Fig. 2B), consistent with our observation that both N-terminal and C-terminal EntE fusions were functionally active. These findings were useful in guiding us in the selection of BACTH constructs to use in our bacterial two-hybrid assays. Since pKT25-*entA* and pUT18C-*entA* could complement the *entA*⁻ phenotype, we proceeded with using them for BACTH since we were confident that the EntA portions of expressed N-terminal EntA fusions were functional. The pKNT25-*entA* and pUT18-*entA* constructs were rejected for BACTH due to their lack of functionality. We proceeded to use all *entE* BACTH constructs for our two-hybrid studies since they were all found to be functional *via* CAS assays and growth studies.

Table 2: BACTH Constructs: Summary of CAS assays and growth studies

| Vector | Reporter | Reporter | EntA | EntE |
|--------|----------|------------|------|------|
| | Fragment | Position | | |
| pUT18C | T18 | N-terminal | + | + |
| pUT18 | T18 | C-terminal | - | + |
| pKT25 | T25 | N-terminal | + | + |
| pKNT25 | T25 | C-terminal | - | + |

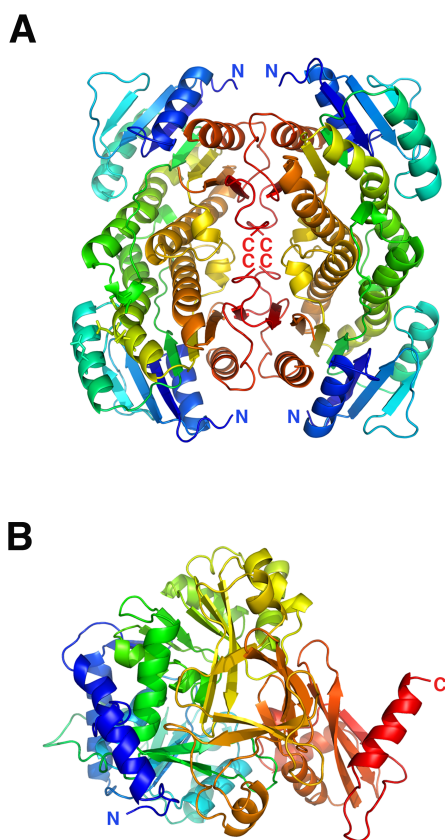


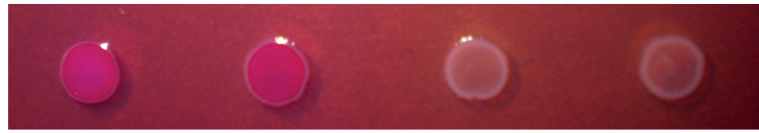
Figure 2: Three-dimensional X-ray crystallographic structures of EntA and EntE.

(A) Crystallographic structure of EntA tetramer (PDB code: 2FWM) [104]. (B) Crystallographic structure of EntE monomer taken from the crystallographic structure of the EntB-EntE chimeric protein (PDB code: 3RG2) [77]. Both proteins are shown as biological assemblies. Chains are colored from N-terminus (blue) to C-terminus (red). Positions of N- and C-termini are indicated.

2.5.2 Detection of the intracellular EntA-EntE interaction by BACTH

BACTH constructs were co-transformed into *E. coli* BTH101 cells. Colonies of co-transformants grown on LB-agar plates were picked and cultured overnight in LB medium. Aliquots (1 μ l) of overnight cultures were spotted onto MacConkey agar plates followed by incubation at 30 °C for 18-24 hours [100]. The co-transformant expressing T25-EntA and T18-EntE demonstrated a positive BACTH signal (Fig. 3A, column 1). Similar results were seen in the co-transformant expressing T18-EntA and T25-EntE (Fig. 3A, column 2). However, the co-transformant expressing T18-EntA and EntE-T25 did not result in a BACTH signal (Fig. 3A, column 3). This was also observed for the co-transformant expressing T25-EntA and EntE-T18 (Fig. 3A, column 4). Taken together, BACTH signals were only observed when T18/T25 fusions were located at the N-termini of both EntA and EntE. β -galactosidase assay results for the complete set of co-transformants that we investigated in this study are shown in Fig. 3B. Consistent with our MacConkey agar plate assays, EntA and EntE co-transformants containing N-terminal T18/T25 fusions produced the highest levels of β -galactosidase activity (363 ± 38 Miller units and 308 ± 14 Miller units, respectively), confirming that the EntA-EntE interaction was only observed with N-terminally fused EntA and EntE (Fig. 3B, columns 1 and 2). We observed a lack of BACTH signal for co-transformants in which N-terminal T18/T25-EntA fusions were co-expressed with C-terminal EntE-T25/T18 fusions (Fig. 3B, columns 3 and 4). The positive BACTH signals seen for N-terminally fused EntA and EntE co-transformants were significantly higher than all negative controls in which BTH101 cells were co-transformed with empty vectors (Fig. 4B, columns 5-11). An additional control was performed in which pKT25-*entA* was co-transformed with a BACTH construct expressing a protein unrelated to enterobactin biosynthesis (pUT18C-*mobA*). This co-transformant also resulted in β -galactosidase activity no higher than the vector

controls (Fig. 3B, column 12). The *E. coli* protein MobA is involved in molybdenum cofactor biosynthesis, and N-terminally fused MobA BACTH constructs have previously been shown to be active [106]. In contrast, a leucine zipper positive control (BTH101 cells co-transformed with pKT25-*zip* and pUT18C-*zip* provided in Euromedex kit) yielded $4,539 \pm 222$ Miller units under identical assay conditions (not shown). The lack of BACTH signal in the T25/T18-EntA and EntE-T25/T18 co-transformants (Fig. 3B, columns 3 and 4) indicates that the EntE C-terminus is distant from EntA N-termini in the EntA-EntE complex since the BACTH signal relies on proximity of T18 and T25 fragments for reconstitution of adenylate cyclase activity. Taken together, our BACTH results provide initial evidence of the relative orientations of EntA and EntE subunits in the EntA-EntE complex upon formation of the interaction interface.

A

| | | | | |
|---------|------|------|------|------|
| T25 (N) | EntA | EntE | | EntA |
| T18 (N) | EntE | EntA | EntA | |
| T25 (C) | | | EntE | |
| T18 (C) | | | | EntE |

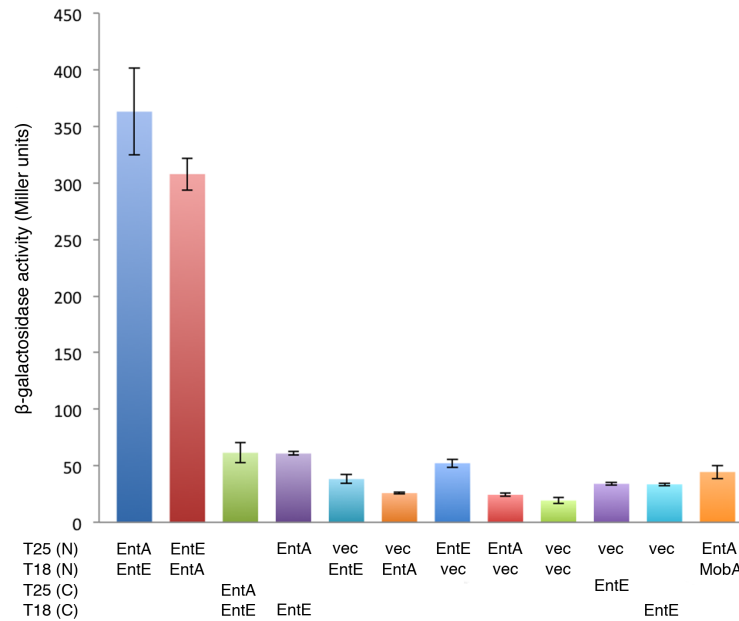
B

Figure 3: BACTH assays of the EntA-EntE interaction. BACTH constructs encoding EntA or EntE fused N- or C-terminally to T25 or T18 were co-transformed into *E. coli* BTH101 cells and assessed for two-hybrid signals. Plasmids used for BACTH constructs were: pKT25 (T25 (N)), pUT18C (T18 (N)), pKNT25 (T25 (C)), and pUT18 (T18 (C)). (A) *E. coli* BTH101 co-transformants spotted onto MacConkey agar. Red colonies are indicative of a positive two-hybrid signal. Left to right: BTH101 co-transformed with pKT25-*entA* and pUT18C-*entE*; BTH101 co-transformed with pUT18C-*entA* and pKT25-*entE*; BTH101 co-transformed with pUT18C-*entA* and pKNT25-*entE*; BTH101 co-transformed with pKT25-*entA* and pUT18-*entE*. (B) Bar graph showing β-galactosidase assays of BACTH co-transformants in (A), as well as relevant empty vector controls ('vec'). An additional control assay in which pKT25-*entA* was co-transformed with pUT18C-*mobA* is also shown. Error bars represent standard deviations from mean values (n=3).

2.5.3 Intracellular expression of BACTH fusion proteins

In order to confirm that the lack of two-hybrid signal observed for co-transformants expressing T18-EntA/EntE-T25 and T25-EntA/EntE-T18 was not due to impaired protein expression, all eight constructs were individually transformed into *E. coli* BW25113 for protein expression studies. BACTH vectors are under the control of the *lac* promoter and require cAMP for expression [107]. It is recommended that studies of fusion protein expression from these vectors should be performed in a *cyd*⁺ strain such as BW25113 [100,108]. We therefore examined BACTH fusion protein expression in *E. coli* BW25113 whole-cell lysates following transformation of individual BACTH constructs and IPTG induction. For Western analysis of whole-cell lysates, membranes were probed with appropriate anti-T18 (3D1), anti-T25 (bN-13), and anti-HA antibodies (Fig. 4). All transformants were found to express T25/T18 fusion proteins. Furthermore, C-terminal fusion proteins containing HA tags were detected by anti-HA antibody. These results confirmed that the lack of two-hybrid signals for co-transformants containing N-terminally fused EntA and C-terminally fused EntE was not due to impaired intracellular protein expression from the BACTH constructs.













| Vector | Reporter Fragment | HA Tag | Primary Antibody | EntA | EntE |
|--------|-------------------|--------|------------------|---|---|
| pUT18C | N-terminal T18 | - | 3D1 |  |  |
| pUT18 | C-terminal T18 | ✓ | 3D1 |  |  |
| | | | HA |  |  |
| pKT25 | N-terminal T25 | - | bN-13 |  |  |
| pKNT25 | C-terminal T25 | ✓ | bN-13 |  |  |
| | | | HA |  |  |

Figure 4: Verification of protein expression from BACTH constructs by Western blotting. Western blot analysis of protein expression from entA and entE BACTH constructs. Whole-cell lysates from IPTG-induced *E. coli* BW25113 transformants (equivalent wet cell weights) were analyzed by Western blotting using antibodies against polypeptide fusions as follows: T18 fragments were detected using anti-T18 monoclonal antibody (3D1); T25 fragments were detected by an anti-T25 polyclonal antibody (bN-13); C-terminally tagged T18 and T25 constructs containing an HA tag as a linker were also detected using an anti-HA monoclonal antibody. HRP-conjugated secondary antibodies were detected by chemiluminescence imaging.

2.5.4 Computational prediction of the EntA-EntE complex

To gain further insights into the nature of EntA-EntE interaction revealed by our two-hybrid approach, we submitted X-ray crystallographic structures of EntA (PDB code: 2FWM) and EntE (PDB code: 3RG2) to the SwarmDock server [103], which was chosen for its ability to introduce flexibility in the automated docking operation as well as for its high-scoring performance in the CAPRI competition [109,110]. Full-blind docking of monomeric EntE to the EntA tetramer resulted in the highest-scoring and lowest-energy ensemble shown in Figure 5. The docked ensemble (top-ranked out of a total of 444 candidate ensembles returned by the server) was found to contain one EntE monomer interacting with one face of the EntA tetramer. Furthermore, the EntE C-terminal domain (residues 432-536), which has been proposed to undergo conformational

rearrangement as part of domain alternation mechanism [8], is facing away from the EntA-EntE interaction interface (Fig. 5A). A similar blind docking job was submitted to the ClusPro server [111], which also returned its highest-scoring ensemble with the same stoichiometry and orientation of EntE relative to the EntA tetramer (data not shown). We focus here on the SwarmDock ensemble since flexible docking algorithms are more robust in predicting atomic positions of unstructured regions such as protein termini [111]. Flexible modeling of termini positions is important in the context of BACTH in order to model exit points for T18 and T25 fusions. In the SwarmDock model, EntE residues at the interaction interface are entirely from the N-terminal portion of the protein (Fig. 5A). This orientation is consistent with the BACTH outcomes reported here in which the C-terminus of EntE is distant from EntA N-termini. In the model, the N-terminus of EntE exits the complex at a position such that when fused to T18 or T25, it could be proximal to T25 or T18 fused to the N-termini of EntA subunits C or D. A contact map generated from the predicted complex indicates that residues from all four subunits of the EntA tetramer occur at the interaction interface (Fig. 5B).

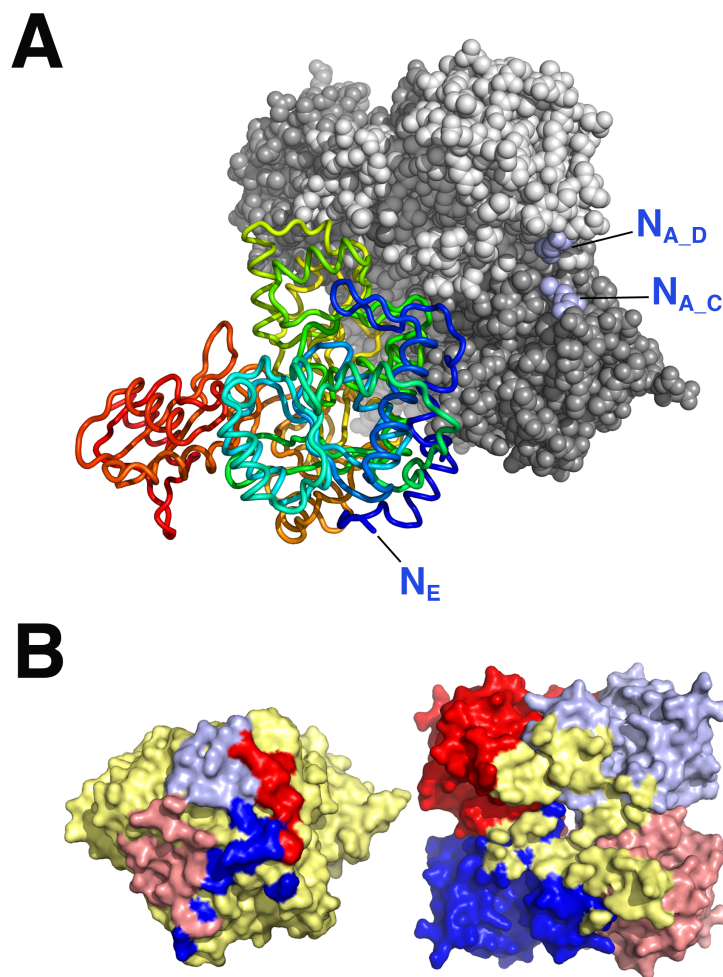


Figure 5: Automated docking of monomeric EntE to tetrameric EntA. (A) Highest-scoring SwarmDock model showing interaction of EntE monomer (coils, colored from N-terminus (blue) to C-terminus (red)) binding to EntA tetramer (spheres; chains A&D: light grey, chains C&B: dark grey; spheres corresponding to N-terminal atoms of chains C&D are shown as light blue spheres). N-termini of proteins are labeled as follows: NE: N-terminus of EntE; NA_C: N-terminus of EntA C chain; NA_D: N-terminus of EntA D chain. (B) EntE-EntA interaction interface. Proteins in the SwarmDock-predicted complex were computationally separated by rotating EntE (left: yellow surface) by 180° and then translating it in the x-axis relative to EntA tetramer (right: chain A: blue surface, chain B: red surface, chain C: pink surface, chain D: light blue surface). EntE residues within 4 Å of EntA are colored according to EntA subunit. EntA residues within 4 Å of EntE are colored yellow.

This is in agreement with our CAS results suggesting that the EntA tetramer is required for biological functionality, and is consistent with our previous report of EntE being unable to interact favorably with EntA in the dimeric or monomeric forms [65]. Although SwarmDock only modeled EntE interaction at one face of the EntA tetramer, EntA possesses two symmetric solvent-exposed surfaces. The overall stoichiometry of the intracellular complex consistent with the SwarmDock model would therefore be two EntE monomers binding per EntA tetramer. This agrees with the stoichiometry value (0.79 ± 0.19) that we previously determined by isothermal titration microcalorimetry [65].

In conclusion, the experimental outcomes reported here provide initial information on the overall subunit orientation of the EntA-EntE complex as it occurs in *E. coli* cells. A blind docking simulation supports our experimental data that elucidate the orientation of EntA and EntE in the complex as well as the biological importance of the quaternary structure of EntA. This knowledge will be useful in further exploring the EntA-EntE protein interaction interface at the functional hinge of the DHB biosynthetic and NRPS modules.

Chapter 3: A Novel Set of Vectors for Fur-controlled Protein Expression Under Iron Deprivation in *Escherichia coli*

3.1 Preface

The work presented in this chapter has been submitted to the journal *BMC Biotechnology*, and is currently under revision: Pakarian, P. & Pawelek, P.D., (2016) “A Novel Set of Vectors for Fur-controlled Protein Expression Under Iron Deprivation in *Escherichia coli*”

3.2 Abstract

Background: In the presence of sufficient iron, the *Escherichia coli* protein Fur (Ferric Uptake Regulator) represses genes controlled by the Fur box, a consensus sequence near or within promoters of target genes. De-repression of Fur-controlled genes occurs upon iron deprivation. In the *E. coli* chromosome, there is a bidirectional intercistronic promoter region with two non-overlapping Fur boxes. This region controls Fur-regulated expression of *entCEBAH* in the clockwise direction and *fepB* in the anticlockwise direction.

Results: We cloned the *E. coli* bidirectional *fepB/entC* promoter region into low-copy-number plasmid backbones (pACYC184 and pBR322) along with downstream sequences encoding epitope tags and a multiple cloning site (MCS) compatible with the bacterial adenylate cyclase two-hybrid (BACTH) system. The vector pFCF1 allows for iron-controlled expression of FLAG-tagged proteins, whereas the pFBH1 vector allows for iron-controlled expression of HA-tagged proteins. We showed that *E. coli* knockout strains transformed with pFCF1-*entA*, pFCF1-*entE* and pFBH1-*entB* express corresponding proteins with appropriate epitope tags when grown under iron restriction. Furthermore, transformants exhibited positive chrome azurol S (CAS) assay signals under iron deprivation, indicating that the transformants were functional for siderophore

biosynthesis. Western blotting and growth studies in rich and iron-depleted media demonstrated that protein expression from these plasmids was under iron control. Finally, we produced the vector pFCF2, a pFCF1 derivative in which a kanamycin resistance (*KanR*) gene was engineered in the direction opposite of the MCS. The *entA* ORF was then subcloned into the pFCF2 MCS. Bidirectional protein expression in an iron-deprived pFCF2-*entA* transformant was confirmed using antibiotic selection, CAS assays and growth studies.

Conclusions: The vectors pFCF1, pFCF2, and pFBH1 have been shown to use the *fepB/entC* promoter region to control bidirectional *in trans* expression of epitope-tagged proteins in iron-depleted transformants. In the presence of intracellular iron, protein expression from these constructs was abrogated due to Fur repression. The compatibility of the pFCF1 and pFBH1 backbones allows for iron-controlled expression of multiple epitope-tagged proteins from a single co-transformant.

3.3 Background

Bacterial iron acquisition is tightly controlled in order to ensure adequate iron uptake to support cellular survival and growth while preventing an over-accumulation of iron leading to oxidative damage [112]. To promote iron homeostasis, most genes involved in iron uptake mechanisms are only abundantly expressed under conditions of low intracellular iron, and are typically repressed when the cell is replete with iron. In *Escherichia coli*, one of the major regulators of iron homeostasis is the protein Fur (Ferric Uptake Regulator), a homodimeric protein with 17 kDa subunits [113-115]. Given its central role in regulating iron homeostasis and oxidative stress, Fur, along with the small RNA RyhB, are known virulence factors in a number of pathogenic bacterial species that require iron from host organisms [116]. Fur, in the iron-bound *holo* form, binds tightly to a recognition site known as the Fur box. Although there is variation in Fur box

sequences, they all share identity with a 19-bp consensus sequence 5'-(GATAATGAT(A/T)ATCATTATC)-3' [117,118]. In addition to its classical role as a repressor, *holo*-Fur has been reported to activate a number of gene targets [119,120]. A recent genome-wide study has also reported that Fur regulates 82 genes in *E. coli*, both by *apo*- and *holo*-Fur activation and *holo*-Fur repression [121]. In the classical *holo*-Fur repression mechanism, iron-bound Fur binds to a Fur box sequence that overlaps with, or is proximal to, promoters of iron-responsive genes, thus preventing their transcription [122]. When intracellular iron is depleted, Fe²⁺ is released from Fur, causing conformational changes in the protein resulting in dissociation from the Fur box [123]. This de-repression results in the up-regulation of Fur-controlled genes. Numerous genes are controlled by *holo*-Fur, including those that encode: (i) proteins involved in siderophore-mediated iron uptake [124], (ii) small RNAs such as *ryhB* that regulate bacterial iron uptake [21], (iii) some TCA cycle enzymes [125], (iv) superoxide dismutase [21,126], and (v) Fur itself [127].

Here we report a novel set of vectors that contain the *E. coli* *fepB-entC* promoter region that has two bidirectional Fur box sequences (Fig. 1A) identified from previous studies [128-130]. Fur box 1 (5'-AAAATGAGAAGCATTATT-3') and Fur box 2 (5'-ATAAATGATAATCATTAT-3') differ from the consensus sequence by five and three nucleotides, respectively (Fig. 1B). When incorporated into the vectors, this region controls plasmid-borne protein expression by Fur de-repression upon iron restriction. They can be used for iron-controlled expression of any subcloned ORF, even those not typically found under Fur control. We designed these vectors for expression of epitope-tagged proteins using an MCS compatible with the bacterial adenylate cyclase two-hybrid (BACTH) system, allowing for subcloning of ORFs of interest from a BACTH system to the Fur-controlled protein expression system reported here. Proteins expressed

from these vectors contain cleavable N-terminally fused epitope tags (FLAG or HA) that are useful for various immunochemical approaches.

3.4 Methods

3.4.1 Reagents, plasmids, software and primers

All reagents were purchased from Bioshop Canada, Inc. (Burlington, Ontario) unless otherwise indicated. Plasmids used in this study are summarized in Table 1. All plasmid maps were generated using SnapGene[®] Viewer (GSL Biotech; <http://www.snapgene.com>). All primer sequences used in this study are found in Table S1 (Supplementary material 3.8).

Table 1: Plasmids used in this study

| Plasmid name | Resistance | Source |
|--------------|-------------------------------------|-----------|
| pACYC184 | Cm ^R , Tet ^R | NEB |
| pBR322 | Amp ^R , Tet ^R | NEB |
| pUT18C | Amp ^R | Euromedex |
| pKT25 | Kan ^R | Euromedex |
| pFCF1 | Tet ^R | This work |
| pFBH1 | Amp ^R | This work |
| pFCF2 | Tet ^R , Kan ^R | This work |

NEB = New England Biolabs.

Amp^R: ampicillin resistance; Cm^R: chloramphenicol resistance.

Kan^R: kanamycin resistance; Tet^R: tetracycline resistance.

3.4.2 Production of pFCF1 and pFCF2

A 489-bp DNA fragment (gBlock1; Fig. S1, part 3.8) with flanking NcoI and EcoRI sites containing: (i) the *E. coli fepB/entC* bidirectional promoter region, (ii) the FLAG tag sequence, (iii) the TEV protease cleavage site sequence, and (iv) the multiple cloning site (MCS) from pUT18C (Euromedex) was synthesized as a gBlock[®] (Integrated DNA Technologies, San Diego,

California). This fragment was digested with NcoI and EcoRI (NEB) and cloned into pACYC184 linearized with the same restriction enzymes. The resulting vector was named pFCF1. In order to create pFCF1-*entA*, pFCF1-*entE*, and pFCF1-T25, *E. coli entA* and *entE* ORFs were PCR-amplified from pCA24N-based constructs as reported previously [131]. The *B. pertussis* T25 fragment was PCR-amplified from pKT25 (Euromedex). PCR products were subcloned into the KpnI and EcoRI sites of the pFCF1 MCS.

A 903-bp DNA fragment (gBlock2; Fig. S2, part 3.8) containing: (i) the HA tag sequence and (ii) the kanamycin resistance (*KanR*) gene from pKT25 (Euromedex) was synthesized as a gBlock[®] (Integrated DNA Technologies, San Diego California). The ends of this fragment contained ~40-nucleotide regions that overlapped with corresponding sequences upstream and downstream of NcoI and ScaI sites, respectively, in pFCF1. The synthesized fragment was inserted into pFCF1 digested with NcoI and ScaI using the Gibson Assembly Master Mix (New England Biolabs) according to manufacturer's protocol. The resulting vector was named pFCF2. The *E. coli entA* ORF was subcloned between KpnI and EcoRI sites of digested pFCF2 to generate pFCF2-*entA*. pFCF1 and pFCF2 constructs were verified by DNA sequencing (McGill University and Génome Québec Innovation Centre).

3.4.3 Production of pFBH1

A 522-bp DNA fragment (gBlock3; Fig. S3, part 3.8) containing: (i) the *E. coli fepB/entC* bidirectional promoter region, (ii) the HA tag sequence, (iii) the TEV protease cleavage site sequence, and (iv) the multiple cloning site (MCS) from pUT18C (Euromedex) was synthesized as a gBlock[®] (Integrated DNA Technologies, San Diego California). The ends of this fragment contained 25-nucleotide regions that overlapped with corresponding sequences upstream and downstream of EcoRI and Sall sites, respectively, in pBR322. The fragment was inserted into

pBR322 digested with EcoRI and Sall using the Gibson Assembly Master Mix (New England Biolabs) according to the manufacturer's protocol. The resulting vector was named pFBH1. The *E. coli entB* ORF was subcloned into the KpnI and EcoRI sites of the pFBH1 MCS. The pFBH1 construct was verified by DNA sequencing (McGill University and Génome Québec Innovation Centre).

3.4.4 CAS assays

All plasmid constructs and empty vector controls were transformed into respective *E. coli* BW25113 (F^- , $\Delta(\text{araD-araB})567$, $\Delta(\text{lacZ4787}(\text{:rrnB-3}))$, λ^- , *rph-1*, $\Delta(\text{rhaD-rhaB})568$, *hsdR514*) knockout strains [97] that have been modified to remove the kanamycin resistance gene as reported previously [131]. Strains transformed with, pFCF1, pFCF1-*entA*, and pFCF1-*entE* were plated onto LB agar containing 12.5 µg/ml tetracycline. Strains transformed with pFCF2, pFCF2-*entA* were plated onto LB agar containing 12.5 µg/ml tetracycline and 50 µg/ml kanamycin. Strains transformed with pFBH1 or pFBH1-*entB* were plated onto LB agar containing 100 µg/ml ampicillin. All plates were incubated overnight at 37 °C. Overnight cultures (LB broth with appropriate antibiotic) from colony picks were diluted 1:1000 in 1x modified M9 medium [131] and 12.5 µg/ml tetracycline with or without 50 µg/ml kanamycin or 100 µg/ml ampicillin. Minimal medium cultures were grown at 37 °C overnight. CAS-agar plates supplemented with appropriate antibiotics were prepared according to Payne *et al.* [38]. CAS plates were spotted with 1 µL overnight cultures and incubated at 37 °C for approximately 16 hours. Presences of orange halos were indicative of enterobactin biosynthesis [99]. Each CAS assay was performed in triplicate.

3.4.5 Growth studies

Single colony picks of transformants used for CAS assays were used to inoculate LB broth supplemented with appropriate antibiotics. Overnight cultures were diluted 1:100 in LB plus antibiotics and then grown at 30 °C until they reached an A_{600} of 1.00. Cultures were centrifuged for 1 min at 21,000 x g and cell pellets were resuspended in 1X modified M9 medium such that all cultures were diluted to an equivalent cell density ($A_{600} = 1.00$). Cultures for growth measurements were then prepared by 1:1,000 dilution into 1X modified M9 medium plus 50 μ M 2,2'-dipyridyl containing appropriate antibiotic. Diluted cultures were incubated at 30 °C for 16 hours with agitation. Cell densities were measured as A_{600} values. Growth experiments were performed in triplicate.

Additional growth studies of pFCF2-*entA* transformants were performed to demonstrate that the kanamycin resistance gene in this construct was under Fur control. Colony picks from the *E. coli* BW25113 *entA*⁻ strain transformed with pFCF2-*entA* were used to inoculate 3 ml of LB broth containing 12.5 μ g/ml tetracycline and 50 μ g/ml kanamycin. Overnight cultures incubated at 30 °C were diluted 1:100 in LB broth containing 12.5 μ g/ml tetracycline and 50 μ g/ml kanamycin and then grown at 30 °C until an A_{600} of 1.0 was reached. Cultures were centrifuged for 1 min at 21,000 x g and cell pellets were resuspended in 1X modified M9 medium such that all were diluted to an equivalent cell density ($A_{600} = 1.00$). Cultures for growth measurements were then prepared by 1:1,000 dilution into one of the following: (i) 1X modified M9 medium plus 50 μ M 2,2'-dipyridyl containing 12.5 μ g/ml tetracycline, (ii) 1X modified M9 medium plus 50 μ M 2,2'-dipyridyl containing 12.5 μ g/ml tetracycline and 50 μ g/ml kanamycin, (iii) LB broth containing 40 μ M FeSO₄, 12.5 μ g/ml tetracycline, 0.2% glucose, and (iv) LB broth containing 40 μ M FeSO₄, 12.5 μ g/ml tetracycline and 50 μ g/ml kanamycin, 0.2% glucose. Diluted cultures were incubated

at 30 °C for 16 hours with agitation. Cell densities were measured as A_{600} values. Growth experiments were performed in triplicate.

3.4.6 Western blotting

Expression constructs were transformed into competent *E. coli* BW25113 cells. Single colony picks of transformants were used to inoculate LB broth supplemented with appropriate antibiotics. Overnight cultures were diluted 1:100 in LB plus antibiotics and then grown at 30 °C until they reached an A_{600} of 1.0. Cultures were centrifuged for 1 min at 21,000 x g and cell pellets were resuspended in 1X modified M9 medium and then diluted to an equivalent cell density ($A_{600} = 1.00$). Cultures were prepared by 1:1000 dilution into iron-depleted medium (1X modified M9 medium plus 100 μ M 2,2'-dipyridyl and appropriate antibiotics) and/or iron-rich medium (LB broth containing 40 μ M FeSO_4 , 0.2% glucose and appropriate antibiotics), followed by incubation at 30 °C for 16 hours with agitation. Cells (100 mg wet weight) from overnight cultures were pelleted by centrifugation at 3,000 x g at 4° C for 30 minutes and then resuspended in Lysis Buffer (50 mM Tris (pH 8.0), 1% n-octyl-B-D-thioglucopyranoside, 3 μ g/ml DNase I, 3 μ g/ml RNase A, 30 μ g/ml lysozyme, 1 mM DTT, 1X Protease Inhibitor Cocktail). Whole-cell lysates were incubated on a nutating mixer for 30 minutes at room temperature and then centrifuged for 5 minutes at 21,000 x g. Supernatants were recovered for Western blots. Aliquots of cleared cell lysates were separated on 10% SDS-polyacrylamide gels. Following gel electrophoresis, separated proteins were transferred onto a PVDF membrane using a Mini-Trans Blot Electrophoretic Transfer Cell (Bio-Rad Laboratories). The membrane was blocked for 1h at room temperature using 5% skim milk powder in PBST (137 mM NaCl, 2.7 mM KCl, 10 mM Na_2HPO_4 , 1.8 mM KH_2PO_4 , 0.2% Tween 20). Blocked membranes were incubated with one of the following primary antibodies for 1h at room temperature or at 4 °C overnight: (i) mouse

monoclonal anti-FLAG antibody (1:1,000 dilution; Thermo Fisher Scientific), (ii) mouse monoclonal anti-HA antibody (1:1,000 dilution; Pierce), (iii) mouse monoclonal anti-GAPDH antibody (1:10,000; Thermo Fisher Scientific). Goat anti-mouse conjugated with horseradish peroxidase (HRP) (1: 10,000 - 1:20,000 dilution; Santa Cruz Biotechnology) was used as a secondary antibody. HRP activity was visualized using a SuperSignal™ West Pico Chemiluminescent Substrate (Thermo Fisher Scientific).

3.5 Results

3.5.1 Construction of pFCF1, pFCF2 and pFBH1

The vector pFCF1 was constructed by inserting gBlock1 (Fig. S1) into a pACYC184 backbone. gBlock1 encodes the bidirectional Fur promoter region (Fig. 1A) followed by a downstream FLAG epitope tag sequence, TEV protease cleavage site, and a multiple cloning site (MCS) (Fig 2A). We used the pUT18C MCS sequence (Euromedex) for subcloning of ORFs from BACTH vectors directly into pFCF1. Iron-starved *E. coli* transformants harboring ORFs subcloned into pFCF1 would thus express recombinant proteins with cleavable N-terminal FLAG tags. The map of pFCF1 is shown in Figure 2B. We also generated pFCF2, a pFCF1-derived vector, to demonstrate bidirectional expression of two proteins from the plasmid-borne *fepB/entC* promoter region. To construct pFCF2, we designed gBlock2 (Fig S2), which contains an in-frame HA tag sequence upstream of the kanamycin resistance gene (*KanR*) that encodes neomycin-kanamycin phosphotransferase II [132]. To generate pFCF2, gBlock2 was synthesized and then inserted between the *NcoI* and *ScaI* sites of pFCF1. The map of pFCF2 is shown in Figure 2C. The vector pFBH1 was constructed by insertion of gBlock3 (Fig. S3) between the *EcoRI* and *SaII* sites of linearized pBR322. gBlock3 contained DNA encoding the bidirectional Fur promoter region (Fig. 1A), the HA tag sequence, a TEV protease cleavage site, and the MCS from pUT18C (Fig. 3A).

The pFBH1 vector (Fig. 3B) allows for iron-controlled expression of recombinant proteins with cleavable N-terminal HA tags.

A

```

AAATCAGCTTCCTGTTATTAATAAGGTTAAGGGCGTAATGACAAATTCGACAAAGCGCACAAATCCGTCCCCTCGCCCTTTGGGGAGAGGGTTAGGGTGA
TTTAGTCGAAGGACAATAAATTAATCCAAATCCCGCATTACTGTTTAAGCTGTTTCGCGTGTTAGGCAGGGGAGCGGGGAAACCCCTCTCCAATCCCAC

GGGGAACAGCCAGCACTGGTGCGAACATTAACCCCTACCCAGCCCTCACCCCTGGAAGGGAGAGGGGGCAGAACGGCGCAGGACATCACATTGCGCTTAT
CCCCTTGTCCGGTCGTGACCACGCTTGTAATGGGAGTGGGGTCGGGAGTGGGACCTTCCCTCTCCCCGCTTGGCCGCTCCTGTAGTGTAAACGCGAATA

          Fur box 1                                     -35
GCGAATCCATCAATAATGCTTCTCATTTCATTGTAACCACAACCAGATGCAACCCCGAGTTGCAGATTGCGTTACCTCAAGAGTTGACATAGTGGCGGT
CGCTTAGGTAGTTATTACGAAGAGTAAAAGTAAACATTGGTGTGGTCTACGTTGGGGCTCAACGTCTAACGCAATGGAGTTCTCAACTGTATCACGCGCA
          +1          -10          -35
          -10          +1          Fur box 2
TTGCTTTAGGTTAGCGACCGAAAATATAAATGATAATCATTATTAAGCCTTTATCATTGTTGGAGGATGAT
AACGAAAATCCAATCGCTGGCTTTTATATTTACTATTAGTAATAATTCGGAAATAGTAAACACCTCCTACTA
  
```

B

```

consensus GATAATGATAATCATTATC
Fur box 1 -A A A T G A G A A G C A T T A T T

consensus GAT-AATGATAATCATTATC
Fur box 2 -A T A A A T G A T A A T C A T T A T -
  
```

Figure 1: The intergenic bidirectional promoter region between *E. coli* *fepB* and *entC*. (A) The sequence contains all nucleotides between the *fepB* and *entC* start codons (624511-624884 in *E. coli* K12 MG1655 (NCBI Reference Number: NC_000913.3)). Positions of anti-clockwise regulatory elements (Fur box1, +1 -10 and -35 sequences for *fepB* transcriptional regulation) are indicated by dashed lines. Positions of clockwise regulatory elements (Fur box 2, +1 -10 and -35 sequence for *entCEBAH* transcriptional regulation) are shown as solid lines. Fur box 1 and Fur box 2 were identified previously [18, 19]. (B) Sequence alignment of the Fur box consensus sequence with Fur box 1 and Fur box 2. Positions diverging from the consensus sequence are highlighted.

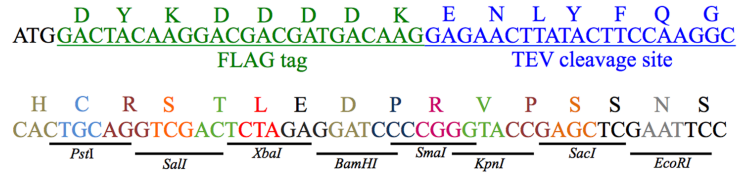
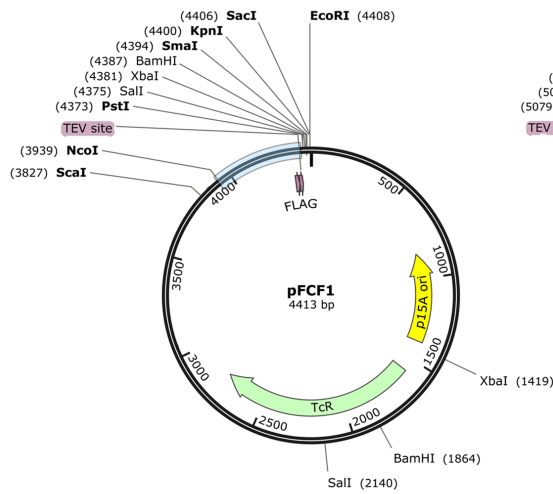
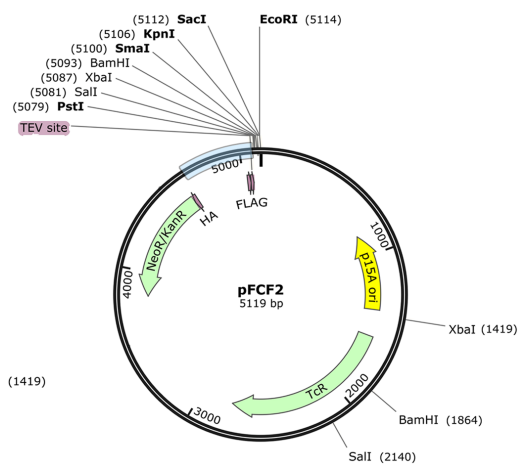
A**B****C**

Figure 2: Vector maps of pFCF1 and pFCF2. (A) Polypeptide sequence immediately downstream of the bidirectional promoter region found in gBlock1. Start codon sequence: black, FLAG sequence: green, TEV cleavage sequence: blue. MCS region from pUT18C colored by codons with restriction endonuclease sites shown below sequence. (B) pFCF1 vector map. Light blue bar indicates the promoter region. Unique restriction endonuclease sites shown in bold. FLAG: FLAG tag sequence; TEV: TEV cleavage site TcR: tetracycline resistance gene; p15A ori: origin of replication. (C) pFCF2 vector map. Light blue bar indicates the promoter region. Unique restriction endonuclease sites shown in bold. FLAG: FLAG tag sequence; TEV: TEV cleavage site; HA: HA tag sequence; NeoR/KanR: neomycin/kanamycin resistance gene; TcR: tetracycline resistance gene; p15A ori: origin of replication.

3.5.2 Assessment of iron-responsive promoter regions

To determine functionality of pFCF1, pFCF2, and pFBH1, we subcloned ORFs encoding *E. coli* enterobactin biosynthetic enzymes into the MCS regions of these vectors and performed complementation experiments using relevant knockout strains. Genes encoding the enterobactin biosynthetic enzymes EntA, EntE, and EntB were prepared by PCR amplification from pCA24N-based constructs as reported previously [131]. Specifically, the *entA* gene was subcloned into pFCF1 and pFCF2 to produce pFCF1-*entA* and pFCF2-*entA*. The *entE* gene was subcloned into pFCF1 to produce pFCF1-*entE*. Finally, the *entB* gene was subcloned into pFBH1 to produce pFBH1-*entB*. The four constructs were transformed into respective *entA*⁻, *entE*⁻ and *entB*⁻ *E. coli* knockout strains, and CAS assays [99] were used to assess complementation of the knockout phenotype (*i.e.*, impaired enterobactin biosynthesis). The CAS assay is a classical technique used to detect for the presence of siderophores. Upon iron chelation by siderophores, a color change of a dye complex (from blue/green to orange) is observed. Transformants containing pFCF1-*entA* and pFCF2-*entA* in an *entA*⁻ background were observed to produce orange halos indicative of iron chelation due to functional enterobactin biosynthesis whereas no halos were observed for empty vector controls (Fig. 4A, upper and lower left panels). Similar results were found for the pFCF1-*entE* transformant in the *entE*⁻ background (Fig. 4A, upper right panel), as well as for the pFBH1-*entB* transformant in the *entB*⁻ background (Fig. 4A, lower right panel). Growth studies (Fig. 4B) were consistent with our CAS assay results. Low growth was observed for *entA*⁻ and *entE*⁻ *E. coli* strains transformed with pFCF1 (Fig. 4B, columns 1 and 3). These knockout strains were rescued by transformation with pFCF1-*entA* and pFCF1-*entE*, respectively (Fig. 4B, columns 2 and 4). An *entB*⁻ strain transformed with pFBH1 also exhibited low growth (Fig. 4B, column 5), while transformation with pFBH1-*entB* complemented the knockout phenotype (Fig.

4B, column 6). Consistent with the above results, the *entA*⁻ strain transformed with pFCF2 did not exhibit significant growth in iron-depleted medium (Fig. 4B, column 7), whereas the pFCF2-*entA* transformant grew well (Fig. 4B, column 8).

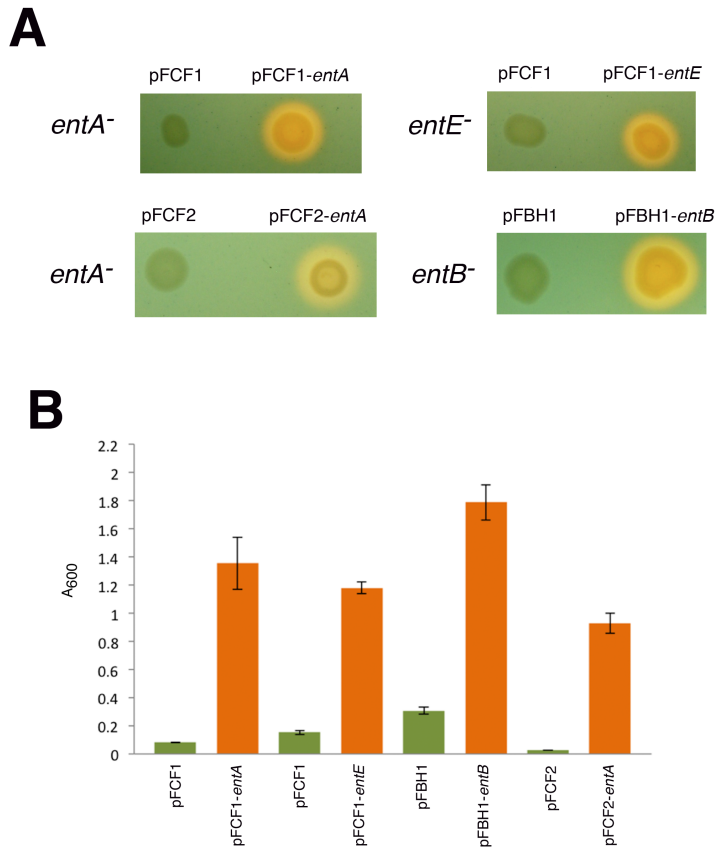


Figure 4: Functional assays for pFCF1, pFCF2 and pFBH1. (A) CAS assays. Images are photographs of CAS agar plates spotted with various *E. coli* transformants. Enterobactin secretion is indicated by orange halos. Upper left panel: *E. coli entA*⁻ strain transformed with pFCF1 (left spot) and pFCF1-*entA* (right spot). Lower left panel: *E. coli entA*⁻ strain transformed with pFCF2 (left spot) and pFCF2-*entA* (right spot). Upper right panel: *E. coli entE*⁻ strain transformed with pFCF1 (left spot) and pFCF1-*entE* (right spot). Lower right panel: *E. coli entB*⁻ strain transformed with pFBH1 (left spot) and pFBH1-*entB* (right spot). (B) Growth studies of transformants in iron-depleted medium. Orange bars indicate strains/transformants that exhibited a positive CAS signal; error bars represent standard deviations from mean values (n=3). Left to right: *E. coli entA*⁻ strain transformed with pFCF1; *E. coli entA*⁻ strain transformed with pFCF1-*entA*; *E. coli entE*⁻ strain transformed with pFCF1; *E. coli entE*⁻ strain transformed with pFCF1-*entE*; *E. coli entB*⁻ strain transformed with pFBH1; *E. coli entB*⁻ strain transformed with pFBH1-*entB*; *E. coli entA*⁻ strain transformed with pFCF2; *E. coli entA*⁻ strain transformed with pFCF2-*entA*.

3.5.3 Iron-controlled protein expression

To investigate iron-controlled protein expression from pFCF1 and pFBH1, we performed Western blotting analysis on isolated soluble proteins from iron-starved *E. coli* cells transformed with pFCF1-*entA* and pFBH1-*entB*. In addition, we used pFCF1 to examine iron-controlled expression of a protein not related to iron metabolism. For this experiment we used the DNA encoding T25, part of the catalytic fragment of adenylate cyclase from *B. pertussis* [102] to produce pFCF1-T25. Proteins from whole-cell lysates (equivalent cell wet weights) of transformants were separated by SDS-PAGE and the presence of epitope-tagged recombinant proteins was detected by Western blotting using appropriate antibodies directed against epitope tags. Expression of FLAG-tagged EntA from pFCF1-*entA* was detected using an anti-FLAG antibody (Fig. 5A, left blot, left lane). As a negative control, untransformed lysate was probed with anti-FLAG antibody and no signal was observed (Fig. 5A, left blot, right lane). Epitope signals were also observed for FLAG-tagged T25 expressed from pFCF1-T25 (Fig. 5A, right blot) and HA-tagged EntB expressed from pFBH1-*entB* (Fig. 5B, left lane). Proteins recovered from untransformed lysate probed with anti-HA antibody resulted in no observable signal (Fig. 5B, right lane).

To determine that the *fepB/entC* Fur promoter region was iron-responsive, we grew *E. coli* BW25113 cells transformed with pFCF1-*entE* under iron-rich conditions using LB medium supplemented with FeSO₄ as well as under iron-restricted conditions using modified M9 medium supplemented with 2,2'-dipyridyl. Cells were recovered from respective overnight cultures and equivalent amounts of proteins from whole-cell lysates were separated by SDS-PAGE. Western blot analysis using an anti-FLAG antibody revealed that FLAG-EntE was only detected in cells grown in iron-depleted medium, whereas no signal was observed from transformants grown in

iron-rich medium (Fig. 5C, upper panel). As a control, proteins from identical lysate loadings were probed with an anti-GAPDH antibody. Comparable GAPDH signals were observed in lysates from cells grown in both iron-depleted and iron-rich media (Fig. 5C, lower panel).

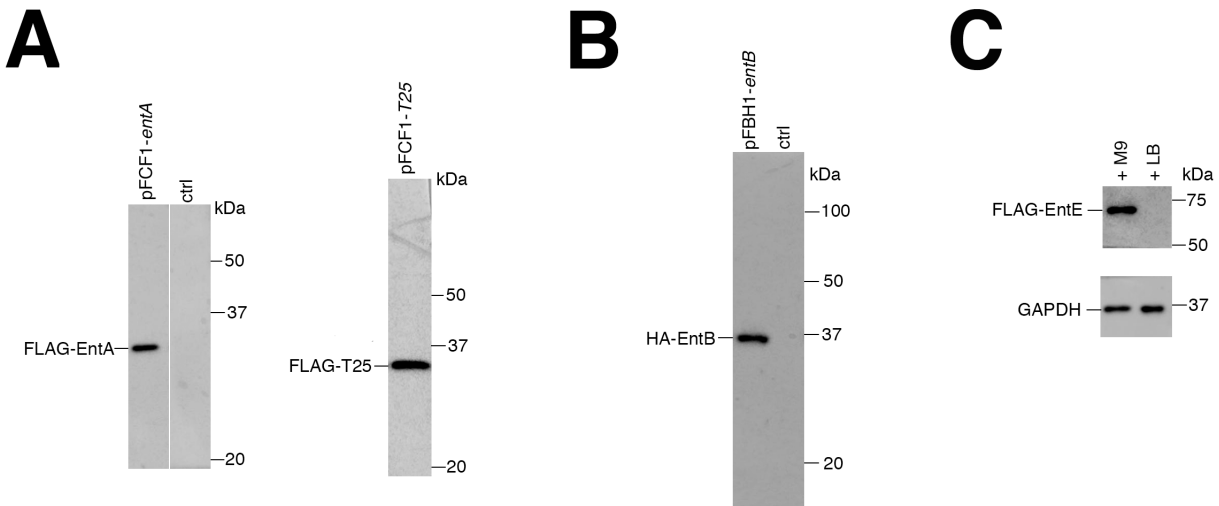


Figure 5: Protein expression from pFCF1 and pFBH1. (A) Whole-cell lysates from iron-starved *E. coli* BW25113 transformants (equivalent wet cell weights) were analyzed by Western blotting. An anti-FLAG antibody was used to detect expression of FLAG-EntA (left blot, left lane) and FLAG-T25 (right blot). Untransformed cell lysate probed with anti-FLAG antibody (left blot, right lane ('ctrl')). (B) Western blot of iron-starved *E. coli* BW25113 lysates probed with anti-HA antibody. Left lane: *E. coli* BW25113 transformed with pFBH1-entB. Right lane: Untransformed cell lysate ('ctrl'). (C) Iron responsiveness of the bidirectional promoter region. Upper panel: anti-FLAG antibody was used to detect expression of FLAG-EntE in lysates from cells grown in minimal M9 medium supplemented with 2,2'-dipyridyl (left) and from cells grown in LB medium supplemented with FeSO₄ (right). Lower panel: anti-GAPDH antibody was used to detect expression of *E. coli* GAPDH from protein samples identical to those in the upper panel.

3.5.4 Iron-controlled bidirectional expression from pFCF2

To test for bidirectional protein expression, we subcloned the *E. coli entA* gene into the MCS of pFCF2, which is under the control of Fur box 2. The pFCF2 vector also contains the *KanR* gene oriented in the opposite direction, under the control of Fur box 1. The resulting pFCF2-*entA* construct was transformed into competent *E. coli* BW25113 *entA*⁻ and transformants were grown

in either iron-rich (LB + FeSO₄) medium or iron-depleted (M9 + 2,2'-dipyridyl) medium in the presence and absence of kanamycin. Growth studies on pFCF2-*entA* transformants revealed that transformants grown in iron-depleted media supplemented with tetracycline grew to similar densities in the presence or absence of kanamycin (Figure 6, columns 1 and 2). Conversely, transformants grown in iron-rich media supplemented with tetracycline grew poorly in the presence of kanamycin (Figure 6, columns 3 and 4) due to Fur repression under iron-replete conditions.

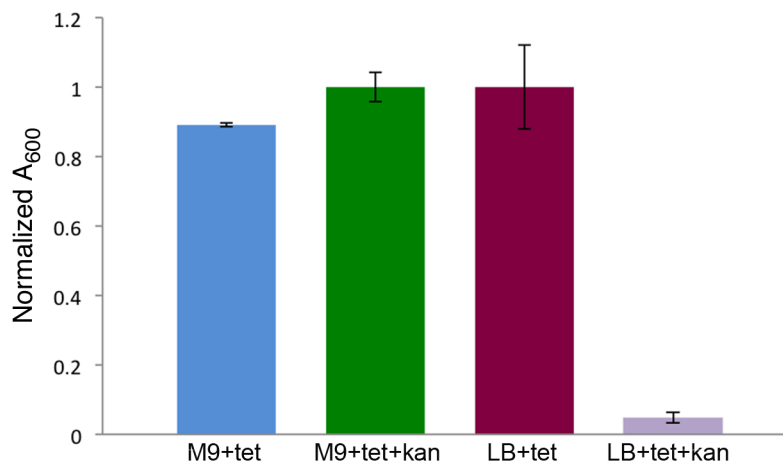


Figure 6: Bidirectional expression from pFCF2. Iron-controlled expression from the anti-clockwise-oriented *KanR* gene in pFCF2 was determined by bacterial growth studies. Shown are normalized cell densities (A_{600}) of *E. coli entA* strains transformed with pFCF2-*entA* grown in (left to right): M9 medium + 2,2'-dipyridyl supplemented with tetracycline; M9 medium + 2,2'-dipyridyl supplemented with tetracycline and kanamycin; LB medium + FeSO₄ supplemented with tetracycline; LB medium + FeSO₄ supplemented with tetracycline and kanamycin. Error bars represent standard deviations from mean values (n=3).

3.6 Discussion

We designed and constructed three vectors (pFCF1, pFCF2, and pFBH1) for iron-controlled protein expression from low-copy-number vectors in *E. coli*. For pFCF1 and pFCF2, the plasmid pACYC184 [133] (origin of replication: p15A; copy number ~ 15) was used as a backbone, whereas for pFBH1 the plasmid pBR322 [134] (origin of replication: pMB1; copy number ~ 20) was used. These low-copy-number plasmids were chosen as backbones in order to avoid protein overexpression found in systems employing high-copy-number plasmids, such as the pBAD series of expression vectors that contain the pUC origin of replication (copy number ~ 500-700 [135]) or the pTZ-derived expression vectors (copy number ~ 1000) [136]. Furthermore, since pFCF1/pFCF2 and pFBH1 have different antibiotic resistance markers along with compatible origins of replication, expression of multiple epitope-tagged proteins from a single co-transformant is possible. For all vectors, gBlock[®] fragments containing: (i) a wild-type *E. coli* Fur-controlled bidirectional promoter region, (ii) sequences encoding epitope tags (FLAG or HA), (iii) sequence encoding the TEV protease cleavage site and (iv) a BACTH-compatible MCS, were designed, synthesized and inserted into respective plasmid backbones (pACYC184 or pBR322).

For iron-controlled expression of epitope-tagged proteins, we used the bidirectional promoter region in the intercistronic space between the *fepB* and *entC* genes in the *E. coli* chromosome (Figure 1A) [128,129]. This region, which contains all nucleotides between the *fepB* and *entC* start codons (624511-624884 in *E. coli* K12 MG1655 (NCBI Reference Number: NC_000913.3)), has two Fur box sequences. Fur box 1 controls expression of *fepB* in the anti-clockwise direction whereas Fur box 2 controls expression of the operon containing *entC*, *entE*, *entB*, *entA*, and *entH*

genes in the clockwise direction. While Fur box 1 overlaps with its cognate -10/-35 sequences, Fur box 2 occurs downstream of its cognate +1/-10/-35 sequences [128,129].

In order to test the functionality of pFCF1, pFCF2 and pFBH1, derivative constructs containing ORFs (*entA*, *entE*, and *entB*) under the control of Fur box 2 were prepared. Chromosomal expression of these ORFs in *E. coli* is under Fur control, and they were therefore logical candidates for testing the plasmid-borne bidirectional promoter region in pFCF1/2 and pFBH1. CAS assays and growth studies (Figure 4) confirmed that the derivative constructs were able to complement respective knockout phenotypes upon iron restriction due to Fur derepression. Western blotting demonstrated that the bidirectional promoter region was controlling expression of epitope-tagged proteins FLAG-EntA and HA-EntB from pFCF1 and pFBH1, respectively. Also, expression of FLAG-T25, a FLAG-tagged *B. pertussis* polypeptide that is typically not under control of *E. coli* Fur, was detected. Taken together, these outcomes demonstrate that the *fepB/entC* promoter region (Fig. 1A) is functional in pFCF1 and pFBH1. Experiments using iron-depleted and iron-rich media showed that expression of FLAG-EntE from pFCF1-*entE* occurred in an iron-controlled manner. This is consistent with recent reports demonstrating that elevated expression of genes under Fur control occurred under iron-restricted conditions [121,137].

Although unidirectional protein expression controlled by Fur box 2 was observed in pFCF1 and pFBH1, the bidirectionality of the *fepB/entC* promoter region had to be tested. We designed pFCF2 such that expression of the *KanR* gene would be controlled by Fur box 1 while Fur box 2 would simultaneously control expression of an ORF subcloned into the MCS in the other direction. A pFCF2-*entA* transformant grown under iron-restricted conditions was expected to exhibit complementation of the *entA*⁻ phenotype with concomitant kanamycin resistance. Using iron-depleted CAS agar plates supplemented with tetracycline and kanamycin, the pFCF2-*entA* transformant complemented the *entA*⁻ phenotype and produced a CAS halo while being resistant

to kanamycin (Figure 4A, lower left panel). This demonstrated that the *KanR* gene in pFCF2-*entA* was under the control of Fur box 1 resulting in iron-regulated expression. Furthermore, growth studies revealed that the pFCF2-*entA* transformant grew more poorly in iron-rich medium supplemented with kanamycin compared to growth in iron-depleted medium plus kanamycin. This suggests that under iron-replete conditions, Fur-controlled expression of the *KanR* gene is repressed relative to that of the same transformant grown under iron-depleted conditions. Taken together our results demonstrate that bidirectional iron-controlled *in trans* protein expression from pFCF2-*entA* occurs in iron-starved *E. coli* transformants. Protein expression controlled by Fur box 1 in pFCF2 is currently restricted to the *KanR* gene. By replacement of this gene with an additional MCS, bidirectional expression of any two epitope-tagged proteins can be achieved in a single transformant. The compatibility of pFCF- and pFBH-derived constructs would further allow for expression of up to four epitope-tagged proteins in a single co-transformant.

3.7 Conclusions

Constructs containing engineered Fur box sequences for unidirectional expression of toxic genes in *E. coli* have previously been reported [137]. To facilitate bidirectional expression of epitope-tagged proteins under iron control, we have designed and constructed three novel low-copy-number vectors derived from pACYC184 and pBR322. These vectors contain the wild-type intercistronic region found between the *fepB* and *entC* genes in the *E. coli* chromosome that can be used for bidirectional expression. As we have demonstrated, when inserted into low-copy-number plasmid vectors, this region can control simultaneous expression of two proteins in a single transformant. Since the pFCF1/2 and pFBH1 have compatible origins of replication and different antibiotic resistance gene markers, they can also be useful for co-transformation.

Our current understanding of Fur regulation indicates that there are approximately 70 *E. coli* genes under the control of Fur [121]. By transferring ORFs naturally found in Fur regulons, the vectors reported here can be used for a wide variety of experiments such as the study of *in trans* complementation of knockout phenotypes, effects of iron-controlled protein expression on cellular processes (*e.g.*, oxidative stress response, TCA cycle, etc.), as well as studies on proteins that are involved in Fur-controlled virulence mechanisms (*e.g.*, Type 3 secretion system)[116]. Furthermore, genes not typically under Fur control can be expressed in an iron-controlled manner. Since the MCS in pFCF1 and pFBH1 is compatible with the BACTH system, ORFs encoding interacting partners detected by BACTH could be easily subcloned into the vectors reported here. Such constructs could be used for follow-up studies such as co-immunoprecipitation experiments using appropriate antibodies directed against vector-encoded epitope-tagged proteins.

3.8 Supplementary Material

Table S1. PCR primer sequences used for preparing pFCF1 and pFBH1 constructs.

| Vector | Gene | Primer Sequence (5'-3') |
|--------|-------------|--|
| | | F: TAGGGGTACCTATGGATTTTCAGCGGTAAAAATGTCTGGG |
| | <i>entA</i> | R: CTACGGAATTCTTATGCCCCAGCGTTGAGCC |
| | | F: TAGGGGTACCTATGAGCATTCCATTCACCCGCTGGC |
| pFCF1 | <i>entE</i> | R: CTACGGAATTCTCAGGCTGATGCGCGTGACG |
| | | F: TAGGGGTACCTATGCAGCAATCGCATCAGGCTGGTTACGCAAACG |
| | <i>T25</i> | R: CTACGGAATTCTTAGGCCCGCCGCGTGCGCGCCAGGTAAT |
| | | F: TAGGGGTACCTATGGCTATTCCAAAATTACAGGCTTACGC |
| pFBH1 | <i>entB</i> | R: CTACGGAATTCTTATTTACCTCGCGGGAGAGTAGC |

F = forward, R = reverse. Underlined sequences indicate *KpnI* (forward) and *EcoRI* (reverse) restriction sites.

Figure S1.

gBlock1

5'-TATTTGCCCATGGAAAATCAGCTTCCTGTTATTAATAAGGTTAAGGGCGTAATGACAAATTC
 GACAAAGCGCACAAATCCGTCCCCTCGCCCCTTTGGGGAGAGGGTTAGGGTGAGGGGAACAGCCAGCAC
 TGGTGCGAACATTAACCCTCACCCAGCCCTCACCTGGAAGGGAGAGGGGCGAGAACGGCGCAGGA
 CATCACATTGCGCTTATGCGAATCCATCAATAATGCTTCTATTTTCATTGTAACCACAACCAGATGCA
 ACCCCGAGTTGCAGATTGCGTTACCTCAAGAGTTGACATAGTGCGCGTTGCTTTTAGGTTAGCGACCG
 AAAATATAAATGATAATCATTATTAAGCCTTTATCATTTTGTGGAGGATGATATGGACTACAAGGACG
 ACGATGACAAGGAGAAGCTTATACTTCCAAGGCCACTGCAGGTGCGACTCTAGAGGATCCCCGGGTAC
 CGAGCTCGAATTCATCGATA-3'

NcoI , EcoRI

Start Codon

Bidirectional promoter region containing two non-overlapping fur boxes: black

FLAG tag

TEV cleavage site

MCS: bold/underlined

Note 1: MCS is from pUT18C vector (Euromedex)

Figure S2.

gBlock2

5'-**CCTTAAAAAATTACGCCCGCCCTGCCACTCATCGCAGT**TCAGAAGA AACTCGTCAAGAA
GGCGATAGAAGGCGATGCGCTGCGAATCGGGAGCGGCGATAACCGTAAAGCACGAGGAAGCGGTCAGC
CCATTCGCCGCCAAGCTCTTCAGCAATATCACGGGTAGCCAACGCTATGTCCTGATAGCGGTCCGCCAC
ACCCAGCCGGCCACAGTCGATGAATCCAGAAAAGCGGCCATTTTCCACCATGATATTCGGCAAGCAGG
CATCGCCATGGGTCACGACGAGATCCTCGCCGTCGGGCATCCGCGCCTTGAGCCTGGCGAACAGTTTCG
GCTGGCGCGAGCCCCTGATGCTCTTCGTCCAGATCATCCTGATCGACAAGACCGGCTTCCATCCGAGTA
CGTGCTCGCTCGATGCGATGTTTCGCTTGGTGGTCAATGGGCAGGTAGCCGGATCAAGCGTATGCAG
CCGCCGATTGCATCAGCCATGATGGATACTTTCTCGGCAGGAGCAAGGTGAGATGACAGGAGATCCT
GCCCCGGCACTTCGCCAATAGCAGCCAGTCCCTTCCCGCTTCAGTGACAACGTCGAGCACAGCTGCGC
AAGGAACGCCCGTTCGTGGCCAGCCACGATAGCCGCGCTGCCTCGTCTTGGAGTTCATTCAGGGCACCG
GACAGGTCGGTCTTGACAAAAAGAACCGGGCGCCCCTGCGCTGACAGCCGGAACACGGCGGCATCAG
AGCAGCCGATTGTCTGTTGTGCCAGTCATAGCCGAATAGCCTCTCCACCCAAGCGGCCGGAGAACCT
GCGTGCAATCCATCTTGTTCAAT**CGCATAATCCGGCACATCATACGGATA****CAT**GAAATCAGCTTCTGT
TATTAATAAGGTTAAGGGCGTAATG-3'

40 bp overlapping region upstream of NcoI site in the vector and 41 bp overlapping region downstream of ScaI site in the vector

Start codon

HA tag

Kanamycin resistance gene: black

Note 1: Start codon, HA tag and Kanamycin resistance gene are reverse complement

Note 2: Kanamycin sequence is from pKT25 vector (Euromedex)

Figure S3.

gBlock3

5'-**ATCACGAGGCCCTTTCGTCTTCAAG**AAATCAGCTTCTGTTATTAATAAGGTTAAGGGCGT
AATGACAAATTCGACAAAGCGCACAAATCCGTCCCCTCGCCCCTTTGGGGAGAGGGTTAGGGTGAGGGG
AACAGCCAGCACTGGTGCGAACATTAACCCTCACCCAGCCCTCACCTGGAAGGGAGAGGGGGCAG
AACGGCGCAGGACATCACATTGCGCTTATGCGAATCCATCAATAATGCTTCTCATTTCATTGTAACCA
CAACCAGATGCAACCCCGAGTTGCAGATTGCGTTACCTCAAGAGTTGACATAGTGCAGGTTGCTTTTA
GGTTAGCGACCGAAAATATAAATGATAATCATTATTAAGCCTTTATCATTGTTGGAGGATGAT**ATGT**
ATCCGTATGATGTGCCGATTATGCGGAGAACTTATACTTCCAAGGCCACTGCAGGTCGACTCTAGA
GGATCCCCGGGTACCGAGCTCGAATTC**CCGATGCCCTTGAGAGCCTTCAACC**-3'

25 nucleotide overlapping regions upstream of EcoRI site of the vector and downstream of SalI site in the vector

Start Codon

Bidirectional promoter region containing two non-overlapping fur boxes: black

HA tag

TEV cleavage site

MCS: bold/underline

Chapter 4: Intracellular Co-Localization of the *Escherichia coli* Enterobactin Biosynthetic Enzymes EntA, EntB, and EntE

4.1 Preface

The work presented in this chapter has been published in the journal: *Biochemical and Biophysical Research Communications*: Pakarian, P. & Pawelek, P.D., (2016) “Intracellular Co-Localization of the Enterobactin Biosynthetic Enzymes EntA, EntB, and EntE from *Escherichia coli*” *Biochem. Biophys. Res. Commun.* 478, 25-32.

4.2 Abstract

Bacteria utilize small-molecule iron chelators called siderophores to support growth in low-iron environments. The *Escherichia coli* catecholate siderophore enterobactin is synthesized in the cytoplasm upon iron starvation. Seven enzymes are required for enterobactin biosynthesis: EntA-F, H. Given that EntB-EntE and EntA-EntE interactions have been reported, we investigated a possible EntA-EntB-EntE interaction in *E. coli* cells. We subcloned the *E. coli* entA and entB genes into bacterial adenylate cyclase two-hybrid (BACTH) vectors allowing for co-expression of EntA and EntB with N-terminal fusions to the adenylate cyclase fragments T18 or T25. BACTH constructs were functionally validated using the CAS assay and growth studies. Co-transformants expressing T18/T25-EntA and T25/T18-EntB exhibited positive two-hybrid signals indicative of an intracellular EntA-EntB interaction. To gain further insights into the interaction interface, we performed computational docking in which an experimentally validated EntA-EntE model was docked to the EntB crystal structure. The resulting model of the EntA-EntB-EntE ternary complex predicted that the IC domain of EntB forms direct contacts with both EntA and EntE. BACTH constructs that expressed the isolated EntB IC domain fused to T18/T25 were prepared

in order to investigate interactions with T25/T18-EntA and T25/T18-EntE. CAS assays and growth studies demonstrated that T25-IC co-expressed with the EntB ArCP domain could complement the *E. coli entB*⁻ phenotype. In agreement with the ternary complex model, BACTH assays demonstrated that the EntB IC domain interacts with both EntA and EntE.

4.2 Introduction

In order to obtain iron from the extracellular environment, many bacteria synthesize and secrete small-molecule chelators known as siderophores. The Gram-negative bacterium *Escherichia coli* produces the catecholate siderophore enterobactin, which is comprised of three 2,3-dihydroxybenzoic acid (DHB) subunits connected to a triserine trilactone core. Seven enzymes are required to synthesize enterobactin in the *E. coli* cytoplasm: EntC, EntB, EntA, EntE, EntF, EntD, and EntH. The DHB precursors are synthesized *via* the sequential activities of EntC, EntB (isochorismatase (IC) domain) and EntA. Three DHB molecules are then condensed with three molecules of L-serine *via* non-ribosomal peptide synthesis (NRPS), the reactions of which are catalyzed by EntE, EntB (aryl carrier protein (ArCP) domain), EntD, and EntF. The DHB biosynthetic enzyme EntA converts 2,3-dihydro-2,3-dihydroxybenzoic acid to DHB in an NAD⁺-dependent oxidation reaction. The biological assembly of EntA is tetrameric, with four identical 26 kDa subunits [104]. EntB is a dimeric protein with two identical 33 kDa subunits [8]. Each EntB subunit has an N-terminal IC domain that is involved in DHB biosynthesis, and a C-terminal ArCP domain involved in NRPS. EntE is a monomeric 59 kDa protein with a stable N-terminal domain and more mobile C-terminal domain that can undergo conformational change due to domain alternation [77]. EntE is the activity in the NRPS arm of the pathway that activates DHB *via* adenylation.

Protein-protein interactions are required for siderophore biosynthesis. It has recently been reported that enzymes involved in biosynthesis of the *Pseudomonas aeruginosa* siderophore pyoverdine are organized into a large multi-enzyme complex known as a siderosome [85,94]. Obligate interactions have been reported between the NRPS enzymes in enterobactin biosynthesis: EntE-EntB [77], EntB-EntF [71], EntB-EntD [9], EntD-EntF [93], EntB-EntH [74]. The EntE-EntB interaction has been elucidated at the atomic level by X-ray crystallography using a chimeric protein in which EntE was fused to the ArCP domain of EntB [77]. Since the chimeric protein lacked the N-terminal isochorismatase (IC) domain of EntB, there is currently no information on possible EntB (IC)-EntE contacts in addition to the crystallized EntB(ArCP)-EntE interface. Our laboratory has reported an interaction between EntA, the terminal enzyme in the DHB biosynthetic arm of the pathway, and EntE, the first enzyme in the NRPS arm of the pathway [65,131]. We used the bacterial adenylate cyclase two-hybrid (BACTH) assay to investigate the intracellular context of this interaction, and have determined the relative orientations of EntA and EntE subunits within the complex [131].

Since EntE-EntB and EntA-EntE interactions are known, we were interested in investigating the possibility of an EntA-EntB interaction, or even a ternary EntA-EntB-EntE complex. Using BACTH assays, we demonstrate here that EntA and EntB interact in *E. coli* cells and that the EntB IC domain interacts with both EntA and EntE. Computational docking supports the existence of a ternary EntA-EntB-EntE complex that is consistent with our BACTH outcomes.

4.3 Material and Methods

4.3.1 Reagents

All chemicals were purchased from Bioshop Canada, Inc. (Burlington, Ontario) unless noted otherwise.

4.3.2 Preparation of constructs

The *E. coli* genes encoding EntA and EntB were amplified from pCA24N-*entA* and pCA24N-*entB* templates [131] by PCR using primers containing KpnI and EcoRI restriction sites. A similar approach was used to amplify DNA encoding the EntB IC (EntB residues 1-207) domain. All primers used in this study are summarized in Table 1. Phusion High-Fidelity DNA polymerase (New England Biolabs) was used for amplification of the above-mentioned genes according to the manufacturer's standard protocol. PCR products were subcloned in-frame between KpnI and EcoRI sites of the BACTH vectors pUT18C and pKT25 to produce constructs encoding N-terminally tagged fusion proteins (T18/T25-EntA, T18/T25-EntB, and T18/T25-IC). BACTH vectors were obtained from the BACTH System Kit (Euromedex). In addition to the BACTH constructs, DNA encoding the EntB ArCP domain (residues 213-285) was subcloned into the KpnI and EcoRI sites of the pBR322-based expression vector pFBH1. The pFBH1 vector contains a Fur promoter region upstream of the MCS that allows for iron-controlled protein expression. All constructs were verified by DNA sequencing (Genome Quebec Innovation Centre, McGill University).

Table 1: PCR primers used in this study

| Vector | Gene | Primer Sequence (5'-3') |
|------------------|-------------|---|
| | | F: TAGGGGTACCTATGGATTTCAGCGGTAAAAATGTCTGGG |
| | <i>entA</i> | R: CTACGGAATTCTTATGCCCCAGCGTTGAGCC |
| | | F: TAGGGGTACCTATGGCTATTCCAAAATTACAGGCTTACGC |
| pUT18C, pKT25 | <i>entB</i> | R: CTACGGAATTCTTATTTACCTCGCGGGAGAGTAGC |
| | | F: TAGGGGTACCTATGGCTATTCCAAAATTACAG |
| | <i>IC</i> | R: CTACGGAATTCTTACAGTAATTCTTCAGTCATC |
| | | F: TAGGGGTACCAGCCAGCAAAGCG |
| pFBH1 | <i>ArCP</i> | R: CTACGGAATTCTTATTTACCTCGC |

F = forward, R = reverse. Underlined sequences indicate *Kpn*I (forward) and *Eco*RI (reverse) restriction sites.

4.3.3 CAS assays and growth studies

An *E. coli* modified knockout background strain deficient in EntB activity (*entB*⁻) was prepared as described previously [131]. The competent *entB*⁻ strain was transformed with BACTH constructs encoding T18/T25-EntB. Also, a T25-IC BACTH construct was co-transformed with pFBH1-*ArCP* into the *entB*⁻ strain. Transformants were plated on LB agar containing 100 µg ml⁻¹ ampicillin or 50 µg ml⁻¹ kanamycin, respectively. T25-IC/*ArCP* co-transformants were plated onto LB agar containing appropriate antibiotics. All plates were incubated overnight at 30 °C. Empty pUT18C, pKT25, and pFBH1 vectors were also transformed into the *entB*⁻ strain as controls. Colonies from transformation plates were used to inoculate LB broth supplemented with appropriate antibiotics. Cultures were incubated with shaking at 30 °C. Overnight cultures were diluted 1:100 in LB broth supplemented with appropriate antibiotics and grown at 30 °C until an A₆₀₀ between 0.5 – 0.7 was reached. Cultures were then diluted 1:1000 in a 1X M9 modified minimal medium [131] and supplemented with appropriate antibiotics. Cultures diluted in minimal medium were grown at 30 °C overnight. CAS-agar plates were prepared according to Payne *et al.* (1994) [38] and then spotted with 1 µL overnight minimal M9 cultures and incubated at 30 °C for 18 hours. Functionality of constructs was assessed by the formation of orange halos on CAS plates [99]. Plate assays were performed in triplicate to ensure reproducibility. Single colony picks of *E. coli* transformants or co-transformants prepared for CAS assays were also used to perform bacterial growth studies as described previously [131].

4.3.4 BACTH assays

Functional BACTH constructs that could rescue the *entB*⁻ phenotype were co-transformed into competent *E. coli* BTH101 cells (*F*⁻, *cya-99*, *araD139*, *galE15*, *galK16*, *rpsL1 (Str^R)*, *hsdR2*, *relA*, *mcrA1*, *mcrB1*) (Euromedex). Co-transformants were incubated on LB plates containing 100 µg

ml⁻¹ ampicillin and 50 µg ml⁻¹ kanamycin at 30 °C for 48 hours. Colony picks were used to inoculate 3 ml of LB medium plus appropriate antibiotics as well as 0.5 mM IPTG. Inoculated cultures were grown at 30 °C overnight [100]. β-galactosidase assays were performed as described by Miller [101] except that reactions were incubated at room temperature. For BACTH plate assays, 1 µl of each overnight culture was spotted onto MacConkey agar base (Difco) plates containing appropriate antibiotics, 0.5 mM IPTG and 1% maltose. Spotted plates were incubated at 30 °C overnight [100]. A positive two-hybrid signal was indicated by the formation of red colonies on plates and elevated β-galactosidase signal. All BACTH assays (plate-based assays and β-galactosidase) were performed in triplicate.

4.3.5 Computational docking

Atomic coordinates of the EntA-EntE docked complex [131] and the dimeric EntB X-ray crystallographic structure (PDB code: 2FQ1; [8]) were submitted to the ClusPro server [110] as a blind docking experiment. Default ClusPro settings were used, and no constraints or prior experimental knowledge was introduced to guide the server towards a docking solution. The selected candidate model of the ternary EntA-EntB-EntE complex was determined as the highest populated cluster in which the docked EntB molecule did not overlap with the EntA-EntE interaction interface. Structural alignments were performed using the Australis server (<http://eds.bmc.uu.se/eds/australis.php>) that employs the LSQMAN alignment program [138].

4.4 Results and Discussion

4.4.1 Intracellular interaction of *E. coli* EntA and EntB

In order to investigate a possible EntA-EntB interaction, the *E. coli* *entA* and *entB* genes were subcloned into the BACTH vectors pUT18C and pKT25. These constructs expressed EntA and

EntB with N-terminal fusions to the *B. pertussis* adenylate cyclase fragments T18 and T25. To ensure that the T18/T25-EntA/EntB fusions were functional, we performed chrome azurol S (CAS) assays and growth studies on transformants. The CAS assay indicates functional siderophore production in bacteria. Secreted siderophores result in the formation of an orange halo due to iron extraction from the dye in the plate media [99]. We had previously used the CAS assay to determine that T18-EntA, T25-EntA, T18-EntE and T25-EntE were functional for enterobactin biosynthesis [131]. Here, the same approach was used to probe for T18/T25-EntB functionality. Competent *E. coli* BW25113 *entB*⁻ cells transformed with pUT18C alone did not yield a CAS halo, indicating impaired enterobactin biosynthesis in this transformant (Fig. 1A, upper left panel, left spot). In contrast, *entB*⁻ cells transformed with pUT18C-*entB* resulted in the formation of an orange halo, indicative of enterobactin biosynthesis due to complementation of the knockout phenotype by T18-EntB (Fig. 1A, upper left panel, right spot). Similar results were found for *entB*⁻ cells transformed with pKT25 and pKT25-*entB*, indicating that T25-EntB could also rescue the knockout phenotype (Fig. 1A, upper right panel). Bacterial growth studies supported our CAS assay results. Significant growth in minimal media was only observed when *entB*⁻ cells were transformed with either pUT18C-*entB* (Fig. 1A, lower left panel) or pKT25-*entB* (Fig. 1A, lower right panel) due to complementation of the knockout phenotype by T18/T25-EntB expression. Taken together, these results established that fusion of T18 or T25 tags to the N-terminus of EntB did not impair enterobactin biosynthesis.

We used the EntB BACTH constructs in a co-transformation experiment to probe for possible interaction with *E. coli* EntA. The BACTH assay is used for the detection of intracellular protein-protein interactions [102]. Intracellular interaction of the partner proteins brings fused T18 and T25 fragments into proximity, thus reconstituting adenylate cyclase activity that could activate reporter genes. When co-transformed into an *E. coli* strain (BTH101) deficient in adenylate

cyclase (*cyaA*), this results in a positive two-hybrid signal (red bacterial colonies on MacConkey agar plates, or elevated β -galactosidase activity in a liquid assay). Co-transformation of pUT18C-*entA* and pKT25-*entB* resulted in a positive two-hybrid signal on MacConkey agar plates (Fig. 1B, upper panel, left spot), whereas no red colony was observed in BTH101 cells co-transformed with pUT18C-*entA* and pKT25 alone (Fig. 1B, upper panel, right spot). In agreement with the plate-based assay, we observed that the pUT18C-*entA*/pKT25-*entB* co-transformant exhibited elevated β -galactosidase activity in comparison with BTH101 cells co-transformed with pUT18C-*entA* and pKT25 empty vector (Fig. 1B, upper bar graph). Similar results were observed when T18/T25 tags were swapped to investigate co-expression of T25-EntA and T18-EntB. The two-hybrid signal was observed on MacConkey agar for the pKT25-*entA*/pUT18C-*entB* co-transformant, but not for cells co-transformed with pKT25-*entA* and pUT18C empty vector (Fig. 1B, lower panel, left and right spots, respectively). We found that co-expression of T25-EntA and T18-EntB in BTH101 cells resulted in elevated β -galactosidase activity relative to cells co-expressing T25-EntA and the unfused T18 fragment (Fig. 1B, lower bar graph). We also performed BACTH control assays on cells co-expressing T18/T25-EntB with T25/T18 tags fused to proteins unrelated to enterobactin biosynthesis. MobA, a protein involved in molybdenum metabolism that we used previously as a BACTH negative control was N-terminally fused to T18 [131]. Furthermore, a vector encoding T25 N-terminally fused to a leucine zipper domain was also used as a control. BTH101 cells co-expressing T18-MobA with T25-EntB resulted in no detectable BACTH signal on MacConkey agar plates (Fig. 1C, left panel). Similarly, no BACTH signal was observed for the T25-ZIP/T18-EntB co-transformant (Fig. 1C, right panel). Liquid assays on these transformants exhibited β -galactosidase activity similar to our other negative controls (120.2 ± 6.0 Miller units and $81.4 + 14.1$ Miller units for T18-MobA/T25-EntB and T25-ZIP/T18-EntB co-transformants, respectively). Taken together, these outcomes demonstrate that

the positive two-hybrid signal was only observed when EntA and EntB were co-expressed in BTH101 cells, indicative of intracellular EntA-EntB interaction.

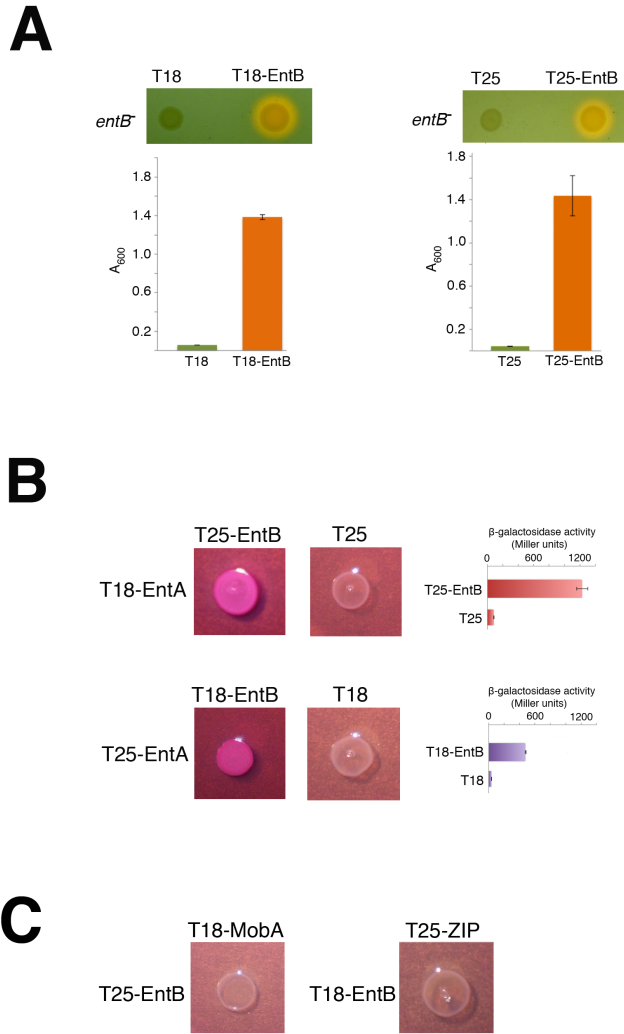


Figure 1: Bacterial two-hybrid assays of EntA with full-length EntB. (A) Validation of BACTH constructs. Upper left panel: Photograph of CAS agar plate spotted with *E. coli entB⁻* cells transformed with pUT18C (left) and pUT18C-*entB* (right). Lower left bar graph: Bacterial growth study of *E. coli entB⁻* cells transformed with pUT18C (left) and pUT18C-*entB* (right). Upper right panel: Photograph of CAS agar plate spotted with *E. coli entB⁺* cells transformed with pKT25 (left) and pKT25-*entB* (right). Lower right bar graph: Bacterial growth study of *E. coli entB⁺* cells transformed with pKT25 (left) and pKT25-*entB* (right). Growth studies were performed in iron-depleted minimal medium at 30 °C. Cell densities measured as absorbances at 600 nm (A_{600}). Orange bars indicate transformants that exhibited a positive CAS signal; error bars represent standard deviations from mean values. All CAS assays and growth studies were performed in triplicate. (B) BACTH assays of T18/T25-EntA co-expressed with T25/T18-EntB. Photographs are of *E. coli* BTH101 co-transformants spotted onto MacConkey agar plates. Bar graphs represent BACTH β -galactosidase assays. *E. coli* BTH101 cells co-transformed with BACTH vectors are indicated as follows. Upper left panel: pUT18C-*entA*/pKT25-*entB*. Upper right panel: pUT18C-*entA*/pKT25. Upper bar graph: β -galactosidase assays of pUT18C-*entA*/pKT25-*entB* co-transformant (upper) and pUT18C-*entA*/pKT25 co-transformant (lower). Lower left panel: pKT25-*entA*/pUT18C-*entB*. Lower right panel: pKT25-*entA*/pUT18C. Lower bar graph: β -galactosidase assays of pKT25-*entA*/pUT18C-*entB* co-transformant (upper) and pKT25-*entA*/pUT18C co-transformant (lower). Error bars represent standard deviations from mean values (n=3). (C) BACTH assays of T25/T18-EntB co-expressed with T18/T25-fused to control proteins. Photographs are of *E. coli* BTH101 co-transformants spotted onto MacConkey agar plates. Left panel: pUT18C-*mobA*/pKT25-*entB*; Right panel: pKT25-*zip*/pUT18C-*entB*.

4.4.2 Computational docking of *E. coli* EntA, EntB, and EntE

Given evidence for pairwise EntA-EntB (this study), EntE-EntB [77] and EntA-EntE [65,131] interactions, we employed computational docking to investigate a possible EntA-EntB-EntE ternary complex. We used the ClusPro docking server [110] given its reported successes at accurately predicting protein complexes [109]. We had previously used experimental approaches to validate a computational model of the EntA-EntE complex [131]. In the EntA-EntE complex model, one EntE monomer was predicted to interact with one face of the EntA tetramer, such that each EntA subunit was required for the entire EntA-EntE interaction interface. Here we used this experimentally validated model along with the crystal structure of dimeric EntB (PDB code: 2FQ1) in blind docking experiment. No constraints were provided to guide ClusPro towards a correct ternary structure model. ClusPro returned 622 possible ensembles of the ternary complex grouped into 30 clusters. As our candidate model, we selected the top-ranked cluster (29 members; weighted score: -856.7) in which the docked EntB protein did not overlap with the EntE-interacting interface of EntA. The top-ranked candidate of EntB docked to the EntA-EntE complex is shown in Figure 2A. Consistent with the reported X-ray crystallographic structure of EntE-EntB (ArCP), most of the EntB-EntE interaction interface was found between the ArCP domain of EntB and a cleft formed between the N- and C-terminal domains of EntE. The EntA-EntB-EntE model indicates direct regions of contact between the EntB IC domain and EntA as well as EntE. In the model, the C-terminal half of EntB IC α 2 (residues 52-71) is found within a pocket formed at the interaction interface between the EntE N-terminal domain and the B-chain of the EntA tetramer. Hydrogen bonding was predicted between EntB Q69 and the main chain amide nitrogen and carbonyl oxygen atoms of EntE E291 (Fig. 2B, left panel). Proximal to EntB α 2 is a loop region in the IC domain (residues 110-120) predicted by the model to directly

interact *via* a hydrophobic interaction between EntB A116 and residue A60 of the EntA B-chain; additional hydrogen bonding was found between the side-chain of EntB D117 and residue Q64 of the EntA B-chain (Fig. 2B, right panel). To validate the ternary complex model, we performed a structural superposition of the EntE C α atoms in the EntE-EntB(ArCP) crystal structure (PDB code: 3RG2) with the EntE C α atoms from the EntA-EntB-EntE ternary complex model. Upon superposition of the EntE backbones, the ArCP domain from the crystal structure superimposed well with the ArCP domain from the ternary complex model (Fig. 2C). Given that the initial docking of EntB to the EntA-EntE complex was blind, the observed superposition of the ArCP domains demonstrates that the ternary complex model obtained by ClusPro is consistent with current knowledge of EntA-EntE and EntE-EntB interactions.

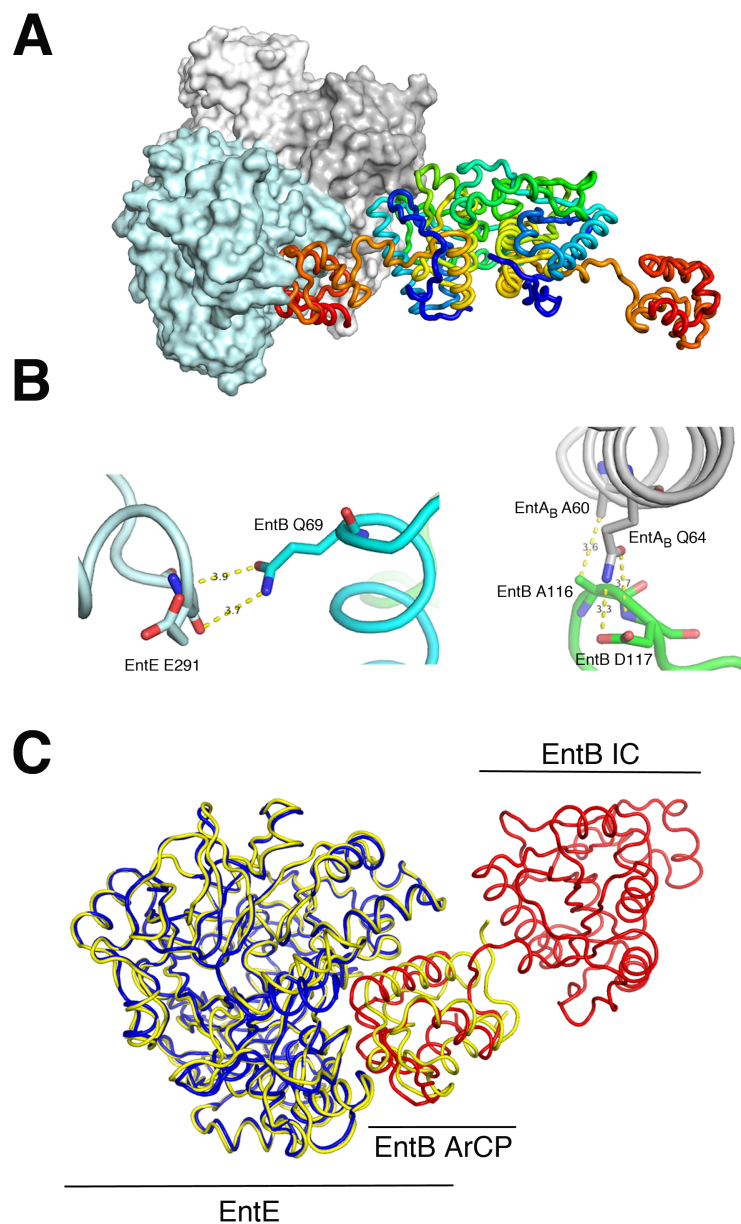


Figure 2: Computational modeling of the *E. coli* EntA-EntB-EntE complex. (A) ClusPro model of EntA-EntB-EntE ternary complex showing EntB dimer (coils, colored from N-terminus (blue) to C-terminus (red)) docked to the EntA-EntE model reported previously [131] (protein subunits shown as van der Waals surfaces; light blue: EntE, dark grey: B-chain of EntA tetramer, light grey: A-chain of EntA tetramer; the D-chain of the EntA tetramer is below the B-chain and also colored light grey; the C chain of the EntA tetramer is not visible in this representation). (B) Left panel: interaction of EntE E291 with EntB Q69; EntE: light blue, EntB: cyan. Right panel: interaction of A60 and Q64 from the B subunit of EntA with EntB residues A116 and D117, respectively; EntA: dark grey, EntB: green. Atoms are shown in stick representations and colored by element. Dotted lines represent predicted contacts; numbers represent distances in Ångstrom units. (C) Superposition of the EntE-EntB (ArCP) crystal structure (yellow) with the EntE (blue) and EntB (red) chains from the ternary complex model. Only one EntB subunit from the model is shown. Protein chains are shown in the coil representation.

4.4.3 Interaction of EntA and EntE with the EntB IC domain

Since the model of EntA-EntB-EntE complex predicted direct interaction of the EntB IC domain with both EntA and EntE, we prepared a BACTH construct expressing the EntB IC domain alone in order to experimentally investigate EntB IC domain interactions. DNA encoding the EntB IC domain (residues 1-207) was cloned into pUT18C and pKT25 to produce BACTH constructs expressing T18-IC and T25-IC. CAS assays and growth studies were used to validate the functionality of the discretely expressed EntB IC domain. To test for functionality of the isolated IC domain, it was co-expressed in *entB*⁻ cells with the isolated EntB ArCP domain. We co-transformed the *entB*⁻ strain with pKT25-IC and pFBH1-ArCP (a protein expression construct under the control of the *E. coli* iron regulator Fur). When grown on CAS agar plates, the co-transformant exhibited an orange halo (Fig. 3A, left spot). In contrast, no CAS halo was observed for *entB*⁻ cells co-transformed with the vector control pKT25 and pFBH1-ArCP (Fig. 3A, middle spot), or with pKT25-IC and the vector control pFBH1 (Fig. 3A, right spot). Bacterial growth studies were in agreement with our CAS assay outcomes. *E. coli entB*⁻ cells co-expressing T25-IC/ArCP grew at wild-type levels in iron-deprived minimal media (Fig 3B, column 1). In contrast, no significant growth was observed when constructs encoding T25-IC or ArCP were co-transformed with respective empty vector controls (Fig. 3B, columns 2 and 3). These outcomes demonstrated that the EntB IC and ArCP domains do not have to be connected in a single polypeptide in order to support intracellular enterobactin biosynthesis. Furthermore, we showed that the IC domain remained functional when N-terminally fused with a BACTH fragment.

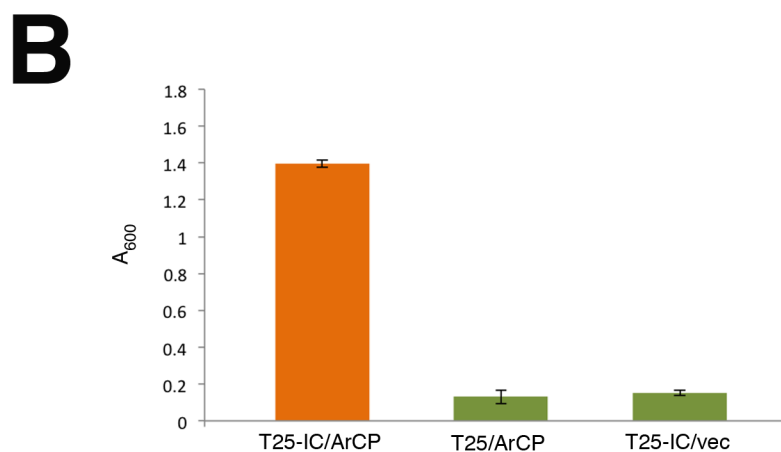
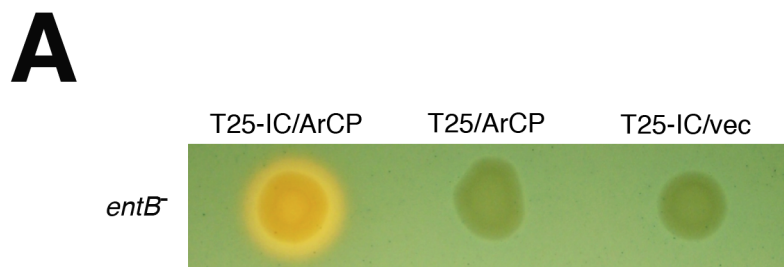


Figure 3: Functional validation of EntB IC domain BACTH construct. (A) Photograph of CAS agar plates spotted with *E. coli entB* cells co-transformed with pKT25-IC/pFBH1-*ArCP* (left spot); pKT25/pFBH1-*ArCP* (middle spot); pKT25-IC/pFBH1 (right spot). (B) Bacterial growth studies of *E. coli entB* co-transformants. Growth studies were performed in iron-depleted minimal medium at 30 °C. Cell densities measured as absorbances at 600 nm (A_{600}). Orange bar indicates transformant that exhibited a positive CAS signal; error bars represent standard deviations from mean values. Left to right: pKT25-IC/pFBH1-*ArCP*; pKT25/pFBH1-*ArCP*; pKT25-IC/pFBH1.

BACTH constructs expressing the isolated EntB IC domain were used in co-transformation experiments with EntA and EntE. Figure 4A shows BACTH outcomes of EntA co-expressed with the EntB IC domain. Co-transformation of pUT18C-*entA* with pKT25-*IC* resulted in a red colony on MacConkey agar media, indicative of a positive two-hybrid signal (Fig. 4A, upper panel, left spot). In contrast, co-transformation of pUT18C empty vector with pKT25-*IC* did not result in a two-hybrid signal (Fig. 4A, upper panel, right spot). Co-transformation of pUT18C-*IC* with pKT25-*entA* also yielded a two-hybrid signal (Fig. 4A, lower panel, left spot), whereas co-transformation of pUT18C-*IC* with pKT25 did not (Fig. 4A, lower panel, right spot). β -galactosidase assays supported the plate-based assays in that elevated β -galactosidase activity was only observed when T18/T25-EntA was co-expressed with T25/T18-*IC*, in comparison with vector controls (Fig. 4A, upper and lower bar graphs). We then investigated potential interaction of EntE with the EntB IC domain (Fig. 4B). Co-transformation of pKT25-*entE* with pUT18C-*IC* in *E. coli* BTH101 cells resulted in a positive two-hybrid signal (Fig. 4B, upper panel, left spot), whereas transformation of pKT25 empty vector with pUT18C-*IC* did not (Fig. 4B, upper panel, right spot). Similarly, the pUT18C-*entE*/pKT25-*IC* co-transformant yielded a positive two-hybrid signal unlike the pUT18C/pKT25-*IC* control (Fig. 4B, lower panel, left and right spots, respectively). Corresponding β -galactosidase assays of co-transformants indicated elevated activity upon co-expression of T25-EntE with T18-*IC* (Fig. 4B, upper bar graph) or co-expression of T18-EntE with T25-*IC* (Fig. 4B, lower bar graph). Taken together, the BACTH outcomes support the computational model of the EntA-EntB-EntE complex since EntB IC was found by BACTH to interact with both EntA and EntE within *E. coli* cells. Since we showed that the EntB IC and ArCP domains are functionally independent, this suggests that they are organized within the EntB protein to structurally anchor an intracellular EntA-EntB-EntE ternary complex. Further experiments are now being performed to directly investigate the ternary

complex as well as the role of EntB as a hub protein, since it is known to also interact with EntD, EntF and EntH [9,71,93].

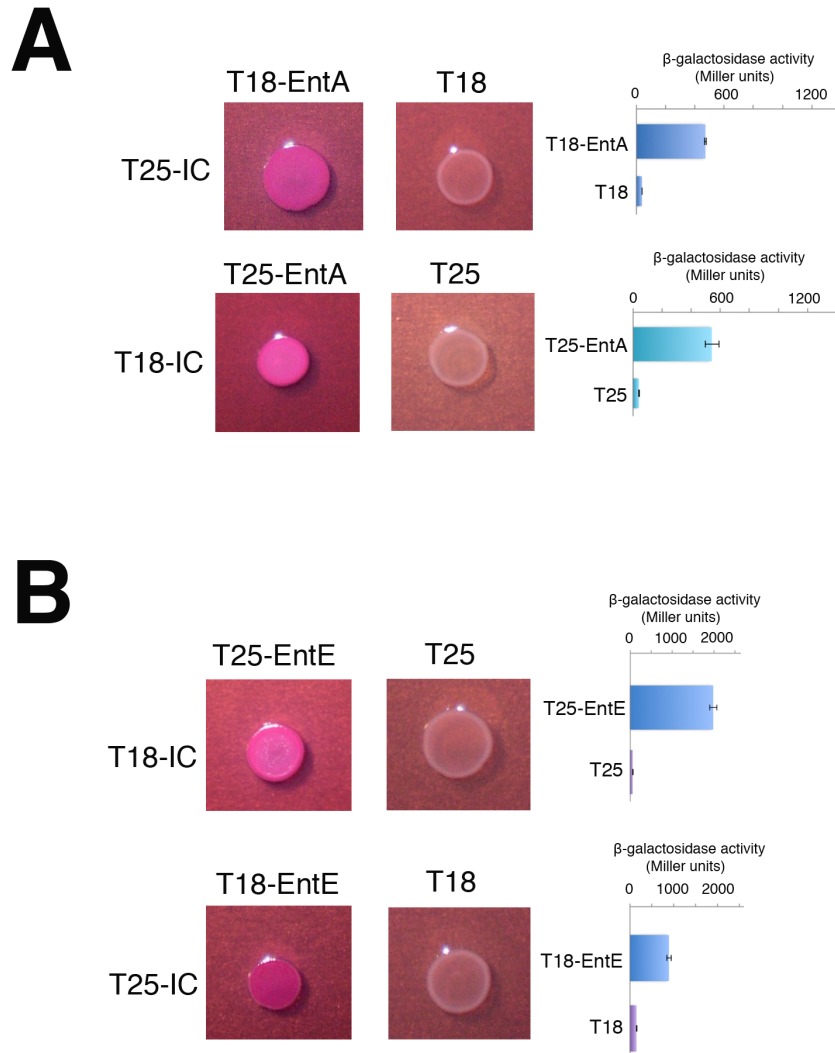


Figure 4: Intracellular co-localization of EntB IC domain with EntA and EntE. Photographs are of *E. coli* BTH101 co-transformants spotted onto MacConkey agar plates. Bar graphs represent BACTH β-galactosidase assays. (A) Interaction of EntB IC domain with EntA. Upper left panel: pUT18C-*entA*/pKT25-*IC*. Upper right panel: pUT18C/pKT25-*IC*. Upper bar graph: β-galactosidase assays of pUT18C-*entA*/pKT25-*IC* co-transformant (upper) and pUT18C/pKT25-*IC* co-transformant (lower). Lower left panel: pKT25-*entA*/pUT18C-*IC*. Lower right panel: pKT25-*entA*/pUT18C. Lower bar graph: β-galactosidase assays of pKT25-*entA*/pUT18C-*IC* co-transformant (upper) and pKT25-*entA*/pUT18C co-transformant (lower). (B) Interaction of EntB IC domain with EntE. Upper left panel: pKT25-*entE*/pUT18C-*IC*. Upper right panel: pKT25/pUT18C-*IC*. Upper right bar graph: β-galactosidase assays of pKT25-*entE*/pUT18C-*IC* co-transformant (upper) and pKT25/pUT18C-*IC* co-transformant (lower).

Chapter 5: General Discussion

Many leading research topics in biology and biochemistry involve processes in which protein complexes have been recognized as critical components. Protein-protein interactions are essential for the majority of cellular functions and can therefore be considered as good druggable targets [4,65].

One cellular process that relies on protein-protein interactions that could be a potential target for drug development is siderophore biosynthesis. Siderophore-mediated iron uptake is a process in which microorganisms such as bacteria scavenge iron from the environment. Iron taken up in this manner is essential for growth and survival of most bacteria [13].

The protein-protein interactions in the biosynthetic pathway of enterobactin, the catecholate siderophore of *E. coli*, are the main focus of this thesis. The enterobactin biosynthetic pathway is divided into two functional arms: the DHB module (EntC, EntB (IC domain) and EntA) and the NRPS module (EntE, EntB (ArCP domain), EntF and EntD). Protein-protein interactions in the NRPS module have been previously identified [6,65]; however, evidence of protein-protein interactions in the DHB module has remained elusive. The research presented in this thesis advances our knowledge of these processes. We studied the subunit orientation in the EntA-EntE complex that bridges the DHB and NRPS modules (Chapter 2). The work in Chapter 3 is centered on the design and generation of the two novel Fur-controlled vectors that can be used for iron-controlled gene expression and the study of protein-protein interactions under iron deprivation. We have also reported a novel protein-protein interaction, EntA-EntB, in the DHB module (Chapter 4).

5.1 Subunit Orientation in the EntA-EntE Complex

Our research group had previously reported and characterized an interaction between EntA, the last enzyme in the DHB module, and EntE, the first enzyme in the NRPS module [65]. We used BACTH and blind docking simulations to gain further insight into the orientation of EntA relative to EntE in the EntA-EntE complex [131]. The outcomes of this study demonstrated that the N-termini of EntA and EntE are proximal in the complex. Further experiments are required to validate the EntA-EntE model that is discussed in Chapter 6, Section 6.1. The bacterial adenylate cyclase two-hybrid (BACTH) assay is a technique used for identification and/or validation of interacting partners within the *E. coli* cells. In this study BACTH was used to validate previously reported biophysical data on EntA-EntE interaction. Furthermore, the presence or absence of a BACTH signal in N- or C-terminally tagged constructs provided some useful information on the directionality of interacting partners, which was supported by the docking simulation experiment. Therefore, two-hybrid approaches could also be useful in studying the subunit orientation in the protein complexes. However, the experimental results obtained by such methods need to be validated by complementary experimental and computational approaches.

The research outcomes presented in Chapter 2, could guide us to identify the exact residues at the interaction interface that could potentially be beneficial for drug discovery approaches where high-throughput screenings are performed to identify the potential small molecule inhibitors of a specific protein-protein interaction [139].

5.2 Design and Generation of Fur-controlled Protein Expression Vectors

The work presented in Chapter 3 focused on the design and generation of two vectors under the control of Fur. Two low copy number plasmids, pACYC184 and pBR322 vectors were used as the backbone for the generation of pFCF1 and pFBH1, respectively. These vectors are comprised

of a bidirectional iron responsive promoter, FLAG or HA epitope tags, TEV cleavage site and a multiple cloning site (MCS) compatible with BACTH vectors. The promoter region exists between *fepB* and *entC* in *E. coli* chromosome and contains two non-overlapping Fur boxes.

Fur is known as a global regulator in bacteria and is involved in various cellular processes such as iron homeostasis, oxidative stress response and acid tolerance [115]. Fur may also have a role in bacterial pathogenicity [69,70,115]. It has been reported that 82 genes in *E. coli* are under the regulation of Fur [121]. Given the importance and ubiquity of Fur regulation, the pFCF1 and pFBH1 vectors could become very handy in the studies of Fur regulated genes. Furthermore, these vectors can be used for expression of genes that are under the regulation of different promoters. The compatibility of the vectors makes it possible to perform co-purification experiments under iron starvation, which could be a convenient follow-up for the BACTH studies. The MCS of pFCF1 and pFBH1 are compatible with BACTH vectors that facilitate the transfer of the genes of interest from one vector set to another. The bidirectionality of the promoter allows for the simultaneous expression of two proteins of interest or one protein of interest along with a reporter protein to monitor the level of protein expression. In addition, engineering the T18 and T25 fragments upstream or downstream of the genes of interest may result in a modified BACTH system where a protein interaction of interest could be studied under iron starvation. This system could therefore be useful to study the siderophore biosynthesis machinery in different microorganisms.

5.3 “ABE Complex”: Ternary Complex Formation between EntA, EntB and EntE

Chapter 4 focused on the ternary complex formation between EntA, EntB and EntE. EntA is the last enzyme in the DHB module of enterobactin biosynthesis. EntB is a bifunctional enzyme that

participates in the DHB module *via* its IC domain and is involved in the NRPS module through its ArCP domain and EntE is the first enzyme in the NRPS module. The interaction between EntE and the ArCP domain of EntB, and EntE and EntA have already been reported [65,77,131]. Using the BACTH assay we reported the first evidence of an interaction between EntB and EntA. Given the previous data on EntB-EntE and EntA-EntE interactions, we hypothesized the formation of ternary complex between EntA, EntB and EntE. Docking simulations and BACTH assays with dissected EntB demonstrated that IC domain of EntB is involved in the interaction with both EntA and EntE. Further experiments for validation and characterization of the hypothesized “ABE complex” are required, which is discussed in Chapter 6, Section 6.2. The work presented in Chapter 4 sheds light on higher-order complexation in *E. coli* enterobactin biosynthesis pathway, which is required for production of enterobactin to be transported to the extracellular environment. Higher-order complexation has also been observed for siderophore biosynthetic proteins in other bacteria, such as pyoverdine biosynthetic proteins in *Pseudomonas aeruginosa* and bacillibactin biosynthetic proteins in *Bacillus subtilis* [85,140,141].

Pyoverdine is a catecholate siderophore that is synthesized in *Pseudomonas* cytoplasm by four NRPS enzymes, PvdL, PvdI, PvdJ and PvdD [85,142]. The siderophore product of the NRPS enzymes is then transferred to the periplasm where it undergoes maturation and is then secreted to the extracellular environment to chelate iron. In addition to NRPS enzymes, PvdH, PvdA and PvdF are involved in the biosynthesis of pyoverdine [143]. It has been shown that PvdA is a membrane bound protein; the interaction and co-localization of the NRPS enzymes with the PvdA have also been reported [144]. Thus, it has been suggested that pyoverdine NRPS enzymes form a multienzyme complex that is anchored to the membrane by virtue of PvdA. The name “siderosome” has been proposed for this multienzyme complex that is believed to increase the efficiency of precursor transfer between biosynthetic enzymes and the secretion machinery [85].

Bacillibactin is the catecholate siderophore of *B. subtilis*. Similar to enterobactin biosynthesis in *E. coli*, bacillibactin is produced in two steps. First, DHB is synthesized through the action of DhbC, DhbB (IC domain) and DhbA. In the second step bacillibactin, a cyclic trimer of DHB-glycine-threonine, is synthesized *via* the NRPS enzymes DhbE, DhbB (ArCP domain) and DhbF [141,145]. The NRPS module in bacillibactin biosynthesis requires obligate protein interactions similar to what has been observed for the enterobactin biosynthetic NRPS enzymes [141]. It has been reported that secretion of bacillibactin is mediated by YmfE, an MFS-type exporter, which is comprised of six transmembrane domains. The 13-amino acid conserved domain, which is believed to be involved in substrate channeling in MFS-type exporters, exists in the YmfE [140]. Therefore, it is possible that substrate channeling may exist in the bacillibactin biosynthesis and secretion pathways, similar to what we hypothesize for enterobactin biosynthesis and secretion.

5.4 Conclusion

The outcomes of the current thesis will pave the way to investigate the possibility of substrate channeling in the enterobactin biosynthesis pathway. Substrate channeling is a process through which an intermediate product of an enzyme is directly transferred to the consecutive enzyme. This process increases the efficiency of the intermediate transport and lowers the degradation of the intermediate product in solution. Furthermore, substrate channeling could prevent the competition between the enzyme of interest and other enzymes for the same intermediate product [146]. Substrate channeling could occur between multiple sequential enzymes that form transient association during the process. The multi-enzyme complex involved in substrate channeling has been referred to as a "metabolon", which could be anchored to the membrane or cytoskeleton [147,148]. In a recent study, the structural evidence of substrate channeling in the Krebs cycle metabolon in mitochondria has been reported [147]. The presence of a membrane transport

metabolon in *E. coli* has also been suggested as a result of co-crystallization of YchM, a member of the family of anion transporters, and acyl carrier protein (ACP) that is involved in fatty acid metabolism [149,150].

Extending the research outcomes reported in this thesis, we hypothesize that enterobactin biosynthetic enzymes form a metabolon that is anchored to the inner membrane of *E. coli* by virtue of EntF, the last enzyme in the NRPS module, and EntS, an MFS inner membrane transporter, interaction. To further study this hypothesis, remaining protein-protein interactions between Ent proteins need to be exhaustively characterized. Such a comprehensive mapping approach will also be useful in the development of high-throughput screening approaches to identify small-molecule inhibitors of Ent protein-protein interactions. Membrane localization of the hypothesized “Ent metabolon” also needs to be investigated, which will be discussed in more detail in Chapter 6, Section 6.4.

Chapter 6: Work in Progress and Future Directions

6.1 Identification of Residues at the Interaction Interface of EntA-EntE Complex

Based on the work presented in Chapter 2, the N-termini of EntA and EntE are proximal in the EntA-EntE complex. Using the A-E docked model, the residues at the interaction interface can be identified and mutated. Site directed mutagenesis would allow us to study the effects of mutations on EntA-EntE interaction. Furthermore, the BACTH technique used successfully in the research reported here can be used to study the impact of small-molecule inhibitors on disrupting the EntA-EntE interaction [151,152], which could potentially lead to identification of antimicrobial agents.

6.2 Validation and Characterization of EntA and EntB Interaction

The BACTH outcomes for EntA-EntB suggest that these two proteins interact. However, more experiments are required to validate BACTH results. To confirm the EntA-EntB interaction, pull-down assays will need to be performed in which pFBH1-*entB* (Chapter 3) would be transformed into *E. coli* BW25113 and grown under iron deprivation and cell lysate from the iron starved bacterial cultures will be incubated with the bait protein, GST-EntA. Furthermore, the formation of the EntA-EntB-EntE complex could be studied by co-transforming pFBH1-*entB* and pFCF1-*entE* into *E. coli* cells and the EntB-E complex can be pulled down using GST-EntA as bait.

The above proposed work is already in progress. Prey constructs have been generated and their functionality validated (Chapter 3). The bait construct pGEX-*entA* has also been prepared using pGEX-4tev vector (this vector was kindly provided by Dr. Alisa Piekny). The functionality of pGEX-*entA* construct was confirmed by performing CAS assay and growth studies (Fig. 1A) as

described in previous chapters. The GST-EntA bait was purified on glutathione beads (GE Healthcare) (Fig. 1B) and stored at -80 °C for future use. The pull-down experiment conditions are currently under optimization.

In support of the pull-down assays, purified EntA and EntB proteins could be used to further characterize the interaction using biophysical techniques such as ITC to determine the binding constant (K_A) of the EntA-EntB complex.

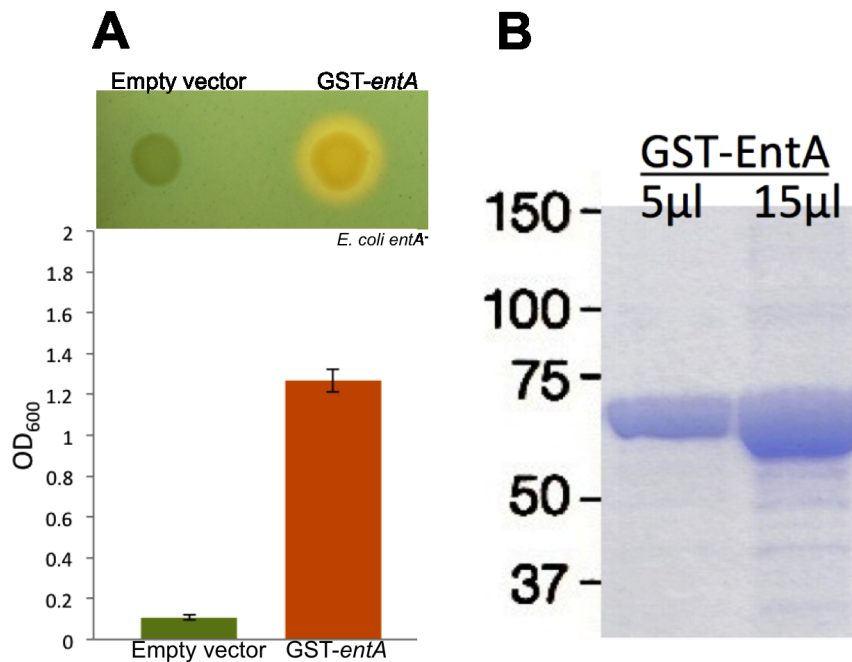


Figure 1: Functionality assays and protein purification for pGEX-*entA* construct. (A) CAS assay and growth studies for pGEX-*entA* construct and vector control, pGEX-*entA* complemented the knockout phenotype in both experiments while the empty vector control neither produced orange halo on CAS plate nor exhibited high growth signal, (B) GST-EntA was purified on glutathione beads.

6.3 Identification of Novel Protein Interactions in the DHB Module

In addition to EntA-EntB interaction, our research group is also interested in the study of the interaction between EntC and EntB. The BACTH constructs for *entC* have been prepared and the

functionality of the constructs was verified by CAS assay and growth studies. We found that the T18/T25-*entC* construct rescued the knockout phenotype regardless of the directionality of the reporter fragments (Fig. 2). BACTH experiments were also performed on a T18/T25-*entC* and T25/T18-*entB* co-transformant, however the BACTH outcomes were inconclusive due to stickiness of EntC and BACTH reporter fragment. To circumvent this problem, the BACTH experimental conditions will need to be optimized or another two-hybrid technique should be employed. Furthermore, the BACTH protocol could be replaced by a pull-down assay as the primary means of identification of the potential interaction between EntC and EntB.

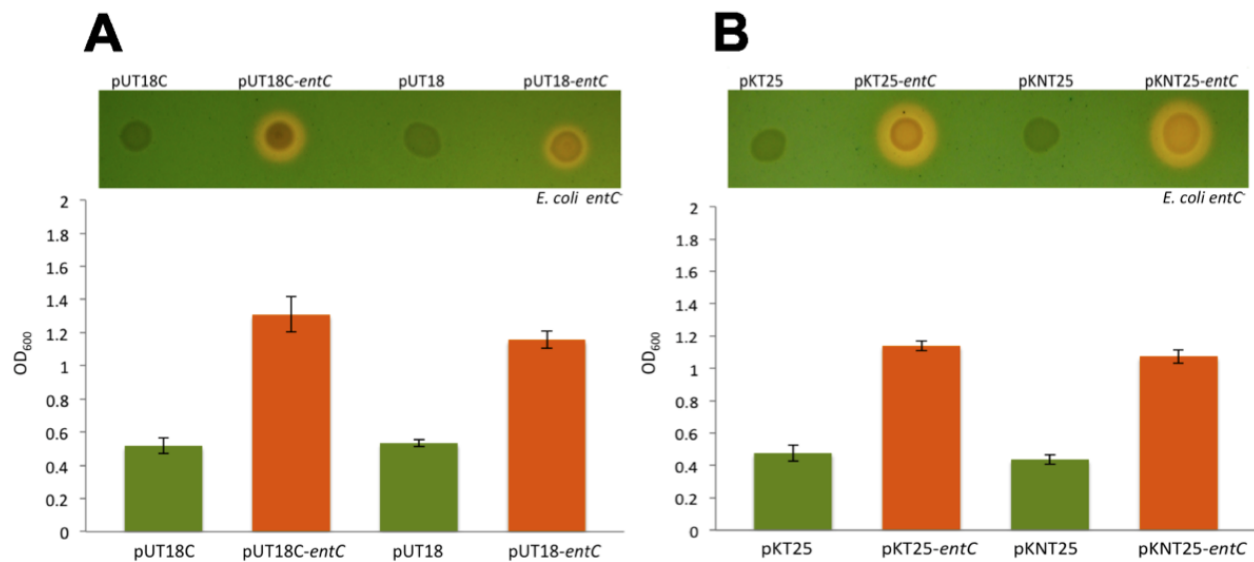


Figure 2: CAS assays and growth studies for *entC* BACTH constructs. Both N and C-terminally T18/T25 tagged EntC complemented the knockout phenotype in CAS assays and growth studies.

6.4 Membrane Localization of Enterobactin Biosynthetic Machinery

As mentioned earlier, it has been shown that the pyoverdine biosynthetic module is anchored to the *Pseudomonas* membrane [85]. Furthermore, Hantash and Earhart have shown the presence of small fraction of EntB, EntE and EntF in membrane in addition to cytoplasm [84]. Our laboratory hypothesize that the enterobactin biosynthetic machinery is anchored to the *E. coli* inner membrane by virtue of EntF-EntS interaction. To further investigate our hypothesis, in collaboration with Dr. Johan Hofkens group (KU Leuven, Belgium), we employed photo-activated localization microscopy (PALM) to study the co-localization and membrane localization of the Ent proteins. Super resolution microscopy is an imaging technique that has pushed the limits of optical resolution from ~250 nm to ~10 nm [153,154]. Photoactivated localization microscopy (PALM) is a super-resolution technique, which has a resolution around 10 nm. Therefore, it can be used for detection of protein interactions in *E. coli* cells (cell dimension ~ 2 microns). This method has been successfully used to visualize near membrane localization of *E. coli* protein, OmpR, under acidic conditions [155], in another study PALM was used to study the dynamics of RNA polymerase in nutrient rich (LB) vs. nutrient poor (M9) media [156]. To visualize proteins in PALM two major classes of fluorescent proteins (FPs) can be used: photoconvertible and photoswitchable FPs. The former class can be converted into a red fluorescent state by illumination of the UV light (*e.g.*, mEos2, Dendra) while the latter converts from dark state to fluorescent state upon photoactivation (*e.g.*, Dronpa, PAmCherry) [157,158].

As part of the research related to this thesis, numerous FPs were fused to Ent proteins (PAmCherry, eYFP, mEos2, mEos3.2, Dronpa and Dendra were fused to EntA, EntB, EntE and EntS). PALM imaging of Ent-FP fusion proteins is currently in progress in collaboration with the Hofkens lab. If successful, this microscopy approach will provide the first direct evidence of co-

localized interacting Ent proteins in a living cell. Furthermore, we will be able to directly determine if these co-localizing proteins are anchored to the *E. coli* inner membrane.

References

1. Perry J. A., Westman E. L., Wright G. D. (2014) The antibiotic resistome: what's new?, *Curr. Opin. Microbiol.* **21**: 45-50.
2. Hoerr, V., Duggan, G.E., Zbytniuk, L., Poon, K. K. H., Große, C., Neugebauer, U., Methling, K., Löffler, B., Vogel, H. J. (2016) Characterization and prediction of the mechanism of action of antibiotics through NMR metabolomics, *BMC Microbiology*, **16**:82, 1-14.
3. Marceau, A. H., Bernstein, D. A., Walsh, B. W., Shapiro, W., Simmons, L. A., Keck, J. L., (2013) Protein Interactions in Genome Maintenance as Novel Antibacterial Targets. *PLoS ONE* **8**(3): e58765.
4. London, N., Raveh, B., Schueler-Furman, O. (2013) Druggable protein–protein interactions – from hot spots to hot segments, *Curr. Opin. Chem. Biol.*, **17**: 952-959.
5. Arkin, M. R., Tang, Y., Wells, J. A. (2014) Small-Molecule Inhibitors of Protein-Protein Interactions: Progressing toward the Reality, *Chem. & Biol.*, **21**: 1102-1114.
6. Khalil, S., Pawelek, P. D. (2009) Ligand-induced conformational rearrangements promote interaction between the *Escherichia coli* enterobactin biosynthetic proteins EntE and EntB, *J. Mol. Biol.* **393**: 658-671.
7. Berggård, T., Linse, S., James, P. (2007) Methods for the detection and analysis of protein–protein interactions, *Proteomics* **7**:2833-2842.
8. Drake, E. J., Nicolai, D. A., Gulick, A. M. (2006) Structure of the EntB multidomain nonribosomal peptide synthetase and functional analysis of its interaction with the EntE adenylation domain, *Chem. Biol.* **13**: 409-419.
9. Lai, J. R., Fischbach, M. A., Liu, D. R., Walsh, C. T. (2006) Localized protein interaction surfaces on the EntB carrier protein revealed by combinatorial mutagenesis and selection, *J. Am. Chem. Soc.* **128**: 11002-11003.
10. Earhart, C. F. (1996) Uptake and metabolism of iron and molybdenum, *Escherichia coli* and *Salmonella*: cellular and molecular biology. *ASM Press, Washington* **1,2**, 1075-1090.
11. Anderson, G. J., Vulpe, C. D. (2009) The cellular physiology of iron, Iron Deficiency and Overload: From Basic Biology to Clinical Medicine (Nutrition and Health). Humana Press, 3-29.
12. Johnstone, T. C., Nolan E. M. (2015) Beyond iron: non-classical biological functions of bacterial siderophores, *Dalton Trans.***44**: 6320-6339.
13. Miethke, M., Marahiel, M. A. (2007) Siderophore-based iron acquisition and pathogen control, *Microbiol. Mol. Biol. Rev.* **71**: 413-451.
14. Beauchene, N. A., Myers, K. S., Chung D., Park D. M., Weisnicht, A. M., Keles S., Kiley, P. J. (2015) Impact of Anaerobiosis on Expression of the Iron-Responsive Fur and RyhB Regulons, *mBio.* **6**: e01947-15.
15. de Lorenzo, V., Perez-Martin, J., Escolar, L., Pesole, G., Bertoni, G. (2004) Mode of binding of the Fur protein to target DNA: negative regulation of Iron-controlled gene expression, In Iron transport in bacteria (Crosa, J. H., Mey, A. R., and Payne, S. M., Eds.), *ASM Press, Washington D.C.*
16. Ghassemian M., Straus N. A. (1996) Fur regulates the expression of iron-stress genes in the cyanobacterium *Synechococcus* sp. strain PCC 7942, *Microbiology* **142**: 1469-1 476.

17. Lewin, A. C., Doughty, P. A., Flegg, L., Moore, G. R., Spiro, S. (2002) The ferric uptake regulator of *Pseudomonas aeruginosa* has no essential cysteine residues and does not contain a structural zinc ion, *Microbiology* **148**: 2449–2456.
18. Xiong, A., Singh, V. K., Cabrera, G., Jayaswal R. K. (2000) Molecular characterization of the ferric-uptake regulator, Fur, from *Staphylococcus aureus*, *Microbiology* **146**, 659–668.
19. De Zoysa, A., Efstratiou, A., Hawkey, P.M. (2005) Molecular Characterization of Diphtheria Toxin Repressor (dtxR) Genes Present in Nontoxigenic *Corynebacterium diphtheriae* Strains Isolated in the United Kingdom, *J. Clin. Microbiol.* **43**: 223-228.
20. Porcheron, G., Habib, R., Houle, S., Caza, M., Lépine, F., Daigle, F., Massé, E., Dozoisa, C. M. (2014) The Small RNA RyhB Contributes to Siderophore Production and Virulence of Uropathogenic *Escherichia coli*, *Infection & Immunity*, **82**: 5056-5068.
21. Masse, E., Gottesman, S. (2002) A small RNA regulates the expression of genes involved in iron metabolism in *Escherichia coli*, *Proc. Natl. Acad. Sci. USA* **99**: 4620-4625.
22. Gozzelino, R., Arosio, P. (2016) Iron Homeostasis in Health and Disease, *Int. J. Mol. Sci.* **17**, 130.
23. Lawen, A., Lane, D. J. R. (2013) Mammalian Iron Homeostasis in Health and Disease: Uptake, Storage, Transport, and Molecular Mechanisms of Action, *Antioxidants & Redox Signaling*, **18**: 2473-2507.
24. Perkins-Balding, D., Ratliff-Griffin, M., Stojiljkovic, I. (2004) Iron Transport Systems in *Neisseria meningitidis*, *Microbiol. Mol. Biol. Rev.* **68**: 154-171.
25. Jenssen, H., Hancock, R. E. W. (2009) Antimicrobial properties of lactoferrin, *Biochimie* **91**:19-29.
26. González-Chávez, S. A., Arévalo-Gallegos, S., Rascón-Cruz, Q. (2009) Lactoferrin: structure, function and applications, *Int. J. of Antimicrobial Agents* **33**: 301.e1–301.e8.
27. Farnaud, S., Evans, R. W. (2003) Lactoferrin—a multifunctional protein with antimicrobial properties, *Molecular Immunology* **40**: 395–405.
28. Pakdaman, R., Petitjean, M. El Hage Chahine, J. M. (1998) Transferrins-A mechanism for iron uptake by lactoferrin, *Eur. J. Biochem.* **254**, 144-153.
29. Zhang, A. S., Enns, C. A. (2009) Iron Homeostasis: Recently Identified Proteins Provide Insight into Novel Control Mechanisms, *J. Biol. Chem.* **284**: 711–715.
30. Finazzi, D., Arosio, P. (2014) Biology of Ferritin in Mammals: an Update on Iron Storage, Oxidative Damage and Neurodegeneration, *Arch Toxicol* **88**:1787–1802.
31. Sandy, M., Butler, A. (2009) Microbial Iron Acquisition: Marine and Terrestrial Siderophores, *Chem. Rev.* **109**: 4580–4595.
32. Segond, D., Abi Khalil, E., Buisson, C., Daou, N., Kallassy, M., Lereclus, D., Arosio, P., Bou-Abdallah, F., Le Roux, C. N. (2014) Iron Acquisition in *Bacillus cereus*: The Roles of IIsA and Bacillibactin in Exogenous Ferritin Iron Mobilization, *PLoS Pathog.* **10(2)**: e1003935.
33. Pawelek, P. D., Coulton, J. W. (2004) Hemoglobin-binding protein HgbA in the outer membrane of *Actinobacillus pleuropneumoniae*: homology modelling reveals regions of potential interactions with hemoglobin and heme, *J. Mol. Graphics and Modelling* **23**: 211–221.
34. Cescau, S., Cwerman, H., Letoffee, S., Delepelaire, P., Wandersman, C., Biville, F. (2007) Heme acquisition by Hemophores, *Biometals* **20**:603–613.
35. Hider, R. C., Kong, X. (2010) Chemistry and biology of siderophores, *Nat. Prod. Rep.* **27**:637–657.

36. Ahmed, E., Holmström, S. J. M. (2014) Siderophores in environmental research: roles and applications, *Biotechnology*, **7**:196–208
37. Masse, E., Pawelek, P. D. (2009) Iron as Nutrient: Strategies for Iron Acquisition and Usage by Pathogenic Microorganisms, Iron Deficiency and Overload: From Basic Biology to Clinical Medicine (Nutrition and Health). Humana Press, 65-76.
38. Payne, S. M. (1994) Detection, isolation, and characterization of siderophores, *Methods Enzymol.* **235**:329-344.
39. Furrer, J. L., Sanders, D. N., Hook-Barnard, I. G., McIntosh, M. A. (2002) Export of the siderophore enterobactin in *Escherichia coli*: involvement of a 43 kDa membrane exporter, *Mol. Microbiol.* **44**:1225-1234.
40. Hertlein G, Muller S, Garcia-Gonzalez E, Poppinga L, Sussmuth RD, Genersch, E. (2014) Production of the Catechol Type Siderophore Bacillibactin by the Honey Bee Pathogen *Paenibacillus larvae*. *PLoS ONE* **9**(9): e108272.
41. Balbontin, R., Villagra, N., de la Gandara, M. P., Mora, G., Figueroa-Bossi, N., Bossi, L. (2016) Expression of IroN, the salmochelin siderophore receptor, requires mRNA activation by RyhB small RNA homologues, *Mol. Microbiol.* **100**: 139–155
42. Lin, H., Fischbach, M. A., Liu, D. R., Walsh, C.T. (2005) *In Vitro* Characterization of Salmochelin and Enterobactin Trilactone Hydrolases IroD, IroE, and Fes, *J. Am. Chem. Soc.* **127**:11075-11084.
43. Cornelis, P., Dingemans, J. (2013) *Pseudomonas aeruginosa* adapts its iron uptake strategies in function of the type of infections, *Front Cell Infect Microbiol*, **3**(75): 1-7
44. Braud, A., Geoffroy, V., Hoegy, F., Mislin, G. L. A., Schalk, I. J. (2010) Presence of the siderophores pyoverdine and pyochelin in the extracellular medium reduces toxic metal accumulation in *Pseudomonas aeruginosa* and increases bacterial metal tolerance, *Environ Microbiol Rep.* **2**:419–425.
45. Haas, H. (2014) Fungal siderophore metabolism with a focus on *Aspergillus fumigatus*, *Nat. Prod. Rep.* **31**: 1266-1276.
46. Sutak, R., Lesuisse, E., Tachezy, J., Richardson, D. R. (2008) Crusade for iron: iron uptake in unicellular eukaryotes and its significance for virulence, *Trends Microbiol.* **6**: 261–268.
47. Gómez-Galera, S., Sudhakar, D., Pelacho, A. M., Capell, T., Christou, P. (2012) Constitutive expression of a barley Fe phytosiderophore transporter increases alkaline soil tolerance and results in iron partitioning between vegetative and storage tissues under stress, *Plant Phys. Biochem.* **53**: 46-53.
48. Devireddy, L. R., Hart, D. O., Goetz, D. H., Green, M. R. (2010) A Mammalian Siderophore Synthesized by an Enzyme with a Bacterial Homolog Involved in Enterobactin Production *Cell* **141**:1006–1017.
49. Bao, G., Clifton, M., Hoette, T. M., Mori, K., Deng, S. X., Qiu, A., Viltard, M., Williams, D., Paragas, N., Leete, T., Kulkarni, R., Li, X., Lee, B., Kalandadze, A., Ratner, A. J., Pizarro, J. C., Schmidt-Ott, K. M., Landry, D. W., Raymond, K. N., Strong, R. K., Barasch, J. (2010) Iron traffics in circulation bound to a siderocalin (Ngal)-catechol complex, *Nat Chem Biol.* **6**: 602-609.
50. Liu, Z., Reba, S., Chen, W. D., Porwal, S. K., Boom, W. H., Petersen, R. B., Rojas, R., Viswanathan, R., Devireddy, L. (2014) Regulation of mammalian siderophore 2,5-DHBA in the innate immune response to infection, *J Exp Med.* **211**:1197-213.

51. Xiao, X., Yeoh, B. S., Saha, P., Olvera, R. A., Singh, V., Vijay-Kumar, M. (2016) Lipocalin 2 alleviates iron toxicity by facilitating hypoferremia of inflammation and limiting catalytic iron generation, *Biometals*. **29**: 451-65.
52. Fischbach, M. A., Lin, H., Liu, D. R., Walsh, C.T. (2006) How pathogenic bacteria evade mammalian sabotage in the battle for iron, *Nat Chem Biol*. **2**:132-138.
53. Allred, B. E., Correnti, C., Clifton, M. C., Strong, R.K., Raymond, K.N. (2013) Siderocalin outwits the coordination chemistry of vibriobactin, a siderophore of *Vibrio cholera*, *ACS Chem Biol*. **8**:1882-1887.
54. Li, W., Cui, T., Hu, L., Wang, Z., Li, Z., He, Z. G. (2015) Cyclic diguanylate monophosphate directly binds to human siderocalin and inhibits its antibacterial activity, *Nat Commun*. **6**:8330.
55. O'Brien, S., Hodgson, D. J., Buckling, A. (2014) Social evolution of toxic metal bioremediation in *Pseudomonas aeruginosa*, *Proc Biol Sci*. **281**: 20140858.
56. Zheng, T., Bullock, J. L., Nolan, E. M. (2012) Siderophore-mediated cargo delivery to the cytoplasm of *Escherichia coli* and *Pseudomonas aeruginosa*: syntheses of monofunctionalized enterobactin scaffolds and evaluation of enterobactin-cargo conjugate uptake, *J Am Chem Soc*. **134**: 18388-18400.
57. Page, M. G., Dantier, C., Desarbre, E. (2010) *In vitro* properties of BAL30072, a novel siderophore sulfactam with activity against multiresistant gram-negative *bacilli*, *Antimicrob Agents Chemother*. **54**:2291-2302.
58. Schalk, I. J., Guillon, L. (2013) Pyoverdine biosynthesis and secretion in *Pseudomonas aeruginosa*: implications for metal homeostasis, *Environ Microbiol*. **15**: 1661-1673.
59. Gao, Q., Wang, X., Xu, H., Xu, Y., Ling, J., Zhang, D., Gao, S., Liu, X. (2012) Roles of iron acquisition systems in virulence of extraintestinal pathogenic *Escherichia coli*: salmochelin and aerobactin contribute more to virulence than heme in a chicken infection model, *BMC Microbiol*. **12**:143-155.
60. Ling, J., Pan, H., Gao, Q., Xiong, L., Zhou, Y., Zhang, D., Gao, S., Liu, X. (2013) Aerobactin synthesis genes *iucA* and *iucC* contribute to the pathogenicity of avian pathogenic *Escherichia coli* O2 strain E058, *PLoS One*. **8**:e57794.
61. Bailey, D. C., Drake, E. J., Grant, T. D., Gulick, A. M. (2016) Structural and Functional Characterization of Aerobactin Synthetase *IucA* from a Hypervirulent Pathotype of *Klebsiella pneumonia*, *Biochemistry*. **55**: 3559-3570.
62. Schmiederer, T., Rausch, S., Valdebenito, M., Mantri, Y., Mösker, E., Baramov, T., Stelmaszyk, K., Schmieder, P., Butz, D., Müller, S. I., Schneider, K., Baik, M. H., Hantke, K., Süssmuth, R. D. (2011) The *E. coli* siderophores enterobactin and salmochelin form six-coordinate silicon complexes at physiological pH, *Angew Chem Int Ed Engl*. **50**:4230-42333.
63. Raymond, K. N., Dertz, E. A., Kim, S. S. (2003) Enterobactin: an archetype for microbial iron transport, *Proc Natl Acad Sci U S A*. **100**:3584-3588.
64. Abergel, R. J., Clifton, M. C., Pizarro, J. C., Warner, J. A., Shuh, D. K., Strong, R. K., Raymond, K. N. (2008) The siderocalin/enterobactin interaction: a link between mammalian immunity and bacterial iron transport, *J Am Chem Soc*. **130**:11524-11534.
65. Khalil, S., Pawelek, P. D. (2011) Enzymatic adenylation of 2,3-dihydroxybenzoate is enhanced by a protein-protein interaction between *Escherichia coli* 2,3-dihydro-2,3-dihydroxybenzoate dehydrogenase (EntA) and 2,3-dihydroxybenzoate-AMP ligase (EntE), *Biochemistry* **50**: 533-545.

66. Ma, L., Payne, S. M. (2012) AhpC is required for optimal production of enterobactin by *Escherichia coli*, *J Bacteriol.* **194**: 6748-6757.
67. Strieker, M., Tanović, A., Marahiel, M. A. (2010) Nonribosomal peptide synthetases: structures and dynamics, *Curr Opin Struct Biol.* **20**:234-240.
68. Caboche, S., Pupin, M., Leclère, V., Fontaine, A., Jacques, P., Kucherov, G. (2008) NORINE: a database of nonribosomal peptides, *Nucleic Acids Res.* **36**(Database issue): D326-31.
69. Gehring, A. M., Mori, I., Walsh, C. T. (1998) Reconstitution and characterization of the *Escherichia coli* enterobactin synthetase from EntB, EntE, and EntF, *Biochemistry*, **37**: 2648-2659.
70. Winn, M., Fyans, J. K., Zhuo, Y., Micklefield, J. (2016) Recent advances in engineering nonribosomal peptide assembly lines, *Nat Prod Rep.* **33**:317-347.
71. Lai, J. R., Fischbach, M. A., Liu, D. R., Walsh, C. T. (2006) A protein interaction surface in nonribosomal peptide synthesis mapped by combinatorial mutagenesis and selection, *Proc. Natl. Acad. Sci. U. S. A.* **103**: 5314-5319.
72. Frueh, D. P., Arthanari, H., Koglin, A., Vosburg, D. A., Bennett, A. E., Walsh, C. T., Wagner, G. (2008) Dynamic thiolation-thioesterase structure of a non-ribosomal peptide synthetase, *Nature*, **454**: 903-906.
73. Drake, E. J., Miller, B. R., Shi, C., Tarrasch, J. T., Sundlov, J. A., Allen, C. L., Skiniotis, G., Aldrich, C. C., Gulick, A. M. (2016) Structures of two distinct conformations of holo-non-ribosomal peptide synthetases, *Nature*, **529**:235-238.
74. Leduc, D., Battesti, A., Bouveret, E. (2007) The hotdog thioesterase EntH (YbdB) plays a role in vivo in optimal enterobactin biosynthesis by interacting with the ArCP domain of EntB, *J. Bacteriol.* **189**: 7112-7126.
75. Chen, D., Wu, R., Bryan, T. L., Dunaway-Mariano, D. (2009) In vitro kinetic analysis of substrate specificity in enterobactin biosynthetic lower pathway enzymes provides insight into the biochemical function of the hot dog-fold thioesterase EntH, *Biochemistry*, **48**:511-513.
76. Ehmann, D. E., Shaw-Reid, C. A., Losey, H. C., Walsh, C. T. (1999) The EntF and EntE adenylation domains of *Escherichia coli* enterobactin synthetase: Sequestration and selectivity in acyl-AMP transfers to thiolation domain cosubstrates, *Proc. Natl. Acad. Sci. U.S.A.* **97**: 2509-2514.
77. Sundlov, J. A., Shi, C., Wilson, D. J., Aldrich, C. C., Gulick, A. M. (2012) Structural and functional investigation of the intermolecular interaction between NRPS adenylation and carrier protein domains, *Chem. Biol.* **19**: 188-198.
78. Putman, M., van Veen, H. W., Konings, W. N. (2000) Molecular properties of bacterial multidrug transporters, *Microbiol. Mol. Biol. Rev.* **64**: 672-693.
79. Bleuel, C., Grosse, C., Taudte, N., Scherer, J., Wesenberg, D., Krauss, G. J., Nies, D. H., Grass, G. (2005) TolC is involved in enterobactin efflux across the outer membrane of *Escherichia coli*, *J. Bacteriol.* **187**: 6701-6707.
80. Vega, D. E., Young, K. D. (2014) Accumulation of periplasmic enterobactin impairs the growth and morphology of *Escherichia coli* tolC mutants, *Mol Microbiol.* **91**: 508-521.
81. Horiyama, T., Nishino, K. (2014) AcrB, AcrD, and MdtABC multidrug efflux systems are involved in enterobactin export in *Escherichia coli*, *PLoS One.* **9**:e108642.
82. Koronakis, V., Sharff, A., Koronakis, E., Luisi, B., Hughes, C. (2000) Crystal structure of the bacterial membrane protein TolC central to multidrug efflux and protein export, *Nature*, **405**: 914-919.

83. Tatsumi, R., Wachi, M. (2008) TolC-dependent exclusion of porphyrins in *Escherichia coli*, *J. Bacteriol.* **190**: 6228-6233.
84. Hantash, F. M., Earhart, C. F. (2000) Membrane association of the *Escherichia coli* enterobactin synthase proteins EntB/G, EntE, and EntF, *J Bacteriol.* **182**:1768-1773.
85. Imperi, F. Visca, P. (2013) Subcellular localization of the pyoverdine biogenesis machinery of *Pseudomonas aeruginosa*: a membrane-associated "siderosome". *FEBS Lett.* **587**: 3387-3391.
86. Krewulak, K. D., Vogel, H. J. (2011) TonB or not TonB: is that the question?, *Biochem Cell Biol.* **89**:87-97.
87. Pawelek, P. D., Croteau, N., Ng-Thow-Hing, C., Khursigara, C. M., Moiseeva, N., Allaire, M., Coulton, J. W. (2006) Structure of TonB in complex with FhuA, *E. coli* outer membrane receptor, **Science**, **312**:1399-1402.
88. Matzanke, B. F., Anemüller, S., Schünemann, V., Trautwein, A. X., Hantke, K. (2004) FhuF, part of a siderophore-reductase system, *Biochemistry.* **43**:1386-1392.
89. Caza, M., Garénaux, A., Lépine, F., Dozois, C. M. (2015) Catechol siderophore esterases Fes, IroD and IroE are required for salmochelins secretion following utilization, but only IroD contributes to virulence of extra-intestinal pathogenic *Escherichia coli*, *Mol Microbiol.* **97**:717-732.
90. de Lorenzo, V., Bindereif, A., Paw, B. H., Neilands, J. B. (1986) Aerobactin biosynthesis and transport genes of plasmid ColV-K30 in *Escherichia coli* K-12. *J Bacteriol.* **165**: 570-578.
91. Ma, L., Kaserer, W., Annamalai, R., Scott, D. C., Jin, B., Jiang, X., Xiao, Q., Maymani, H., Massis, L. M., Ferreira L. C., Newton S. M., Klebba P. E. (2007) Evidence of ball-and-chain transport of ferric enterobactin through FepA. *J Biol Chem.* **282**: 397-406.
92. Crosa, J. H., Walsh, C. T. (2002) Genetics and assembly line enzymology of siderophore biosynthesis in bacteria. *Microbiology and Molecular Biology Reviews.* **66**: 223-249.
93. Lambalot, R. H., Gehring, A. M., Flugel, R. S., Zuber, P., LaCelle, M., Marahiel, M. A., Reid, R., Khosla, C. Walsh, C. T. (1996) A new enzyme superfamily - the phosphopantetheinyl transferases. *Chem Biol.* **3**: 923-936.
94. Gasser, V., Guillon, L., Cunrath, O. Schalk, I.J. (2015) Cellular organization of siderophore biosynthesis in *Pseudomonas aeruginosa*: Evidence for siderosomes. *J. Inorg. Biochem.* **148**: 27-34.
95. Kitagawa, M., Ara, T., Arifuzzaman, M., Ioka-Nakamichi, T., Inamoto, E., Toyonaga, H. Mori, H. (2005) Complete set of ORF clones of *Escherichia coli* ASKA library (a complete set of *E. coli* K-12 ORF archive): unique resources for biological research. *DNA Res.* **12**: 291-299.
96. Datsenko, K.A. Wanner, B. L. (2000) One-step inactivation of chromosomal genes in *Escherichia coli* K-12 using PCR products. *Proc Natl Acad Sci U S A.* **97**: 6640-6645.
97. Baba, T., Ara, T., Hasegawa, M., Takai, Y., Okumura, Y., Baba, M., Datsenko, K.A., Tomita, M., Wanner, B.L., Mori, H. (2006) Construction of *Escherichia coli* K-12 in-frame, single-gene knockout mutants: the Keio collection. *Mol Syst Biol.* **2**: 2006.0008.
98. Green, M.R., Sambrook, J. (2012) Molecular cloning: a laboratory manual. Cold Spring Harbor Laboratory Press New York.
99. Schwyn, B., Neilands, J.B. (1987) Universal chemical assay for the detection and determination of siderophores. *Anal Biochem.* **160**: 47-56.
100. Battesti, A., Bouveret, E. (2012) The bacterial two-hybrid system based on adenylate cyclase reconstitution in *Escherichia coli*. *Methods.* **58**: 325-334.

101. Miller, J.H. (1992) A short course in bacterial genetics: a laboratory manual and handbook for *Escherichia coli* and related bacteria. Cold Spring Harbor Laboratory Press, Plainview, N.Y.
102. Karimova, G., Pidoux, J., Ullmann, A., Ladant, D. (1998) A bacterial two-hybrid system based on a reconstituted signal transduction pathway. *Proc Natl Acad Sci U S A.* **95**: 5752-5756.
103. Torchala, M., Moal, I. H., Chaleil, R. A., Fernandez-Recio, J., Bates, P.A. (2013) SwarmDock: a server for flexible protein-protein docking. *Bioinformatics* **29**: 807-809.
104. Sundlov, J. A., Garringer, J. A., Carney, J. M., Reger, A. S., Drake, E. J., Duax, W. L., Gulick, A.M. (2006) Determination of the crystal structure of EntA, a 2,3-dihydro-2,3-dihydroxybenzoic acid dehydrogenase from *Escherichia coli*. *Acta Crystallogr D Biol Crystallogr.* **62**: 734-740.
105. Mattaini, K. R., Brignole, E. J., Kini, M., Davidson, S. M., Fiske, B. P., Drennan, C. L., Vander Heiden, M.G. (2015) An epitope tag alters phosphoglycerate dehydrogenase structure and impairs ability to support cell proliferation. *Cancer. Metab.* **3**: 5.
106. Magalon, A., Frixon, C., Pommier, J., Giordano, G., Blasco, F. (2002) *In vivo* interactions between gene products involved in the final stages of molybdenum cofactor biosynthesis in *Escherichia coli*. *J. Biol. Chem.* **277**: 48199-48204.
107. Reznikoff, W. S. (1992) The lactose operon-controlling elements: a complex paradigm. *Mol. Microbiol.* **6**: 2419-2422.
108. Sawma, P., Roth, L., Blanchard, C., Bagnard, D., Crémel, G., Bouveret, E., Duneau, J. P., Sturgis, J. N., Hubert, P. (2014) Evidence for new homotypic and heterotypic interactions between transmembrane helices of proteins involved in receptor tyrosine kinase and neuropilin signaling. *J. Mol. Biol.* **426**: 4099-4111.
109. Lensink, M. F., Wodak, S. J. (2013) Docking, scoring, and affinity prediction in CAPRI. *Proteins* **81**: 2082-2095.
110. Comeau, S. R., Gatchell, D.W., Vajda, S., Camacho, C. J. (2004) ClusPro: an automated docking and discrimination method for the prediction of protein complexes. *Bioinformatics* **20**: 45-50.
111. Bonvin, A. M. (2006) Flexible protein-protein docking. *Curr. Opin. Struct. Biol.* **16**: 194-200.
112. Andrews, S. C., Robinson, A. K., Rodríguez-Quñones, F. (2003) Bacterial iron homeostasis. *FEMS Microbiol. Rev.* **27**: 215-237.
113. Hantke, K. (1984) Cloning of the repressor protein gene of iron-regulated systems in *Escherichia coli* K12. *Mol. Gen. Genet.* **197**: 337-341.
114. Pohl, E., Haller, J. C., Mijovilovich, A., Meyer-Klaucke, W., Garman, E., Vasil, M. L. (2003) Architecture of a protein central to iron homeostasis: crystal structure and spectroscopic analysis of the ferric uptake regulator. *Mol. Microbiol.* **47**: 903-915.
115. Fillat, M. F. (2014) The FUR (ferric uptake regulator) superfamily: Diversity and versatility of key transcriptional regulators. *Arch. Biochem. Biophys.* **546**: 41-52.
116. Porcheron, G., Dozois, C. M. (2015) Interplay between iron homeostasis and virulence: Fur and RyhB as major regulators of bacterial pathogenicity. *Vet. Microbiol.* **179**: 2-14.
117. de Lorenzo, V., Wee, S., Herrero, M., Neilands, J. B. (1987) Operator sequences of the aerobactin operon of plasmid ColV-K30 binding the ferric uptake regulation (fur) repressor. *J. Bacteriol.* **169**: 2624-2630.

118. Stojiljkovic, I., Bäumlér, A. J., Hantke, K. (1994) Fur regulon in Gram-negative bacteria. Identification and characterization of new iron-regulated *Escherichia coli* genes by a fur titration assay. *J. Mol. Biol.* **236**: 531-545.
119. Delany, I., Rappuoli, R., Scarlato, V. (2004) Fur functions as an activator and as a repressor of putative virulence genes in *Neisseria meningitidis*. *Mol. Microbiol.* **52**: 1081-1090.
120. Nandal, A., Huggins, C. C., Woodhall, M. R., McHugh, J., Rodríguez-Quñones, F., Quail, M. A., Guest, J. R., Andrews, S. C. (2010) Induction of the ferritin gene (ftnA) of *Escherichia coli* by Fe(2+)-Fur is mediated by reversal of H-NS silencing and is RyhB independent. *Mol. Microbiol.* **75**: 637-657.
121. Seo, S. W., Kim, D., Latif, H., O'Brien, E. J., Szubin, R., Palsson, B. O. (2014) Deciphering Fur transcriptional regulatory network highlights its complex role beyond iron metabolism in *Escherichia coli*. *Nat. Commun.* **5**: 4910.
122. Baichoo, N., Helmann, J. D. (2002) Recognition of DNA by Fur: a reinterpretation of the Fur box consensus sequence. *J. Bacteriol.* **184**: 5826-5832.
123. Pecqueur, L., D'Autréaux, B., Dupuy, J., Nicolet, Y., Jacquamet, L., Brutscher, B., Michaud-Soret, I., Bersch, B. (2006) Structural changes of *Escherichia coli* ferric uptake regulator during metal-dependent dimerization and activation explored by NMR and X-ray crystallography. *J. Biol. Chem.* **281**: 21286-21295.
124. Bagg, A., Neilands, J. B. (1987) Molecular mechanism of regulation of siderophore-mediated iron assimilation. *Microbiol. Rev.* **51**: 509-518.
125. Hantke, K. (1987) Selection procedure for deregulated iron transport mutants (fur) in *Escherichia coli* K 12: fur not only affects iron metabolism. *Mol. Gen. Genet.* **210**: 135-139.
126. Troxell, B., Fink, R. C., Porwollik, S., McClelland, M., Hassan, H. M. (2011) The Fur regulon in anaerobically grown *Salmonella enterica* sv. Typhimurium: identification of new Fur targets. *BMC Microbiol.* **11**: 236.
127. de Lorenzo, V., Herrero, M., Giovannini, F., Neilands, J. B. (1988) Fur (ferric uptake regulation) protein and CAP (catabolite-activator protein) modulate transcription of fur gene in *Escherichia coli*. *Eur. J. Biochem.* **73**: 537-546.
128. Elkins, M. F., Earhart, C. F. (1989) Nucleotide sequence and regulation of the *Escherichia coli* gene for ferrienterobactin transport protein FepB. *J. Bacteriol.* **171**: 5443-5451.
129. Brickman, T. J., Ozenberger, B. A., McIntosh, M. A. (1990) Regulation of divergent transcription from the iron-responsive *fepB-entC* promoter-operator regions in *Escherichia coli*. *J. Mol. Biol.* **212**: 669-682.
130. de Lorenzo V. *et al.* Mode of Binding of the Fur Protein to Target DNA (Chapter 13) (2004) *Iron transport in bacteria*, Crosa, J. H., Mey, A. R., and Payne, S. M., eds. ASM Press.
131. Pakarian, P., Pawelek, P. D. (2016) Subunit orientation in the *Escherichia coli* enterobactin biosynthetic EntA-EntE complex revealed by a two-hybrid approach. *Biochimie*, **127**:1-9.
132. Brzezinska, M., Davies, J. (1973) Two enzymes which phosphorylate neomycin and kanamycin in *Escherichia coli* strains carrying R factors. *Antimicrob. Agents Chemother.* **3**:266-269.
133. Chang, A. C., Cohen, S. N. (1978) Construction and characterization of amplifiable multicopy DNA cloning vehicles derived from the P15A cryptic miniplasmid. *J. Bacteriol.* **134**: 1141-1156.

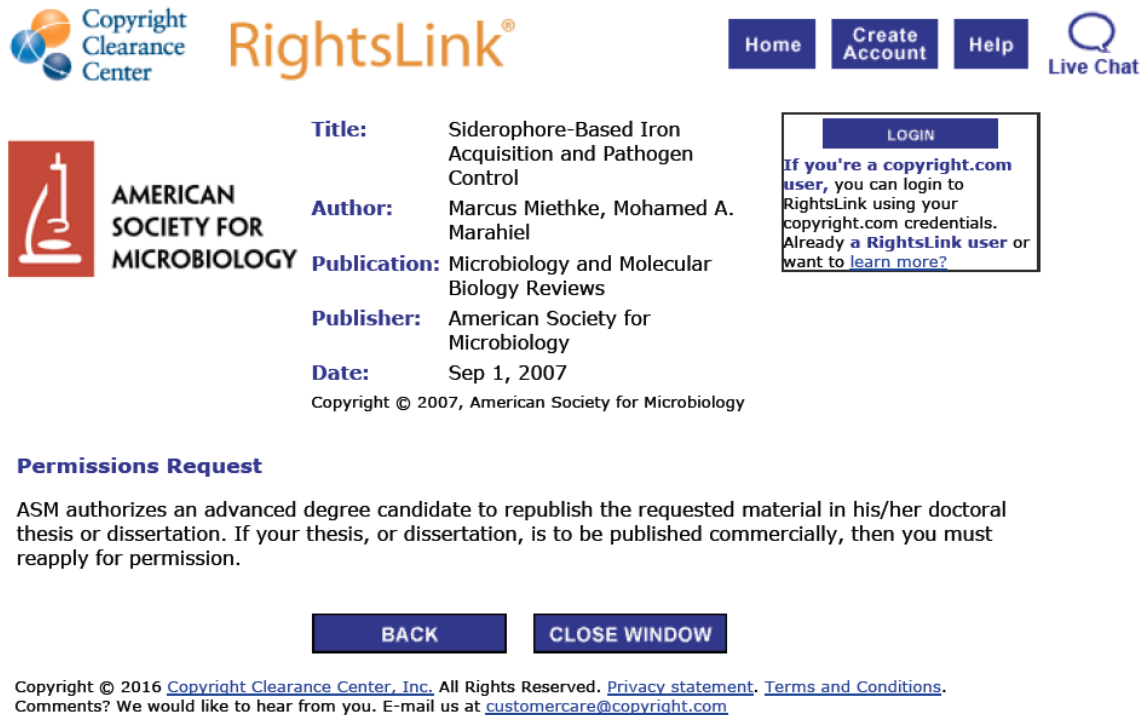
134. Bolivar, F., Rodriguez, R. L., Greene, P. J., Betlach, M. C., Heyneker, H. L., Boyer, H. W., Crosa, J. H., Falkow, S. (1977) Construction and characterization of new cloning vehicles. II. A multipurpose cloning system. *Gene*, **2**: 95-113.
135. Lin-Chao, S., Chen, W. T., Wong, T. T. (1992) High copy number of the pUC plasmid results from a Rom/Rop-suppressible point mutation in RNA II. *Mol. Microbiol.* **6**:3385-3393.
136. Mead, D. A., Szczesna-Skorupa, E., Kemper, B. (1986) Single-stranded DNA 'blue' T7 promoter plasmids: a versatile tandem promoter system for cloning and protein engineering. *Protein Eng.* **1**: 67-74.
137. Guan, L., Liu, Q., Li, C., Zhang, Y. (2013) Development of a Fur-dependent and tightly regulated expression system in *Escherichia coli* for toxic protein synthesis. *BMC Biotechnol.* **13**: 25.
138. Kleywegt, G. J. (1996) Use of non-crystallographic symmetry in protein structure refinement, *Acta Crystallogr D Biol Crystallogr.* **52**: 842-857.
139. Johnson, D. K., Karanicolas, J. (2013) Druggable Protein Interaction Sites Are More Predisposed to Surface Pocket Formation than the Rest of the Protein Surface. *PLoS Comput Biol* **9**: e1002951.
140. Miethke, M., Schmidt, S., Marahiel, M. A. (2008) The major facilitator superfamily-type transporter YmfE and the multidrug-efflux activator Mta mediate bacillibactin secretion in *Bacillus subtilis*, *J Bacteriol.* **190**: 5143-5152.
141. May, J. J., Wendrich, T. M., Marahiel, M. A. (2001) The *dhb* operon of *Bacillus subtilis* encodes the biosynthetic template for the catecholic siderophore 2,3-dihydroxybenzoate-glycine-threonine trimeric ester Bacillibactin, *J Biol Chem.* **276**:7209-7217.
142. Hannauer, M., Schäfer, M., Hoegy, F., Gizzi, P., Wehrung, P., Mislin, G. L., Budzikiewicz, H., Schalk, I. J. (2012) Biosynthesis of the pyoverdine siderophore of *Pseudomonas aeruginosa* involves precursors with a myristic or a myristoleic acid chain, *FEBS Lett.* **586**: 96-101.
143. Nadal-Jimenez, P., Koch, G., Reis, C. R., Muntendam, R., Raj, H., Jeronimus-Stratingh, C. M., Cool, R. H., Quax, W. J. (2014) PvdP is a tyrosinase that drives maturation of the pyoverdine chromophore in *Pseudomonas aeruginosa*, *J Bacteriol.* **196**:2681-2690.
144. Imperi, F., Putignani, L., Tiburzi, F., Ambrosi, C., Cipollone, R., Ascenzi, P., Visca, P. (2008) Membrane-association determinants of the omega-amino acid monooxygenase PvdA, a pyoverdine biosynthetic enzyme from *Pseudomonas aeruginosa*, *Microbiology*, **154**: 2804-2813.
145. Zhang, K., Nelson, K. M., Bhuripanyo, K., Grimes, K. D., Zhao, B., Aldrich, C. C., Yin, J. (2013) Engineering the substrate specificity of the DhbE adenylation domain by yeast cell surface display, *Chem Biol.* **20**: 92-101.
146. James, C. L., Viola, R. E. (2002) Production and characterization of bifunctional enzymes. Substrate channeling in the aspartate pathway, *Biochemistry.* **41**: 3726-3731.
147. Wu, F., Minter, S. (2015) Krebs cycle metabolon: structural evidence of substrate channeling revealed by cross-linking and mass spectrometry, *Angew Chem Int Ed Engl.* **54**: 1851-1854.
148. Gitai, Z. (2005) The new bacterial cell biology: moving parts and subcellular architecture, *Cell*, **120**: 577-586.
149. Moraes, T. F., Reithmeier, R. A. (2012) Membrane transport metabolons, *Biochim Biophys Acta.* **1818**: 2687-2706.

150. Babu, M., Greenblatt, J. F., Emili, A., Strynadka, N. C., Reithmeier, R. A., Moraes, T. F. (2010) Structure of a SLC26 anion transporter STAS domain in complex with acyl carrier protein: implications for *E. coli* YchM in fatty acid metabolism, *Structure*, **18**:1450-1462.
151. Smith, M. A., Coinçon, M., Paschos, A., Jolicœur, B., Lavallée, P., Sygusch, J., Baron, C. (2012) Identification of the binding site of Brucella VirB8 interaction inhibitors, *Chem Biol.* **19**: 1041-1048.
152. Paschos, A., den Hartigh, A., Smith, M. A., Atluri, V. L., Sivanesan, D., Tsolis, R. M., Baron, C. (2011) An in vivo high-throughput screening approach targeting the type IV secretion system component VirB8 identified inhibitors of *Brucella abortus* 2308 proliferation, **79**:1033-1043.
153. Kostecki, J. S., Li, H., Turner, R. J., Delisa, M. P. (2010) Visualizing interactions along the *Escherichia coli* twin-arginine translocation pathway using protein fragment complementation, *PLoS One*, **5**: e9225.
154. Haung, B. (2010) Super-resolution optical microscopy: multiple choices, *Curr. Opin. Chem. Biol.* **14**: 10-14.
155. Foo, Y. H., Spahn, C., Zhang, H., Heilemann, M., Kenney, L. J. (2015) Single cell super-resolution imaging of *E. coli* OmpR during environmental stress, *Integr. Biol.* **7**:1297-1308.
156. Spahn, C., Cella-Zannacchi, F., Endesfelder, U., Heilemann, M. (2015) Correlative super-resolution imaging of RNA polymerase distribution and dynamics, bacterial membrane and chromosomal structure in *Escherichia coli*, *Methods Appl. Fluoresc.* **3**: 014005.
157. Fernández-Suárez, M., Ting, A. Y. (2008) Fluorescent probes for superresolution imaging in living cells, *Nature Reviews* **9**, 929-943.
158. Subach, F. V., Patterson, G. H., Manley, S., Gillette, J. M., Lippincott-Schwartz, J., Verkhusa, V. V. (2009) Photoactivatable mCherry for high-resolution two-color fluorescence microscopy, *Nat. Methods.* **6**:153-159.

Appendix 1

Permission for republishing figures 1, 4 and 5 in the introduction section.

Figure 1:



The screenshot shows the RightsLink interface. At the top left is the Copyright Clearance Center logo. To its right is the RightsLink logo. Further right are navigation buttons for Home, Create Account, and Help, along with a Live Chat icon. The main content area features the American Society for Microbiology logo on the left. To its right, the article details are listed: Title: Siderophore-Based Iron Acquisition and Pathogen Control; Author: Marcus Miethke, Mohamed A. Marahiel; Publication: Microbiology and Molecular Biology Reviews; Publisher: American Society for Microbiology; Date: Sep 1, 2007. Below this is a copyright notice: Copyright © 2007, American Society for Microbiology. A 'Permissions Request' section follows, stating that ASM authorizes an advanced degree candidate to republish the material in a thesis or dissertation, but requires a permission request for commercial publication. A 'LOGIN' button is visible in a box on the right side of the article details. At the bottom of the page are 'BACK' and 'CLOSE WINDOW' buttons, and a footer with copyright information and contact details for Copyright Clearance Center, Inc.

Copyright Clearance Center RightsLink®

Home Create Account Help Live Chat

AMERICAN SOCIETY FOR MICROBIOLOGY

Title: Siderophore-Based Iron Acquisition and Pathogen Control

Author: Marcus Miethke, Mohamed A. Marahiel

Publication: Microbiology and Molecular Biology Reviews

Publisher: American Society for Microbiology

Date: Sep 1, 2007

Copyright © 2007, American Society for Microbiology

Permissions Request

ASM authorizes an advanced degree candidate to republish the requested material in his/her doctoral thesis or dissertation. If your thesis, or dissertation, is to be published commercially, then you must reapply for permission.

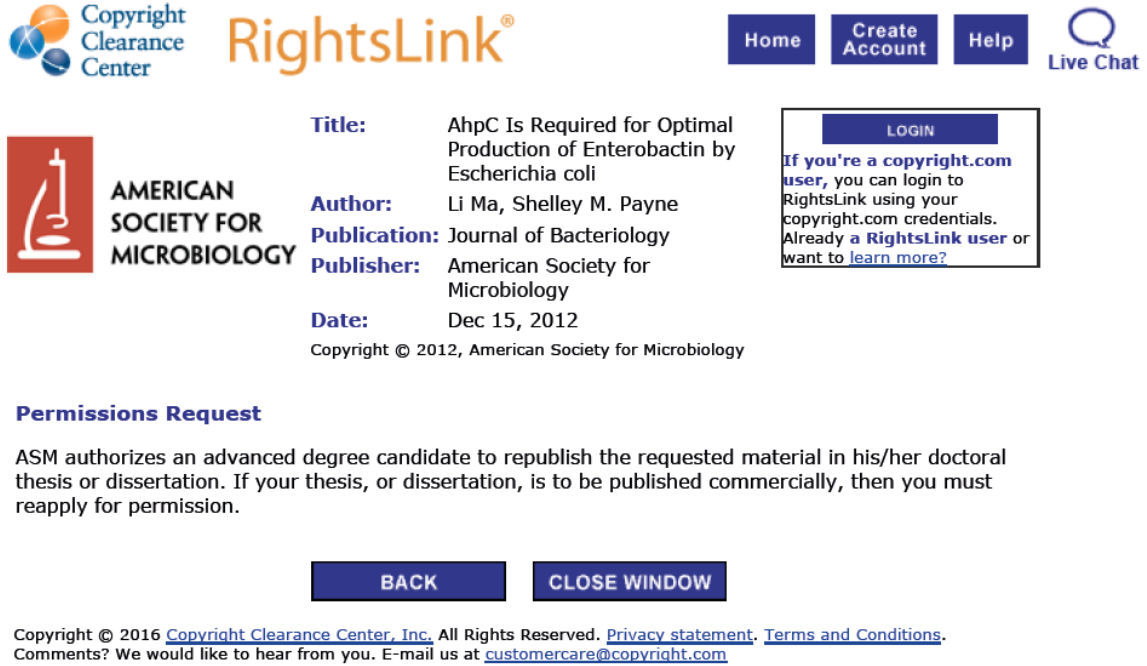
LOGIN

If you're a [copyright.com user](#), you can login to RightsLink using your [copyright.com](#) credentials. Already a [RightsLink user](#) or want to [learn more?](#)

BACK CLOSE WINDOW


Copyright © 2016 [Copyright Clearance Center, Inc.](#) All Rights Reserved. [Privacy statement](#). [Terms and Conditions](#). Comments? We would like to hear from you. E-mail us at customercare@copyright.com

Figure 4:



Copyright Clearance Center RightsLink®

Home Create Account Help Live Chat

 **AMERICAN SOCIETY FOR MICROBIOLOGY**

| | |
|---------------------|---|
| Title: | AhpC Is Required for Optimal Production of Enterobactin by Escherichia coli |
| Author: | Li Ma, Shelley M. Payne |
| Publication: | Journal of Bacteriology |
| Publisher: | American Society for Microbiology |
| Date: | Dec 15, 2012 |

Copyright © 2012, American Society for Microbiology

LOGIN

If you're a [copyright.com user](#), you can login to RightsLink using your [copyright.com](#) credentials. Already a [RightsLink user](#) or want to [learn more?](#)

Permissions Request

ASM authorizes an advanced degree candidate to republish the requested material in his/her doctoral thesis or dissertation. If your thesis, or dissertation, is to be published commercially, then you must reapply for permission.

BACK **CLOSE WINDOW**

Copyright © 2016 [Copyright Clearance Center, Inc.](#) All Rights Reserved. [Privacy statement.](#) [Terms and Conditions.](#) Comments? We would like to hear from you. E-mail us at customer@copyright.com

Figure 5:

The screenshot displays the Copyright Clearance Center RightsLink interface. At the top left is the Copyright Clearance Center logo. To its right is the RightsLink logo. Further right are navigation buttons for Home, Create Account, and Help, along with a Live Chat icon. Below the logos, the ACS Publications logo is shown on the left, followed by a list of publication details: Title, Author, Publication, and Date. A LOGIN button is visible, with a text box explaining that users can log in with their copyright.com credentials or learn more. At the bottom of the details section, a copyright notice for 2006 by the American Chemical Society is present.

Copyright Clearance Center RightsLink®

Home Create Account Help Live Chat

ACS Publications Most Trusted. Most Cited. Most Read.

Title: Localized Protein Interaction Surfaces on the EntB Carrier Protein Revealed by Combinatorial Mutagenesis and Selection

Author: Jonathan R. Lai, Michael A. Fischbach, David R. Liu, et al

Publication: Journal of the American Chemical Society

Publisher: American Chemical Society

Date: Aug 1, 2006

Copyright © 2006, American Chemical Society

LOGIN

If you're a copyright.com user, you can login to RightsLink using your copyright.com credentials. Already a RightsLink user or want to learn more?

PERMISSION/LICENSE IS GRANTED FOR YOUR ORDER AT NO CHARGE

This type of permission/license, instead of the standard Terms & Conditions, is sent to you because no fee is being charged for your order. Please note the following:

- Permission is granted for your request in both print and electronic formats, and translations.
- If figures and/or tables were requested, they may be adapted or used in part.
- Please print this page for your records and send a copy of it to your publisher/graduate school.
- Appropriate credit for the requested material should be given as follows: "Reprinted (adapted) with permission from (COMPLETE REFERENCE CITATION). Copyright (YEAR) American Chemical Society." Insert appropriate information in place of the capitalized words.
- One-time permission is granted only for the use specified in your request. No additional uses are granted (such as derivative works or other editions). For any other uses, please submit a new request.

If credit is given to another source for the material you requested, permission must be obtained from that source.

BACK

CLOSE WINDOW

Copyright © 2016 Copyright Clearance Center, Inc. All Rights Reserved. [Privacy statement](#), [Terms and Conditions](#). Comments? We would like to hear from you. E-mail us at customer@copyright.com